2000

Transport and Magnetic Measurements of Mono - Silicides.

Ncholu Ignatius Manyala
Louisiana State University and Agricultural & Mechanical College

INFORMATION TO USERS

This manuscript has been reproduced from the microfilm master. UMI films the text directly from the original or copy submitted. Thus, some thesis and dissertation copies are in typewriter face, while others may be from any type of computer printer.

The quality of this reproduction is dependent upon the quality of the copy submitted. Broken or indistinct print, colored or poor quality illustrations and photographs, print bleedthrough, substandard margins, and improper alignment can adversely affect reproduction.

In the unlikely event that the author did not send UMI a complete manuscript and there are missing pages, these will be noted. Also, if unauthorized copyright material had to be removed, a note will indicate the deletion.

Oversize materials (e.g., maps, drawings, charts) are reproduced by sectioning the original, beginning at the upper left-hand corner and continuing from left to right in equal sections with small overlaps.

Photographs included in the original manuscript have been reproduced xerographically in this copy. Higher quality 6" x 9" black and white photographic prints are available for any photographs or illustrations appearing in this copy for an additional charge. Contact UMI directly to order.

Bell & Howell Information and Learning
300 North Zeeb Road, Ann Arbor, MI 48106-1346 USA
800-521-0600

UMI®

TRANSPORT AND MAGNETIC MEASUREMENTS OF MONO-SILICIDES

A Dissertation

Submitted to the Graduate Faculty of the
Louisiana State University and
Agricultural and Mechanical College
in partial fulfillment of the
requirements for the degree of
Doctor of Philosophy

in

The Department of Physics and Astronomy

by
Ncholu Ignatius Manyala
B.Sc., National University of Lesotho, 1989
M.Sc., University of Witwatersrand, 1992
May 2000

DEDICATION

In the memory of my mother and my three brothers

ACKNOWLEDGMENTS

In my six years of graduate work at Louisiana State University I have benefited very much from friendship of many people to who I wish to pass special thanks.

First, I thank members of my special committee. My thesis advisor John F. DiTusa has taught me so much about experimental techniques of low temperature physics and has always been helpful with advice and creative solutions to the problems that I faced. His enthusiasm and talent for defining cutting-edge research problems has been a continuous source of inspiration.

I would like to thank Drs. Michael Cherry and Dana Browne for serving in my committee. Dr. Philip Adams was a co-principal investigator for half part of the work outline in this thesis, and has been a great help. I would like to thank Yvan Sidis for many helpful suggestions and discussions regarding the experiment to be done and the meaning of results of this experiment. I also like to thank Gabriel Aeppli, David Young and Zack Fisk for their wonderful contributions to this work. The discussion with Alem Telku were also a great help.

Special thanks to my colleagues and friends Alem Telku, Reginald Madjoe, Phillip Walsh, Alexey Koveshnikov and Cabir Terzoiglu for their friendship which helped a great deal during this stressful time. I would also like to thank the following undergraduates students for their help in the laboratory during the course of this work Joseph Langdale, Brian Perone, Martin Bitner, and Jonathan Hanson.

My thanks to Randy Gould, Marcus A. Sen, Steven B. Ellison, Donnie Olano, Allen Young, Bobby Sullivan and Phillip Nurse for their technical assistance in numerous ways. I would also like to thank Xiaogang Xie and Wanda Leblanc from Geology department for their great help in the characterization of the samples used in this work. I am grateful to all the past and present secretaries and staff: Arnell Jackson, Karla Lockwood, Beverly Rodriguez, Karen Richard, Cathy Mixon, Ophelia Dudley,

Karen Cashio, Jim Fernandez, Hortensia Valdes, and Conner Campion, for the numerous ways they have provided assistance.

I would like to acknowledge the financial support I have received from the Fulbright shcolarship, Teaching Assistantship from the Department of Physics and Astronomy and research assistantship from Dr. John DiTusa.

I would like to thank all of my family, my father and all my bothers and sisters and their families for their love and support through out my graduate career. They have all answered my long letters outlining difficult times of being away from home and being all alone during the last six years. I wish my mother is still here to see it to the end as she had always thought high of me.

The greatest thanks goes to my wife Mataoana and my daughter Ithabeleng for being my best friends. My wife helped me through all rough times, and celebrated all my accomplishments with me. She deserves a special credit for making it though these years married to a graduate student of whom she never saw much of. I would like to thank her from the bottom of my heart for taking care of our daughter all these years that I had not been there for her. This time I am coming home forever. Finally, all glory and honor to my Lord and Saviour Jesus Christ for giving me life and purpose.

TABLE OF CONTENTS

LIST OF FIGURES

ABSTRACT

The purpose of this dissertation is to investigate the magnetic and transport properties of the dilution series connecting the mono-silicides FeSi, CoSi, and MnSi. We have focused on these materials since they allow the exploration of carrier doping of an unusual insulator, FeSi, whose properties are dominated by strong Coulomb interactions. These monosilicides all have the same cubic B-20 crystal structure making them ideal for an exploration of $Fe_{1-x}Mn_xSi$ and $Fe_{1-y}Co_ySi$ for all x and y between 0 and 1. The carrier sign and densities, as well as the proximity to magnetic phases can be controlled by the level of chemical substitution across this series. We have investigated the transport and magnetic behavior of this system, centered on the Kondo insulator FeSi, by carrying out magnetization, Hall effect, resistivity and magnetoresistence measurements. We have discovered that MnSi and $Fe_{1-y}Co_ySi$, which both are itinerant helimagnetic compounds, differ in that the Co doped FeSi is nearly spin polarized and has a novel temperature and field dependent conductivity. We discovered that the MR in $Fe_{1-y}Co_ySi$ is due to quantum interference effects which are substantial in this compound up to 100 K. $Fe_{1-y}Co_ySi$ ($0 < y \leq 0.3$) is a strongly scattering low charge density metal in which we have also discovered an extraordinarily large anomalous Hall effect. In contrast the hole doped insulator, $Fe_{1-x}Mn_xSi$, remains paramagnetic up to $x <$ 0.9 with a large quasiparticle mass and a conductivity (σ) that is dominated by electron-electron (e-e) interaction effects. At low temperatures the hole carriers are localized beyond that due to the usual square-root singularity associated with quantum interference effects. In fact, the σ and susceptibility are comparable to the diluted magnetic semiconductors, such as the Mn doped II-VI compounds.

CHAPTER 1

INTRODUCTION

In this work we present investigations of the magnetic and transport properties of the dilution series of the mono-silicides FeSi, CoSi, and MnSi. These materials have a common B-20 cubic crystal structure, allowing an investigation of their electronic and magnetic properties as we vary the number of d electrons on the transition metal site.

1.1 Background and Motivation

The doping of magnetic or nonmagnetic semiconductors and insulators has resulted in interesting and useful electronic and magnetic properties, and has led to recent discoveries in materials where Coulomb interactions are significant. Recent discoveries include "colossal" magnetoresistance (CMR) of manganites[1-3], and low density magnetic systems[4, 5]. Along side of these discoveries, the development of micro-structures of magnetic materials has led to the discovery of the MR of magnetic superlayers referred to as giant magnetoresistance (GMR)[6], spin dependent electronics (spintronics)[7, 8], as well as MRs in several other systems[5, 9, 10]. These discoveries have led to the technological applications in magnetoelectronics, such as the increased sensitivity of read/write heads and thus the information density of magnetic storage devices.

Our motivation was to search for novel behavior in magnetic systems when the carrier density can be controlled –a doped semiconductor. We have chosen the strongly correlated insulator FeSi which is distinct from classic semiconductors such as Si, Ge, and Mott-Hubbard insulators. Since the monosilicides FeSi, CoSi, and MnSi all have the same cubic B-20 crystal structure, they allow the exploration of the $Fe_{1-x}Mn_xSi$ and $Fe_{1-y}Co_ySi$ for all x and y between 0 and 1. In this way we controlled the carrier density and disorder in a magnetically interesting phase diagram (Fig. 1.1 (a)). This system has been known to have varied ground state properties dependent on composition including Kondo insulating or metallic, as well as helimagnetic, paramagnetic, or even diamagnetic. It is the

existence of the strongly correlated insulator FeSi at the center of this series which determines the charge and magnetic ground state properties of this transition metal silicide dilution series (see Fig. 1.1). The ferromagnetic fluctuations of this parent insulating system combined with the low carrier concentration and concomitant dominance of the Coulomb interactions of a diffusively conducting system give this series its unique electronic properties.

The electronic and magnetic properties of carrier doped classic semiconductors like Si near metal-insulator transition (MI) have been found to be determined by disorder and electron-electron (e-e) interactions[11,12]. The importance of Coulomb interactions has been further highlighted by investigations of systems such as the Mott-Hubbard insulators, where the Coulomb interactions are responsible for the insulating behavior. The resulting metals have interesting and unusual magnetic and superconducting ground states. These investigations have found for examples, that V vacancies in $V_{2-x}0_3$ produce a metal with spiral magnetic order[13,14], Sr substitution in $La_{2-x}Sr_xCuO_4$ produces a high-temperature superconductor[15-19], and hydrostatic pressure applied to $Ni(S,Se)_2$ produces a MI transition with novel critical exponents[20]. Recently, another class of insulators with strong e-e interaction effects have emerged, namely "strongly correlated" or "Kondo" insulators[21-25]. The best characterized of these is FeSi[26].

One of the interesting aspects of this work is that FeSi and the Kondo insulators seem to be distinct from the classic semiconductors and the Mott-Hubbard systems. FeSi is thought to belong to the Kondo insulator family which is mostly made up of rare-earth intermetallics. FeSi is the only transition-metal compound to be classified in this group of materials[24, 26, 27]. It is an insulator with a band gap of 60 meV which originally attracted attention over 30 years ago because this material which is half Fe has a low temperature susceptibility that surprisingly approaches zero[26, 28]. The magnetic susceptibility and inelastic neutron scattering spectrum measurements revealed a thermally activated spin susceptibility which has only recently been modeled [25, 28, 29]. Measurements of the ac

conductivity[30] and the photoemission[31] find temperature-dependent features in direct conflict with traditional theories of band-gap insulators. This is considered to be clear evidence that this insulator is distinct from the garden variety of band insulators.

With either hole (Mn or Al) or electron (Co) doping of FeSi an insulator to metal (MI) transition occurs at a level of ~ 0.01 (Fig. 1.1 (b) and (d))[32, 33]. While electron doping beyond the MI transition almost immediately produces a helimagnetic ground state, hole doping produces a simple paramagnetic metal. It is only upon approaching the MnSi phase diagram that a helimagnetic state appears ($x > 0.8$). At this end of the phase diagram shown in Fig. 1.1 (a), both the magnetic and transport behavior are that of a textbook weakly itinerant ferromagnet[34]. Although FeSi is a nonmagnetic insulator and CoSi is a diamagnetic metal, nearly all of the phase diagram between is characterized by a metallic and helimagnetic ground state (see Fig. 1.1 (a))[35-39].

We have investigated the transport and magnetic behavior across this dilution series by carrying out magnetization, Hall effect, resistivity and magnetoresistance measurements. For $Fe_{1-y}Co_ySi$ ($0 < y \leq 0.3$) we find a low charge density *(n)* helimagnetic phase with one of the largest anomalous Hall effects measured to date. Furthermore, we have discovered that MnSi and $Fe_{1-y}Co_ySi$, which both are itinerant helimagnetic compounds, differ in that the Co doped FeSi is nearly spin polarized and has a novel T and field dependent conductivity. In fact, we have discovered a positive MR in $Fe_{1-y}Co_ySi$ up to T exceeding T_C which can be described in terms of the quantum contributions to the conductivity.

In $Fe_{1-x}Mn_xSi$, we have concentrated on the low Mn concentrations ($0 < x \leq 0.08$) with the intention of comparing it to $FeSi_{1-z}Al_z$. In both cases we expect holes to be introduced in FeSi by doping on the two different sites. We found that the basic physics of the metal induced from FeSi by hole doping does not depend on the site at which the holes are introduced. For both $Fe_{1-x}Mn_xSi$ and $FeSi_{1-z}Al_z$ the low T σ is dominated by the

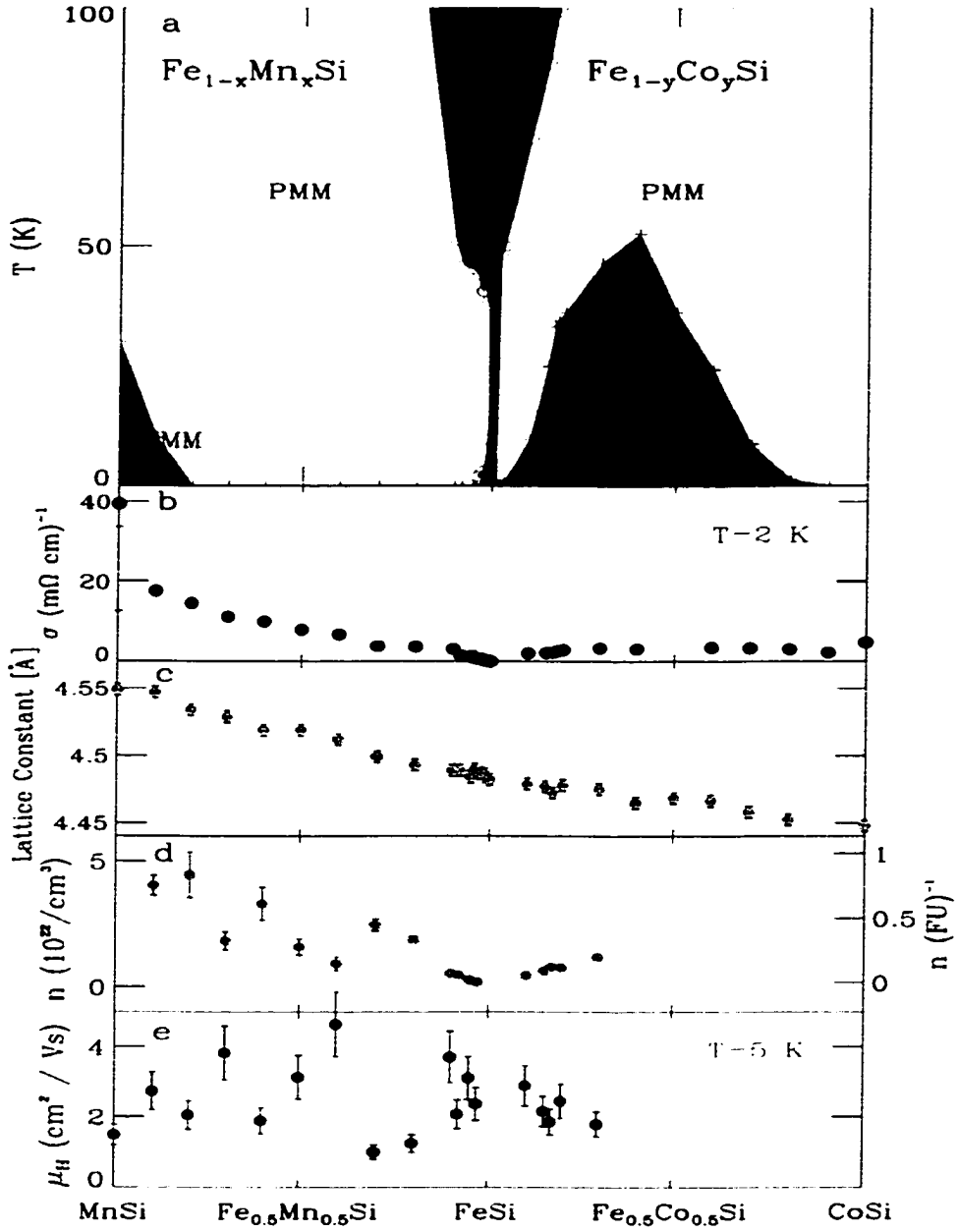

Fig. 1.1 Phase diagram for $Fe_{1-x}Mn_xSi$ and $Fe_{1-y}Co_ySi$. (a) Transition temperature (T_C) vs. nominal Mn and Co concentration (x, y). (b) low T conductivity vs. nominal Mn and Co concentration (x, y). (b) Lattice constant vs. nominal Mn and Co concentration (x, y). (c) Carrier density as determined from Hall effect vs. nominal Mn and Co concentration (x, y). (d) Hall mobility vs. nominal Mn and Co concentration (x, y). (HMM – helimagnetic metal, PMM – paramagnetic metal, PMI – paramagnetic insulator).

correlation effects (e-e interactions) of a disordered metal. In both cases there is a strong enhancement of the quasi-particles mass on the metallic site of the transition- a heavy Fermion metal. There are however, significant differences in the two compounds in both the low T magnetic and transport properties. $Fe_{1-x}Mn_xSi$ appears to be different from $FeSi_{1-z}Al_z$ in that its low temperature properties are similar to the diluted magnetic semiconductors. Associated with this ground state is magnetic field driven insulator to metal transition.

1.2 Organization of the Thesis

Specific questions we hoped to answer are discussed for each system in the following chapters. Chapter two discusses the general overview of measurements of interest. Chapters three through five present the results of the measurements and conclusions reached. In chapter three we discuss the Hall effect measurements of both dilution series $Fe_{1-x}Mn_xSi$ and $Fe_{1-y}Co_ySi$. Chapter four covers the magnetic and transport measurements of $Fe_{1-y}Co_ySi$ with comparisons made to classic helimagnmetic compound MnSi. Chapter five deals with magnetic and transport measurements of $Fe_{1-x}Mn_xSi$ compared to $FeSi_{1-z}Al_z$ in the same hole concentration range. We conclude with chapter six where we sum up our results and conclusions.

1.3 Experimental Details

The samples investigated in our experiments were either polycrystalline pellets or small bars cut from single crystals grown from Sb and Sn fluxes. The polycrystalline samples were produced from high purity (99.995%) starting materials provided by Alfa AESAR, A Johnson Matthey Company, by arc melting in an argon atmosphere. To improve sample homogeneity $Fe_{1-y}Co_ySi$ ($Fe_{1-x}Mn_xSi$) samples were annealed for 24 hrs. at 1200 ^{0}C (four days at 1000 ^{0}C) in evacuated quartz ampoules. We employed x-ray spectra on the ground samples obtained with Cu-Kα radiation on a SIEMENS D5000 equipped with a position sensitive detector to determine that samples were single phase. The lattice constant of the doped samples from the x-ray spectra are shown in Fig. 1.1

(c), where it is apparent that they depend linearly on both Co and Mn concentrations respectively. This observance of Vegard's law demonstrates that both Co and Mn successfully replace Fe in the whole concentration range. We have performed energy-dispersive x-ray microanalysis (EDX) and wavelength dispersive spectroscopy (WDS) on a JEOL Superprobe 733 scanning electron microscope equiped with a Kevex Si (Li) detector to check the stoichiometry of our samples. We used beam current of 10 mA and accelerating voltage of 15 kV for WDS measurements. The data show no evidence that the Co, Mn, Fe, or Si concentration differs from the nominal values.

The resistance and Hall-effect measurements were performed on rectangular samples cut by a string saw and polished with emery paper. Thin Pt wires were attached to four contacts made with silver paste which were arranged linearly with an average spacing between voltage probes of 2 mm along an average cross section of 1×0.5 mm^2. The resistivity (ρ) amd magnetoresistance (MR) measurements were performed at 19 Hz using standard lock-in techniques in a dilution refrigerator with 9-T superconducting magnet, and at high temperatures with a gas flow cryostat in a 5 T superconducting magnet. The contacts for the Hall effect were carefully aligned, and measurements were performed with fields between –5 and 5 T. The Hall voltage (V_H) was taken as $V_H = (V(H) - V(-H)) / 2$, thus correcting for any contamination from the field symmetric MR due to misalignment of the contacts. We have determined the field direction in our superconducting magnet and thus the sign of ordinary Hall constant by measuring the Hall effect of 200 $\mathring{A}$ thick Al film as standard sample[40].

The magnetic susceptibility (χ) of the same samples was measured in a Quantum Design superconducting quantum inteference device (SQUID) magnetometer for fields between 0.05 and 0.1 T and temperatures from 1.7 to 400 K. We collected magnetization (M) measurements between 1.7 and 400 K in fields between –5 and 5 T in a SQUID magnetometer and from 0 to 32 T in a vibrating reed magnetometer at the National High Magnetic Field Laboratory (NHMFL) in Florida.

CHAPTER 2

OUTLINE OF THE MEASUREMENTS

In this work we have measured four properties of the doped FeSi compound as to investigate the influence of doping: resistivity, magnetoresistance, Hall effect and magnetic susceptibility. In this chapter we give an overview of the measurements and what information can be drawn from each.

2.1 Hall Effect

The Hall effect is commonly used to determine the carrier concentration in a material. Consider a material carrying a current i in the $\vec{x}$ direction as shown in upper frame of Fig. 2.1. The material has a concentration of conduction electrons n_e, which has a mobility μ_e. In the absence of a magnetic field the Hall Voltage $V_H = 0$. When a magnetic field H is applied in the $\vec{z}$ direction the electrons which are moving in - $\vec{x}$ direction with drift velocity v_x are deflected in - $\vec{y}$ direction as a result of the Lorentz force thus building up charge on the edge of a material. This build up results in an electric field, $\vec{E}_y = -(V_H / b)\vec{y}$ across the sample, called the Hall Field[41], where b is the width of the sample. The charge build up continues until the force of the Hall field on the moving conduction electrons balances the Lorentz force and halts further accumulation of electrons on the sample edge. Once equilibrium is reached the force in the $\vec{y}$ direction is zero[41]:

$$F_y = -e(\vec{v} \times \vec{B})_y + eE_y = 0, \tag{2.1}$$

where e is the electron charge.

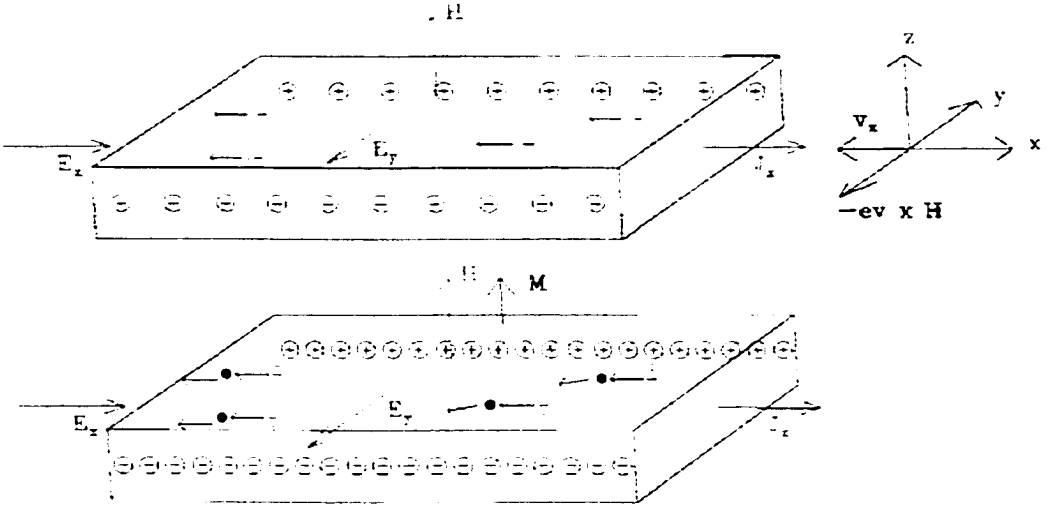

Fig. 2.1. Upper frame: The Hall effect in paramagnetic metals and semiconductors. Lower frame: The Hall effect in ferromagnetic metals.

The current density is [41]:

$$j_x = \frac{i}{bd} = -n_e e v_x, \tag{2.2}$$

where d is sample thickness and thus the Hall field is

$$E_y = \frac{V_H}{b} = -\frac{1}{n_e e} j_x H = -\frac{1}{n_e e}\frac{iH}{bd} = R_0 \frac{iH}{bd}, \tag{2.3}$$

where R_0 is called the ordinary Hall constant.

$$R_0 = \frac{-1}{n_e e}, \tag{2.4}$$

V_H is given by:

$$V_H = R_0 \frac{iH}{d}. \tag{2.5}$$

These can be inverted to find the carrier concentration in terms of the measured quantities V_H, i, H and d,

$$n_e = -\frac{1}{V_H e}\frac{iH}{d}. \tag{2.6}$$

In some materials, there exist both positive (holes) and negative (electrons) charge carriers each of which has a concentration, n_h, and n_e, and a mobility, μ_h, and μ_e. In this case an analogous calculation leads us to a Hall constant which depends on both the concentration and mobility of each carrier species[41]:

$$R_0 = \frac{n_h\mu_h^2 - n_e\mu_e^2}{e(n_h\mu_h + n_e\mu_e)^2}. \tag{2.7}$$

Note that if $n_h = 0$, equation (2.7) reduces to one carrier limit $R_0 = -1/n_e e$, and that if $n_e = 0$, equation (2.7) reduces to $R_H = 1/n_h e$. This demonstrates that the Hall constant is negative for electron carriers and positive for hole carriers.

The ratio E_y / J_x is known as the transverse resistivity (ρ_{xy}) which is usually a few orders of magnitude smaller than longitudinal resistivity (ρ_{xx}). However in magnetic materials a second contribution which is proportional to the magnetization (M) (see Lower frame: Fig. 2.1), known as anomalous or extraordinary Hall effect dominates at low H and can be hundreds of times larger than the ordinary ρ_{xy}[42]. This second contribution is thought to result from both the spin-orbit (SO) scattering and the spin alignment of the carriers. The same mechanism creates an anomalously large ρ_{xy} in heavy fermion metals[43]. In order to highlight this contribution it is customary to write ρ_{xy} as[44, 45]

$$\rho_{xy} = R_0 H + 4\pi M R_S. \tag{2.8}$$

Here R_0 is the Hall effect resulting from Lorentz force on the carriers in the same manner as in paramagnetic materials and R_S is referred to as the anomalous or extraordinary Hall constant. To characterize R_S below T_C where usually $R_S >> R_0$, it is best to extract the spontaneous Hall resistivity ρ_{xyS} by a linear extrapolation of the data at high fields to $H = 0$. Then $R_S = \rho_{xyS} / 4\pi M_S$ and the high field slope gives R_0. Above T_C and for $H \equiv 0$ we have $\chi H = 4\pi M$ and equation (2.8) becomes

$$\rho_{xy} = (R_0 + R_S 4\pi\chi) H \, . \tag{2.9}$$

The accepted theory of the anomalous Hall effect relies on SO coupling between the carrier and the lattice which produces a left-right asymmetry in the scattering[42]. Above T_C the randomization of the spins leads to an insignificant E_y. However, a large E_y results when material has a non-zero M due to the alignment of the carrier spins (see Fig 2.1 lower frame). This alignment creates an abundance of scattering in one particular direction, and net current perpendicular to E_x. Thus an E_y many times larger than that due

to Lorentz force is necessary to cancel this anomalous current. It has been established, both experimentally and theoretically that there is a direct correlation between the extraordinary Hall coefficient and longitudinal resistivity in the form

$$R_S = \lambda \rho_{xx}^n, \tag{2.10}$$

where λ is the SO coupling constant and n depends on the predominant SO scattering mechanism involved: $n = 1$ for skew scattering , and $n = 2$ for side jump scattering[44, 46]. To understand the origin of these two mechanisms, we know that according to quantum mechanics, a free electron (represented by a wave packet) moves on the average with constant velocity, along a straight line. Assume then the electron be scattered at $t \sim 0$ by a central potential. Again, and for the same reasons, the average electron trajectory after scattering ($t >> 0$) will be a straight line. In the presence of SO interaction, the symmetry of the problem is low, and may not coincide. Thus the new effects are expected: First, the two lines can form an angle δ related to asymmetric scattering (skew scattering). Secondly, the two lines may not meet at the center of the scattering potential; there is a small abrupt side jump Δy (side jump scattering). The side jump is of no consequence in the case of a conventional experiment where free particles are scattered by atoms or nuclei. This is understandable, because usually the particle detectors are located at several cm or m from the target, distance much larger than Δy. But Δy is more important in ferromagnetic metals and alloys, where the mean free path Λ_e of a conduction electron after collision may be smaller than 10^{-9}-10^{-8} m.

While asymmetric scattering arises from a collision term of the classical Boltzmann equation, the side jump Δy is non-classical. The physical nature of Δy is easily understood in terms of localized electrons or wave packets, not in terms of plane waves or of momentum representation. Δy exists because the impurity distorts the wave function

locally, and creates a local current density. The skew scattering term, believed to arise from spin-orbit coupling between the magnetic moment and the conduction electron, is expected to dominate in pure materials at low temperatures, whereas the side jump mechanism is predominant in the higher temperatures and in materials with higher resistivities.

2.2 Magnetoresistance in Normal Metals

The field dependence of the resistance (magnetoresistance) in a material often reveals important information about its electronic structure. In a purely classical Drude model of metallic conduction the conductivity $\sigma = 1 / \rho$ is proportional to the conduction electron concentration n and relaxation time τ[40]. At low temperature the dominant scattering is that by impurities which is temperature and field independent. Since τ does not depend on magnetic field the purely classical model predicts, incorrectly, that the resistivity is not field dependent,

$$\sigma = \frac{1}{\rho} = \frac{ne^2\tau}{m_e}. \tag{2.11}$$

What this classical model is missing is the fact that in a metallic material with Fermi surface (with either open or closed orbits), the electron is restricted to travel (in k space) along surface of constant energy. This restriction reduces the rate at which a conduction electron can absorb energy from the driving electric field and results in an increase of the resistivity with increasing field. If the orbits on the Fermi surface are closed the magnetoresistance saturates at high fields, while for open orbits it increases without limit.

The existence of localized magnetic moments like Fe in pure metals such as Cu form dilute alloys where the local moments couple to the conduction electrons (Kondo effect). This coupling has important consequences on the electrical resistivity. At low

temperatures the magnetic impurities act as the main scattering centers. There is a resistivity minimum as the ρ has a crossover between low T and high T due to phonon scattering. When T is lowered, ρ depends on T as $ln(T)$, reflecting the presence of a large resonance at or near Fermi energy E_F in the conduction electron scattering rate as a function of energy (Kondo resonance). The magnetic field destroys the conduction electron screening of localized moments (which is the source of resonance) leading to a decrease in resistance, hence a negative magnetoresistance.

In ferromagnetic metals an anomalous electrical resistance is observed which is characteristic of the magnetization and is additive to the ordinary electrical resistance. The origin of this anomalous electrical resistance below Curie temperature (T_C) is understood as due to spin fluctuations that scatter electrons through the exchange interaction. The temperature dependence of resistivity below T_C due to spin fluctuations is given by:

$$\rho = \rho_0 + B(H)\, T^2. \tag{2.12}$$

As T increases above T_C

$$\rho - \rho_0 \propto T^{5/3} \tag{2.13}$$

and at high temperature the resistivity depends linearly on T as in normal metals. It is also observed that the resistivity of a ferromagnetic metal has a peak in $d\rho / dT$ near T_C[47]. The change of slope above and below T_C is given by the following equations:

$$\frac{1}{\rho_C}\frac{d\rho}{dT} = \frac{A}{\eta}(\kappa^{-\eta} - 1) + B\,, \quad T > T_C \tag{2.14}$$

and

$$\frac{1}{\rho_C}\frac{d\rho}{dT} = \frac{A'}{\eta}(|\kappa|^{-\eta'} - 1) + B', \qquad T < T_C, \tag{2.15}$$

where $\kappa = (T - T_C)/T_C$, η, η', A, A', B, B' are constants, and ρ_C is the resistivity at T_C. Renormalization theory predicts $\eta = \eta' \approx 0.1$ and $A/A' \approx 1.3$ for a three dimensional exchange ferromagnet[48]. The external magnetic field usually suppresses the amplitude of spin fluctuations, and reduces the resistivity due to the fluctuations leading to negative magnetoresistance (MR).

In an insulator, where conduction occurs via thermally activated hopping of electrons across an energy gap Δ, the resistivity can be changed by magnetic field via the field dependence of energy gap. In this case the Zeeman splitting tends to lift the spin degeneracy of the gap edge. Since there is no need for energy conservation for the thermally activated hopping, the net result is a decrease in the gap magnitude $\propto g\mu_B H$, where g is the Lande' factor. Because $\rho \sim exp(\Delta / k_B T)$ depends exponentially on Δ, magnetic fields can often have dramatic effects on the resistivities of insulators.

2.3 Magnetoresistance in Disordered Metals

An insulator can be made metallic by chemical substitution (doping), by pressure, or by application of external magnetic field. Such a transformation is refered to as an insulator-to-metal (MI) transition. For chemical substitution, the metal resulting from this process is very disordered because of the random distribution of the impurities in the host parent compound. Since in this work we are dealing with an insulator (FeSi) where correlations are important, we find that the theory discussed above is not sufficient to explain our data. Hence, in this section we discuss the temperature and magnetic field dependence of the resistivity of disordered, strongly correlated metals.

The metal-insulator (MI) transition in disordered materials has of late been studied by the methods of the theory of second-order phase transitions. Experiments confirmed

that conductivity goes to zero in a continuous manner[49-51] at a metal-insulator transition and does not show a discontinuous jump as was once assumed. In a disordered system, the Anderson localization effect[52, 53] and Coulomb correlations of the diffusing carriers[54, 55] have been shown to be equally important. In the simplest scaling model, the conductivity in proximity to the MI transition has the form

$$\sigma(T,s) = \xi(s)^{-\mu\nu} f[T\tau(s)], \tag{2.16}$$

where s is a parameter that drives the MI transition[56-58]. In our case s will be the Mn or Co concentration, or the external magnetic field. The other parameters in this model are the correlation length ξ which diverges as $(s - s_c)^{-\mu}$ and the time scale τ (s) which diverges as T goes to zero as $(s - s_c)^{\mu\nu}$. In these formulas the critical exponent ν is related to the manner in which σ vanishes at $T = 0$, $\sigma \propto (s - s_c)^{\nu}$. On the insulating side of the transition the conductivity is dominated by hopping, where the assumption is that there are localized states near Fermi energy. The temperature dependence of σ due to hopping is usually given by:

$$\sigma \propto \exp(-[T_0 / T]^{1/4}), \quad T_0 = \frac{5/2}{9\pi\xi_L^3 k_B g}, \tag{2.17}$$

where ξ_L is the localization length and g is the density of states. This is Mott's $T^{1/4}$-law. The assumption that all jumps are over a fixed distance $\overline{R}$ (fixed range hopping) is only justified for hops between nearest neighbors. For $\overline{R} > R^0$ (mean separation of nearest neighbors), hops of different distances will follow one another (variable range hopping). The hopping transport is due to phonon-assisted hopping, and is prevalent among insulators with a small density of extrinsic carriers.

For materials on the metallic side of the MI transition, the effect of disorder on the temperature and field dependence of the conductivity is significant. This sensitivity results from the diffusive motion of the quasiparticles scattered by the disorder. At low T the vast majority of these scattering events are elastic, resulting in an increased probability of coherent interference of the scattered wave functions. Since these effects arise from the interference of the quasi-particle wave functions, they are known as the quantum contribution to the conductivity[59-61]. The quantum contributions are known to result in a $\sqrt{T}$ dependence of σ in three dimensional conductors[11, 60, 62]. This singular behavior has been understood as arising mainly from an enhancement of the Coulomb interactions.

There are two channels of conduction in which the carriers can interfere. One is diffusion interaction channel. In this channel there is an increase in the effective Coulomb coupling constant from λ to $\lambda(1 + \alpha_d)$, due to the probability that the two quasiparticles interact with each other more than once (α_d) in a time $\hbar/\varepsilon$, where ε is the energy difference between two indistinguishable states. The diffusive channel interaction in disordered materials gives rise to the square-root singularity at the DOS. This singularity is in direct conflict with Landau's idea that in a Fermi liquid the coulomb interaction renormalizes the density of states, but leave it as a smooth function of energy[60]. The Landau theory uses essentially the spatial homogeneity of the system, but the introduction of impurities and defects disturbs this homogeneity leading to physical properties different from those predicted by Fermi liquid theory. In three dimensions the correction to the conductivity in the diffusion interaction channel is given by

$$\Delta\sigma_I = \frac{e^2}{\hbar}\frac{1}{4\pi}\frac{1.3}{\sqrt{2}}\left(\frac{4}{3}-\frac{3}{2}\tilde{F}_\sigma\right)\sqrt{\frac{k_B T}{\hbar D}}, \qquad (2.18)$$

where $D = v_F l/3$ is the diffusion constant[60]. This equation includes the contribution from the exchange term $\left(\frac{4}{3}\right)$ and the Hartree term $(3/4\,\tilde{F}_\sigma)$ of the self-energy, where $\tilde{F}_\sigma$ measures the strength of the electron-electron interaction.

The effect of a magnetic field on the diffusion interaction channel can be understood if we consider the total interference amplitude to be composed of spin-singlet and triplet amplitudes. In this picture the spin-singlet amplitude is not influenced by the field, whereas the states with $j = 1$ will be split by $g\mu_B H_{eff}$ (Zeeman splitting). In ferromagnets we have exchange forces being introduced with the field acting on each ionic dipole as an effective field $H_{eff} = H_a + \alpha M$, where H_a is the applied magnetic field and αM is the molecular field. This field is proportional to the magnetization (M), with α the molecular field constant. It is well known that the molecular field in a ferromagnetic material is normally very much larger than any realizable applied field. Thus the effect of an external field can be amplified by the molecular field increasing the magnitude of the MR[63, 64]. The precession of the spins in the magnetic field causes the interference probability to decrease, effectively cutting off the singularity of the triplet term for $g\mu_B H_{eff} > k_B T$. Thus there will be field-dependent and –independent contributions to the conductivity resulting in a field and temperature dependence of this contribution of

$$\Delta\sigma_I = \frac{e^2}{\hbar}\frac{1}{4\pi^2}\left[\frac{1.3}{\sqrt{2}}\left(\frac{4}{3}-\frac{1}{2}\tilde{F}_\sigma\right)-\tilde{F}_\sigma\frac{1}{\sqrt{2}}\left[1.3+g_3(h)\right]\right]\sqrt{\frac{k_B T}{\hbar D}}, \tag{2.19}$$

where $g_3(h) = \int_0^\infty d\Omega \frac{d^2}{d\Omega^2}[\Omega N(\Omega)]\left(\sqrt{\Omega + h} + \sqrt{|\Omega - h|} - 2\sqrt{\Omega}\right)$, $N(\Omega) = 1/\left(e^\Omega - 1\right)$, and $h = g\mu_B H_{eff}/k_B T$ [60]. g_3 has the limiting behavior: $g_3(h) = \sqrt{h} - 1.3$ for $h >> 1$ and $g_3(h) = 0.053h^2$ for $h << 1$.

These equations demonstrate that in the theory of electron-electron interactions the exchange term and $\frac{1}{3}$ of the Hartree term are not changed by the magnetic field. Large

magnetic fields cut off only the part of the singularity associated with the Hartree term, those in Eq. 2.16 which include $\tilde{F}_\sigma$, and the relevant field scale is $g\mu_B H_{eff} \sim \hbar D$[60]. In the diffusion channel the MC can be either negative or positive depending on the sign of coupling constant.

The second contribution to MC is the Cooper interaction channel, which is similar to diffusion channel, except that we consider the case when the path of one quasiparticle is reversed[59]. That is, one quasiparticle diffuses from B to A (time reversed from A to B path). The coupling constant λ is replaced by the effective coupling constant $\lambda = \lambda/(1+\lambda\ln(E_F/k_BT))$, a typically small change since $\lambda << 1$. For superconducting systems where the effective coupling constant is replaced by $1/\ln(T_{SC}/T)$, where T_{SC} is the superconducting critical temperature, and the interaction is attractive, it is found to be significant. The magnetic field destroys the time-reversal symmetry, and thus the phase coherence necessary for the effect. A negative MC is predicted when the Landau orbit size becomes comparable to the thermal length, $2eH/\hbar c > k_BT/D$.

At low temperatures the conductivity in disordered systems can also have contributions from the weak localization. The weak localization is understood as arising from the two series of scattering events during which the phase of the quasiparticles is not affected by the scattering. The key point is that these two partial waves will interfere constructively, resulting in an increased probability for back-scattering. In three dimensions the conductivity increases with temperature as

$$\Delta\sigma_{wl} \propto \frac{e^2 T^{q/2}}{\hbar}\pi^2, \tag{2.20}$$

where q is determined by temperature dependence of the inelastic processes[59].

The effect of magnetic field on the weak localization is to induce a phase difference in the two scattering series. In this way the magnetic field will destroy the coherent back-scattering if the phase difference between the two paths is of the order of π.

All trajectories with an area projected onto a plane perpendicular to magnetic field larger than $L_H^2 = \hbar c/2eH$ will have coherent scattering suppressed[59]. The characteristic field for the suppression is set by the phase breaking scattering time τ_ϕ as $H_\phi = \hbar c/4eD\tau_\phi$. Since the field cuts off the back-scattering probability, the MC is positive, and in fields H >> H_ϕ the conductivity has the form[59]

$$\Delta\sigma_{wl} = 0.605\frac{e^2}{2\pi^2\hbar}\frac{1}{L_H}. \tag{2.21}$$

2.4 Magnetization and Magnetic Susceptibility

Magnetic susceptibility (χ) and magnetization measurements are very powerful probes of the magnetic ground state of the system in question. The temperature dependence of the magnetic susceptibility in paramagnetic doped insulators is usually the sum of different contributions, ranging from low T Curie-Weiss form, T independent Pauli susceptibility, to a thermally activated term for Kondo insulators. For these materials we write χ as the sum of these three terms

$$\chi = \delta\chi + \frac{C_1}{T-\Theta_w} + \frac{C_2}{T}\exp(-\Delta_\chi / Tk_B), \tag{2.22}$$

where C_1, C_2, Θ_w, and Δ_χ are Curie constants, the Weiss temperature, and energy gap respectively. The first term on the right hand side is the Pauli paramagnetic susceptibility,

$$\delta\chi = \mu_B^2 g(\varepsilon_F), \tag{2.23}$$

where $g(\varepsilon_F)$ is the density of states at Fermi level. For a parabolic band this simplifies to $g(\varepsilon_F) = m^* k_F / \hbar^2 \pi^2$. Using the expression for Fermi wave vector $k_F = (3\pi^2 n / \nu')^{1/3}$ Eq. 2.23 can be written as:

$$\delta\chi = \frac{(3\pi)^{1/3} \mu_B^2 m^* \nu'^{2/3}}{\hbar \pi^2} [n - n_c]^{1/3} , \tag{2.24}$$

where n_c and ν' are critical density and the valley degeneracy. It is clear that one can estimate the effective mass from this expression. For ferro- or antiferromagnetic materials the second term of Eq. 2.22 usually describes the data only at $T > T_C$ or T_N (where T_C is Curie temperature for ferromagnets and T_N is the Nee'l temperature for antiferomagnets). The last term of Eq. 2.22 is the thermally activated susceptibility found in intrinsic FeSi. The magnetization of a paramagnetic materials is often interpreted as consisting of the linear $M(H)$ of the free carriers added to the magnetization of non-interacting ions given by

$$M(H) = \delta\chi H + n_l g \mu_B J B_J (g \mu_B H / k_B T), \tag{2.25}$$

where $\delta\chi$ is Puali susceptibility, n_l is the density of local moments, and B_J is the Brillouin function $B_J(x) = (2J + 1/2J) \coth (2J + 1/2J)x - (1/2J) \coth (1/2J)x$.

Some of the materials under study go through a transition to an itinerant magnetic state, such as MnSi. The actual occurence of magnetism in transition metals is considered to be associated with the atomic character of d-band and mainly intra-atomic exchange interactions. There has been a long on-going discussion of the description of d-electrons starting from localized, or itinerant states. Between the 1950s and early 1960s it became clear that d-electrons should be treated as localized in magnetic insulators and as correlated itinerant electrons in transition metals. The Hartree-Fock approximation (HFA) is often

used for the localized model, while the dynamical HFA or the random-phase approximation (RPA) is more appropriate for the itinerant model. Around 1960, Matthias *et. al.* discovered the weakly itinerant ferromagnetic metals $ZrZn_2$[65], and Sc_3In[66], with low T_C (25 K and 6 K respectively) and small magnetization (0.12 μ_B and 0.04 μ_B per atom respectively). To describe the magnetic behavior of these materials one has to go beyond the HF-RPA theory by taking account of the influence of the exchange-enhanced spin-fluctuactions on the thermodynamical quantities.

Thus one has to calculate the renormalized thermal equilibrium state and spin fluctuactions at the same time in a self-consistent fashion. In other words, one has to deal with the mutually coupled modes of spin fluctuactions self-consistently. The quantum statistical mechanical theory of self-consistent renormalization (SCR) of spin fluctuations was put forth by Moriya and Kawabata[67]. This theory is an extension of HF-RPA theory and its success means that two main streams in the theory of itinerant magnetism have rejoined. According to SCR theory magnetization as $T \rightarrow T_C$ has the following temperature dependence[34]

$$M \propto (T_C^{4/3} - T^{4/3})^{1/2}. \tag{2.26}$$

This form can be used to replace the mean field C-W behavior of Eq. 2.22 in magnetic materials.

CHAPTER 3

HALL EFFECT MEASUREMENTS

In this chapter we will discuss the Hall effect measurements of our $Fe_{1-x}Mn_xSi$ and $Fe_{1-y}Co_ySi$ samples with a special emphasis on helimagnetic $Fe_{1-y}Co_ySi$ ($0.1 \leq y \leq 0.3$). We compare our results with other ferromagnetic compounds and find that $Fe_{1-y}Co_ySi$ is a strongly scattering low charge density metal with an extraordinarily large anomalous low T Hall effect. $Fe_{1-y}Co_ySi$ also differs from other magnetic systems in that the anomalous Hall constant (R_S) is nearly temperature independent below T_C.

3.1 Introduction

There has been a recent renewal of interest in the magnetic field dependent transport properties of materials for application in magnetoelectronics. Most of the attention has focused on the magnetoresistive (MR) materials such as the giant MR superlattices[6], the colossal MR manganites[1-3], as well as several other materials[5, 9, 10]. A second method for producing magnetic field sensitive devices that has been ignored is the Hall effect. In this chapter we report on an exploration of a chemical substitutions between monosilicides MnSi, FeSi and CoSi, chosen because this dilution series is known to include semiconducting, itinerant magnetic, and heavy fermion ground states[32, 33, 38]. We have investigated the transport and magnetic behavior across these transition metal silicide series which we find continuously evolves from a classic weak itinerant magnet, to a metallic paramagnet, to a Kondo (or strongly correlated) insulator, and finally a magnetic heavy fermion[33] all without a change in the crystal structure. This has allowed us to systematically examine the effect of magnetism, carrier density (n), and scattering rates on the Hall resistivity.

3.2 Results

Our high field Hall effect data demonstrate that even at the relatively high Co substitution of $0.1 \leq x \leq 0.3$ each impurity donates one electron per added Co (see Fig.

1.1 (d)). Similarly one hole is doped into FeSi for each Mn substitution for Fe and Al[32] substitution for Si in FeSi. The Al data is included here for comparison purposes (see Figs. 1.1 (d) and 3.1). Thus, at low doping, Mn like Al, inserts holes at the same rate into the valence band of FeSi. Figures 3.2 and 3.3 show the ordinary Hall coefficient as function of temperature for Co and Mn concentration respectively. MnSi data is also shown in Fig. 3.2 as comparison to Co data. It is clear in the figure that for both Co doped FeSi and MnSi R_0 increases as T is increased and reaches maximum at about T_C. This maximum is most likely associated to the difficulty of separating R_S from R_0 at the vicinity of T_C. In the case of low Mn concentration in FeSi we observe that R_0 changes sign from positive (holes) to negative (electrons) as T is increased (see Fig. 3.3). This shows that the high temperature conductivity is dominated by the thermally activated carriers consistent with the behavior of doped semiconductor like FeSi as $T \rightarrow \Delta_E$ (energy gap).

Our main result of a large Hall resistivity (ρ_{xy}) as a function of H in Co and Mn doped FeSi can be seen in Figs. 3.4 (a), 3.5 (a), 3.6, and 3.7 (nonmagnetic $Fe_{1-x}Mn_xSi$ samples). In particular Fig. 3.6 (a) shows the low field part of ρ_{xy}, while Fig. 3.5 (a) shows ρ_{xy} vs H up to 32 T at different temperatures for our $Fe_{0.7}Co_{0.3}Si$ sample. As is common for ferromagnets at T below the Curie temperature (T_C) ρ_{xy} has roughly the same H dependence as M (see Figs. 3.4 (b) and 3.5 (b))[42]. Fig. 3.6 (a) shows that ρ_{xy} has a large linear dependence below about 2 kG and then saturates at the same H where M saturates. Beyond 2 kG ρ_{xy} becomes much less H dependent. At these high fields ρ_{xy} has the usual dependence on n and H, $\rho_{xy} = H / nec$ in its simplest form. For H less than 2 kG, ρ_{xy} is proportional to M and the anomalous contribution dominates (see Eq. 2.8)[42].

For comparison we have plotted ρ_{xy} and M for our MnSi and $Fe_{0.1}Mn_{0.9}Si$ along with $Fe_{1-y}Co_ySi$ samples in Figs. 3.4 (a) and (b) respectively. It is apparent from the figure that although M has the same order of magnitude with comparable H dependence, the Hall effect is vastly different in these compounds. In fact, there is a difference of a

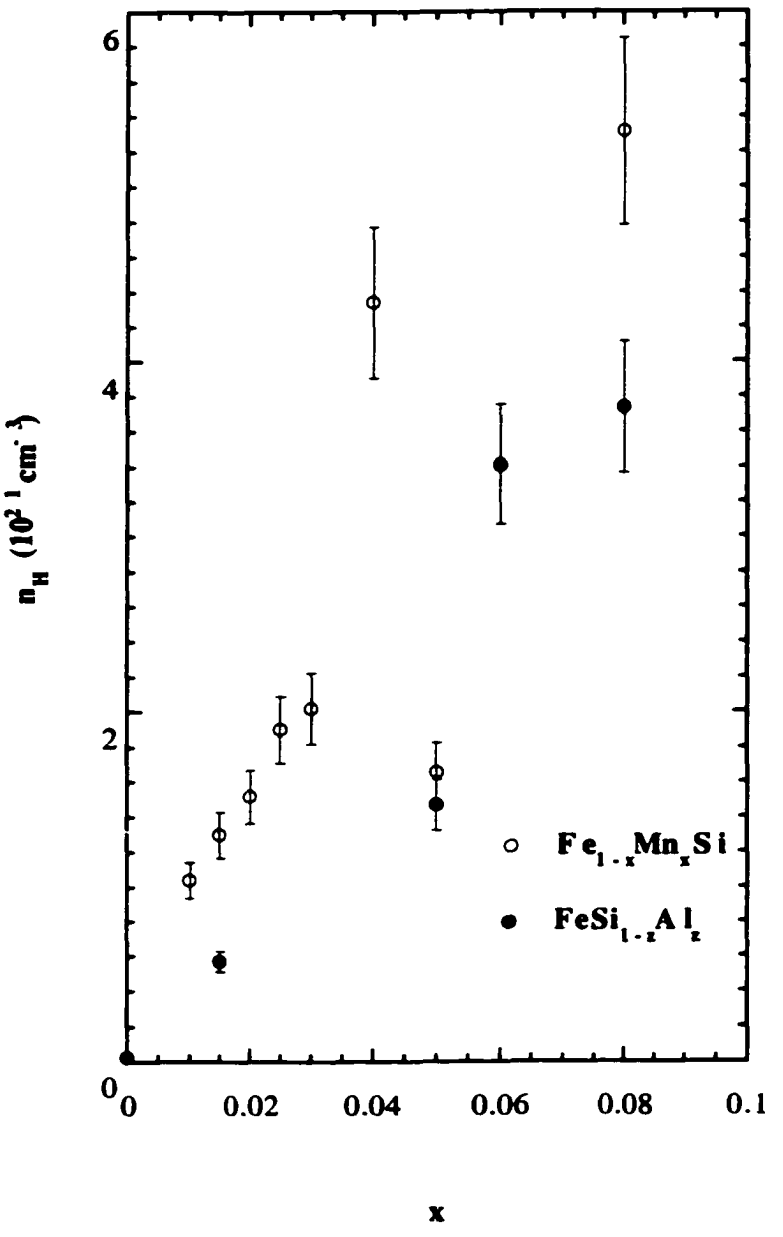

Fig. 3.1 Charge density at 4 K vs. nominal Mn and Al concentrations for $Fe_{1-x}Mn_xSi$ and $FeSi_{1-z}Al_z$.

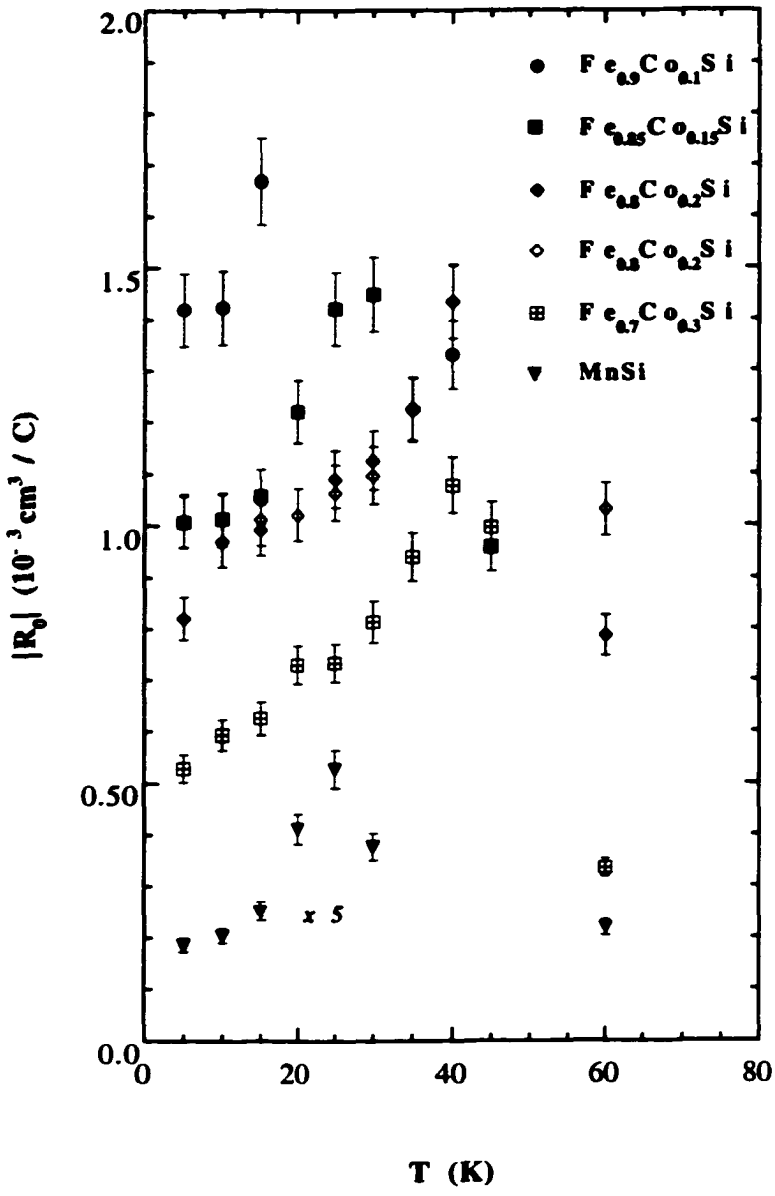

Fig. 3.2 Ordinary Hall coefficient (R_0) vs Temperature for $Fe_{1-y}Co_ySi$ and MnSi samples with symbols noted in the figure.

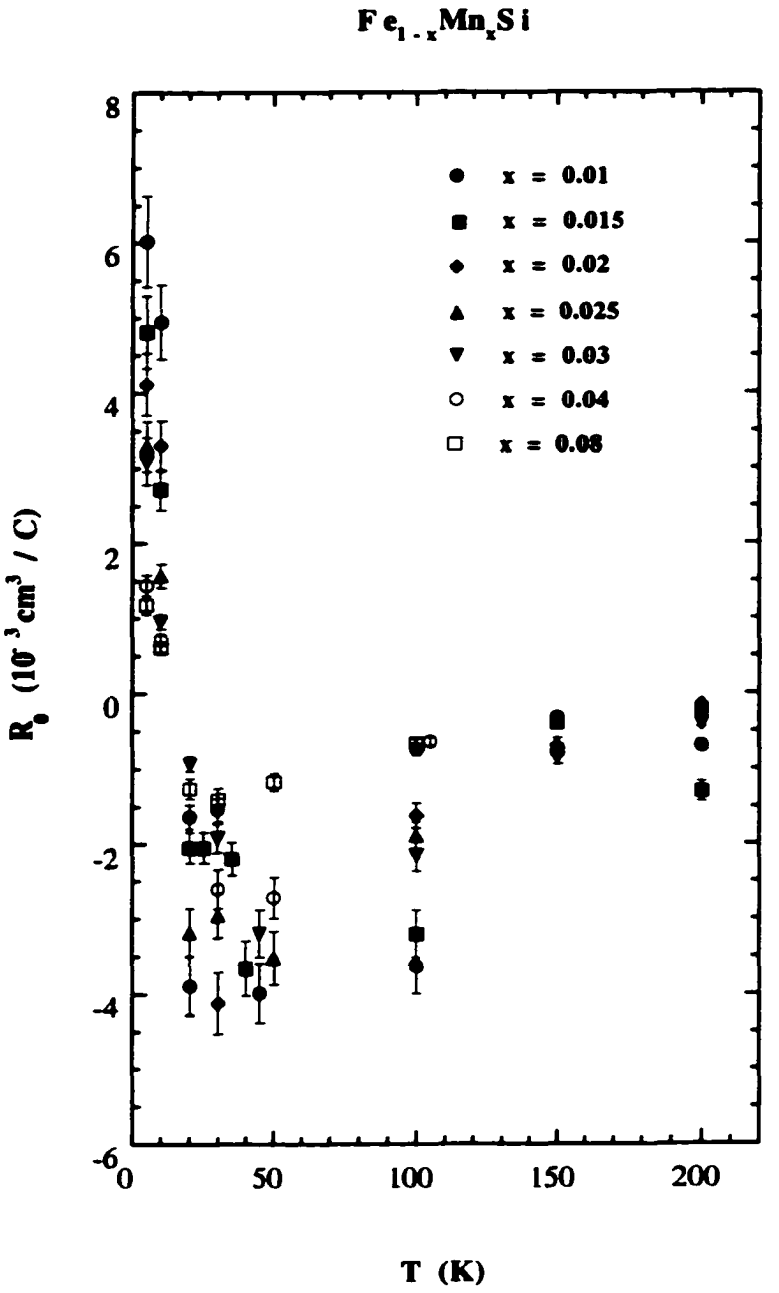

Fig. 3.3 Ordinary Hall coefficient (R_0) vs. Temperature for $Fe_{1-x}Mn_xSi$ in the range of concentration $0.01 \leq x \leq 0.08$.

factor of 150 between the low H ρ_{xy} of the $Fe_{0.9}Co_{0.1}Si$ and $Fe_{0.1}Mn_{0.9}Si$ samples. We have chosen to compare these two samples in detail since they have the same crystal structure, the same level of chemical substitution, and helimagnetic ground states with T_C = 10 K. A further comparison is shown in Figs. 3.8 (a) and (b) where we present the zero field resistivity (ρ_{xx}) and magnetic susceptibility (χ) at 50 G. Again the magnetic properties of these samples appear to be similar, yet the transport is very different. In fact, our $Fe_{0.9}Co_{0.1}Si$ sample is 9 times more resistive than the $Fe_{0.1}Mn_{0.9}Si$ sample and nearly 20 times more resistive than MnSi.

The qualitative difference in ρ_{xx} can be understood by comparing the properties of the nominally pure compounds FeSi and MnSi. FeSi is a nomagnetic band insulator with a 60 eV gap[28] while MnSi is a classic helimagnetic metal with a T_C of 30 K (Fig. 1.1 (a))[34]. The result is that $Fe_{0.9}Co_{0.1}Si$ has 9 times fewer carriers than $Fe_{0.1}Mn_{0.9}Si$ which is reflected both in the high H ρ_{xy} and ρ_{xx}. In fact, the low temperature Hall mobility ($\mu_H = R_0 / \rho_{xx}$) (Fig. 1.1 (e)) is very similar for these two compounds and shows no systematic dependence on x and y, a surprising conclusion given that the Drude model predicts $\mu_H = m^* / e\tau$ and the ground state properties change drastically across this series. This makes our comparison particularly instructive since n alone seems to be responsible for the difference in ρ_{xx} and the high field ρ_{xy}.

As we have pointed out (see Eq. 2.8), the Hall effect in magnetic materials has two contributions, one proportional to H, the second determined by $M(H)$[42]. Since the saturation magnetization M_S of the $Fe_{0.1}Mn_{0.9}Si$ sample is ~ 3.5 times larger than M_S of $Fe_{0.9}Co_{0.1}Si$ sample, R_S of these two compounds differ by a factor of ~ 500 (see Figs. 3.6 (b) and 3.11). The accepted theory of the anomalous Hall effect relies on the SO coupling between the carrier and the lattice which produces a left-right asymmetry in the scattering[42]. Since ρ_{xx} of our $x = 0.9$ and $y = 0.1$ samples differ by a factor of ~ 9 neither of the mechanisms describe by Eq. 2.10 can account for the difference in R_S that we

measure. The only way to make this theory compatible to our data is to assume that only 1/6 of ρ_{xx} in $Fe_{0.1}Mn_{0.9}Si$ (only 1/20 for MnSi) should be included in our analysis. We would have to assume that even though the scattering rates in these materials are similar, the scattering in $Fe_{0.9}Co_{0.1}Si$ is much more effective in producing a perpendicular current. A second option would be to assign a much larger λ to $Fe_{1-y}Co_ySi$ samples than the $Fe_{1-x}Mn_xSi$ samples due to an incompletely quenched orbital moment in $Fe_{1-y}Co_ySi$ as is generally the case for Co^{2+} ions. However, there is a little support in polarized neutron diffraction, ESR, or Co^{59} NMR measurements for orbital moment in $Fe_{1-y}Co_ySi$ to account for a large increase in λ[37, 68-70]. The difference in R_S may be another indication of difference in polarization of the electron gases (80% for $Fe_{0.9}Co_{0.1}Si$ and 20% for $Fe_{0.1}Mn_{0.9}Si$) to be discussed in chapter 4.

It is useful for comparison purposes to present ρ_{xy} and R_S of $Fe_{1-y}Co_ySi$ and $Fe_{1-x}Mn_xSi$ with other materials both magnetic and paramagnetic as we have done in Figs.3.9, 3.10 and 3.11. In Figs. 3.9 and 3.10 we plotted ρ_{xy} of a large number of materials at 1kG and low temperature vs charge density and ρ_{xx} respectively in order to compare magnitudes of the Hall voltage for similar geometry samples. As is well known and apparent in the figures, very large Hall effects result from making semiconductors intrinsic and thus reducing n. However, unlike semiconductors, magnetic materials have large ρ_{xy} (as much as few $\mu\Omega$ cm) while maintaining metallic n and ρ_{xx}. In fact, our $Fe_{1-y}Co_ySi$ samples have ρ_{xy} similar to nonmagnetic semiconductors with a factor of 250 times smaller n while retaining ρ_{xx} 5 to 20 times smaller than these clean crystalline semiconductors. Our $Fe_{1-y}Co_ySi$ samples have the largest ρ_{xy} measured at 4 K for metallic (poly)crystalline ferromagnets without dilution in their insulating host.

Further comparison is made in Fig. 3.11 where R_S is plotted as a function of ρ_{xx}. It is clear from the locus of points from dilute Ni and Fe alloys[71] that $Fe_{1-y}Co_ySi$ is an extension of the $R_S \propto \rho^2_{xx}$ behavior to larger ρ_{xx}, while MnSi and $Fe_{0.1}Mn_{0.9}Si$ seem out of place. In fact, MnSi seems unusual in this plot in that it does not lie within the locus of

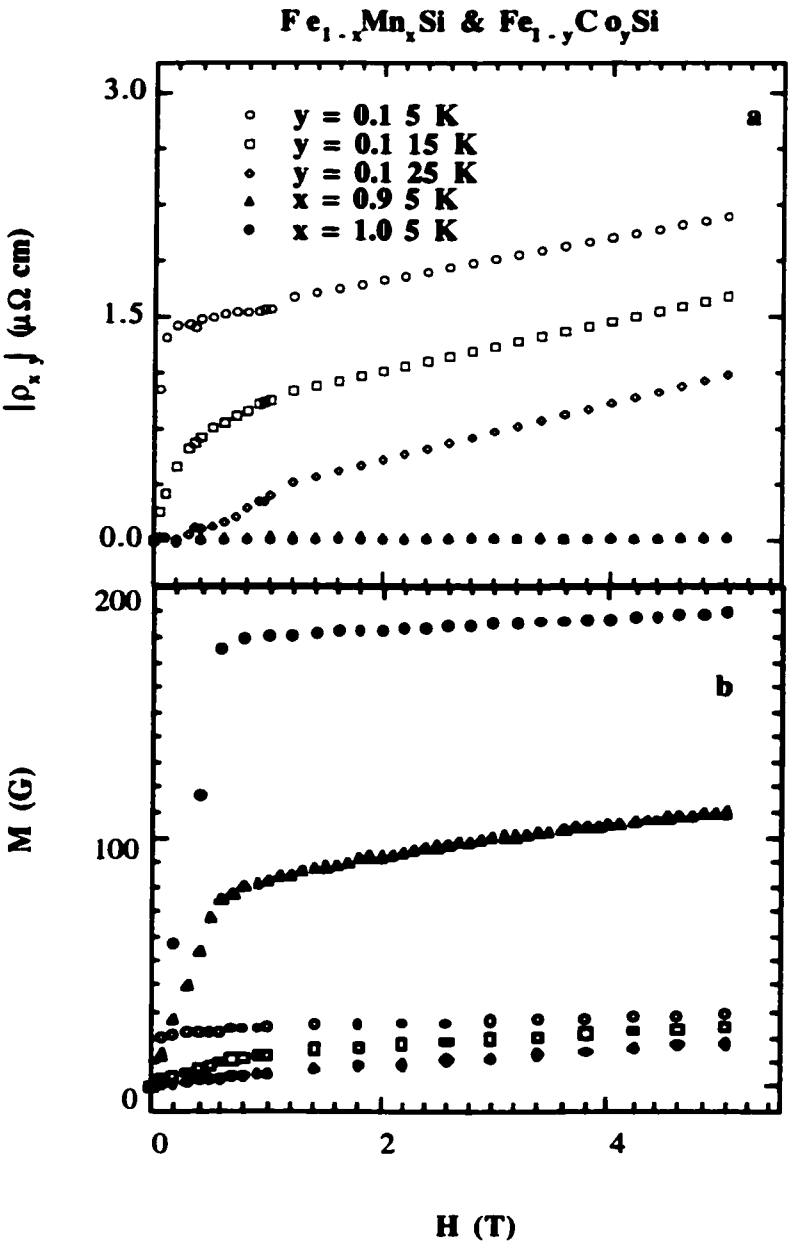

Fig. 3.4. Comparison of $Fe_{0.9}Co_{0.1}Si$, $Fe_{0.1}Mn_{0.1}Si$, and MnSi. (a) Hall resistivity (E_y / J_x) at temperatures labeled in the figure vs. field . (b) Magnetization vs. field (symbols the same as in (a)).

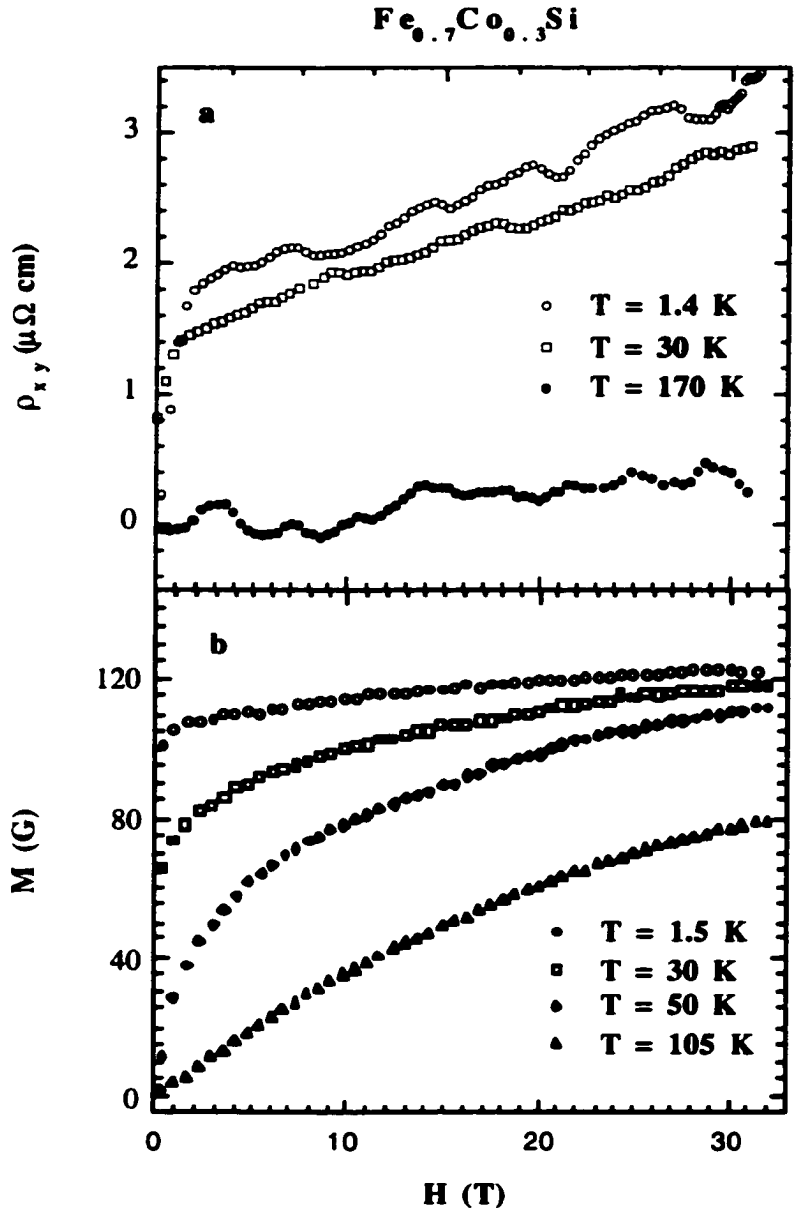

Fig. 3.5. (a) Hall resistivity and (b) magnetization of $Fe_{0.7}Co_{0.3}Si$ vs. field.

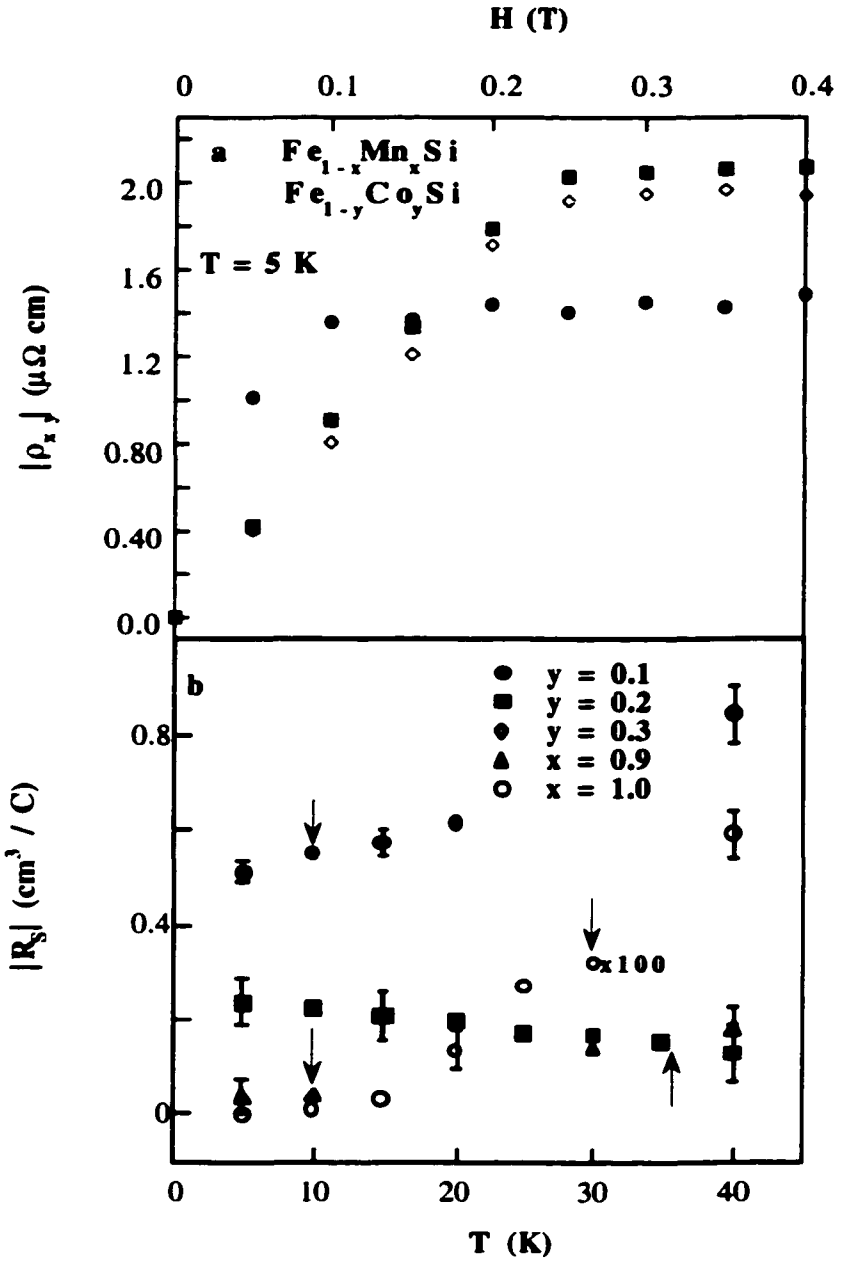

3.6. Comparison of $Fe_{1-y}Co_ySi$, $Fe_{0.1}Mn_{0.9}Si$, and MnSi. (a) Hall resistivity vs. field of $Fe_{1-y}Co_ySi$ samples at 5 K showing a linear in H of low field Hall effect (symbols the same as in (b). (b)) Anomalous Hall coefficient (R_S) vs. T (symbols as in the figure). Arrows identify transition temperature (T_C).

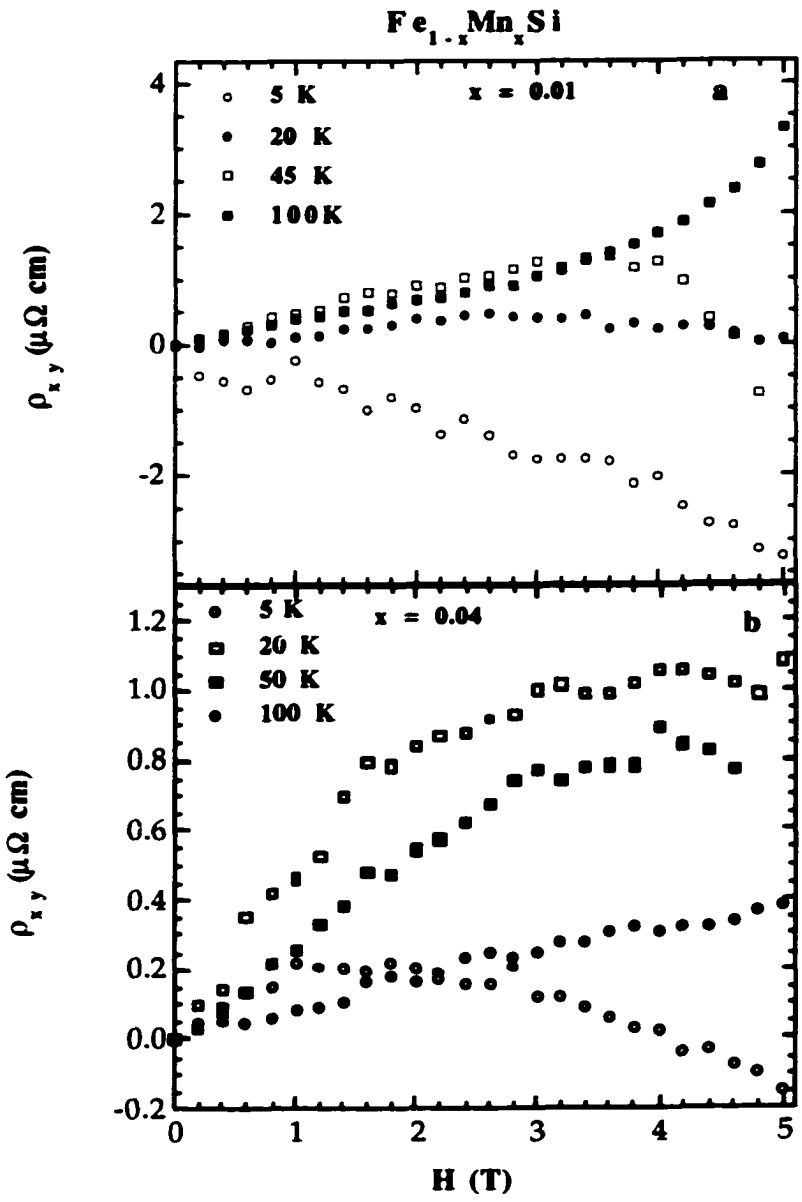

Fig. 3.7 Hall resistivity vs. magnetic field for $Fe_{1-x}Mn_xSi$ (a) $x = 0.01$ and (b) $x = 0.04$ respectively at different temperatures as labeled in the figure.

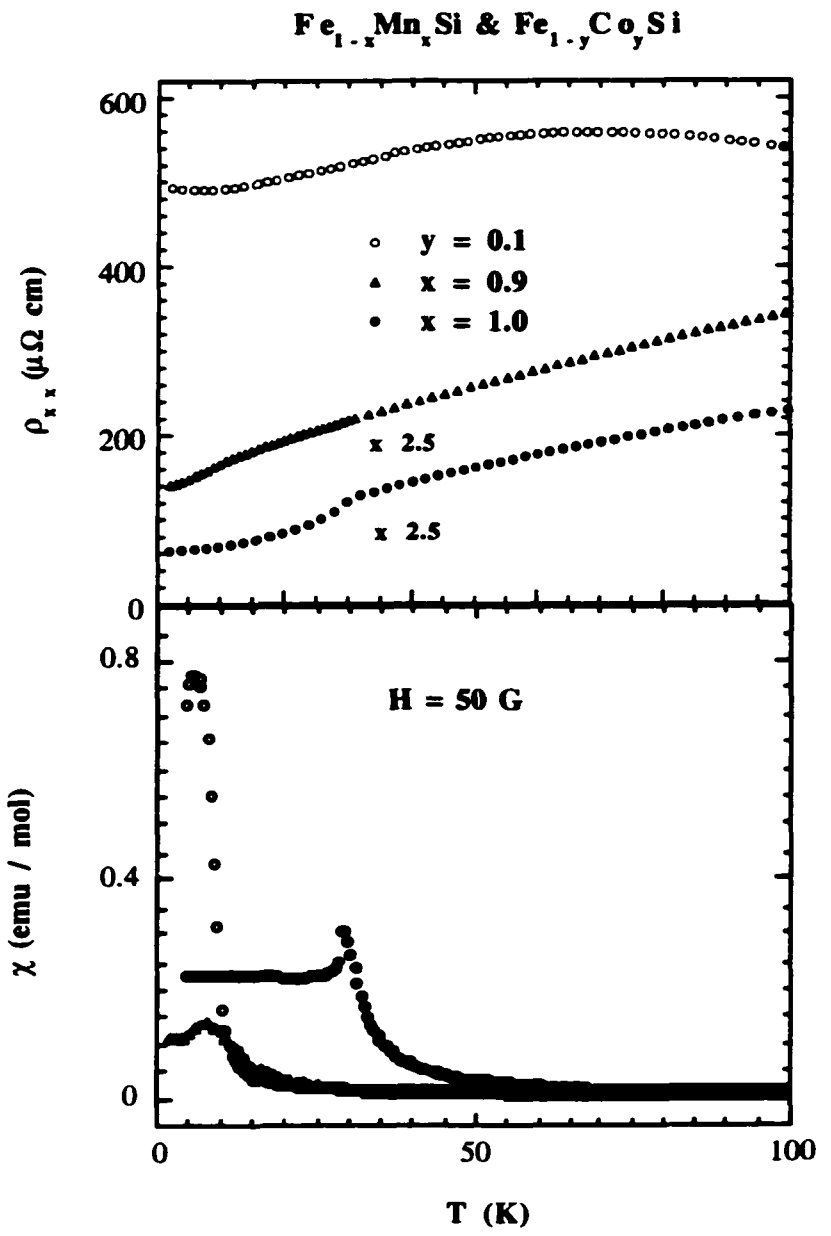

Fig. 3.8. Comparison of $Fe_{0.9}Co_{0.1}Si$, $Fe_{0.1}Mn_{0.9}Si$, and MnSi. (a) Resistivity at zero field and (b) Magnetic susceptibility at 50 G (symbols the same as (a)) vs. T (K).

points for the dilute metal alloys. It is usually assumed that in these dilute alloys the majority of the scattering at low T results from SO scattering from impurities, and in turn large R_S results from these scattering. Since R_S in $Fe_{1-y}Co_ySi$ extends this dependence to larger ρ_{xx} we conclude that nearly all scattering in $Fe_{1-y}Co_ySi$ involves SO scattering, while in MnSi the majority of scattering events do not include an asymmetric scattering.

One further difference that our $Fe_{1-y}Co_ySi$ samples have with the more common ferromagnetic systems in Fig. 3.11, lies in the T dependence of R_S. For nearly all of these materials, including MnSi and $Fe_{0.1}Mn_{0.9}Si$, R_S decrease substantially below T_C[72]. However, our $Fe_{1-y}Co_ySi$ samples show little variation of R_S below T_C (see Fig. 3.6 (b)) perhaps due to the relative T independence of ρ_{xx} (Fig. 3.8 (a)). In clean metals the scattering of carriers from magnetic fluctuations near T_C accounts for a large fraction of the scattering rate. As T is lowered these fluctuations freeze out resulting in a T^2 dependent ρ_{xx} (see Eq. 2.12). Although MnSi and $Fe_{0.1}Mn_{0.9}Si$ follow these behavior accurately, it doesn't seem to be the case in $Fe_{1-y}Co_ySi$.

3.3 Conclusions

Although our materials are not suitable for technology, our data, as well as recent investigations of $La_{1-x}Ca_xCoO_3$[83] and $La_{1-x}Sr_xMnO_3$[82], suggest that doping of anomalous insulators such as Kondo, Mott-Hubbard, and charge transfer insulators can often lead to magnetic metals with large Hall effects. Our comparison of $Fe_{1-y}Co_ySi$ and $Fe_{1-x}Mn_xSi$ reveals that simple models to predict the size of ρ_{xy} from M and ρ_{xx} are not complete, and thus a true exploration of likely materials is necessary. We hope that our data will motivate such investigations since it suggests that this anomalous Hall effect need not be strongly T dependent, can be large in materials with a few hundred $\mu\Omega$cm resistivity, and has a linear field dependence in helimagnets, or soft magnets.

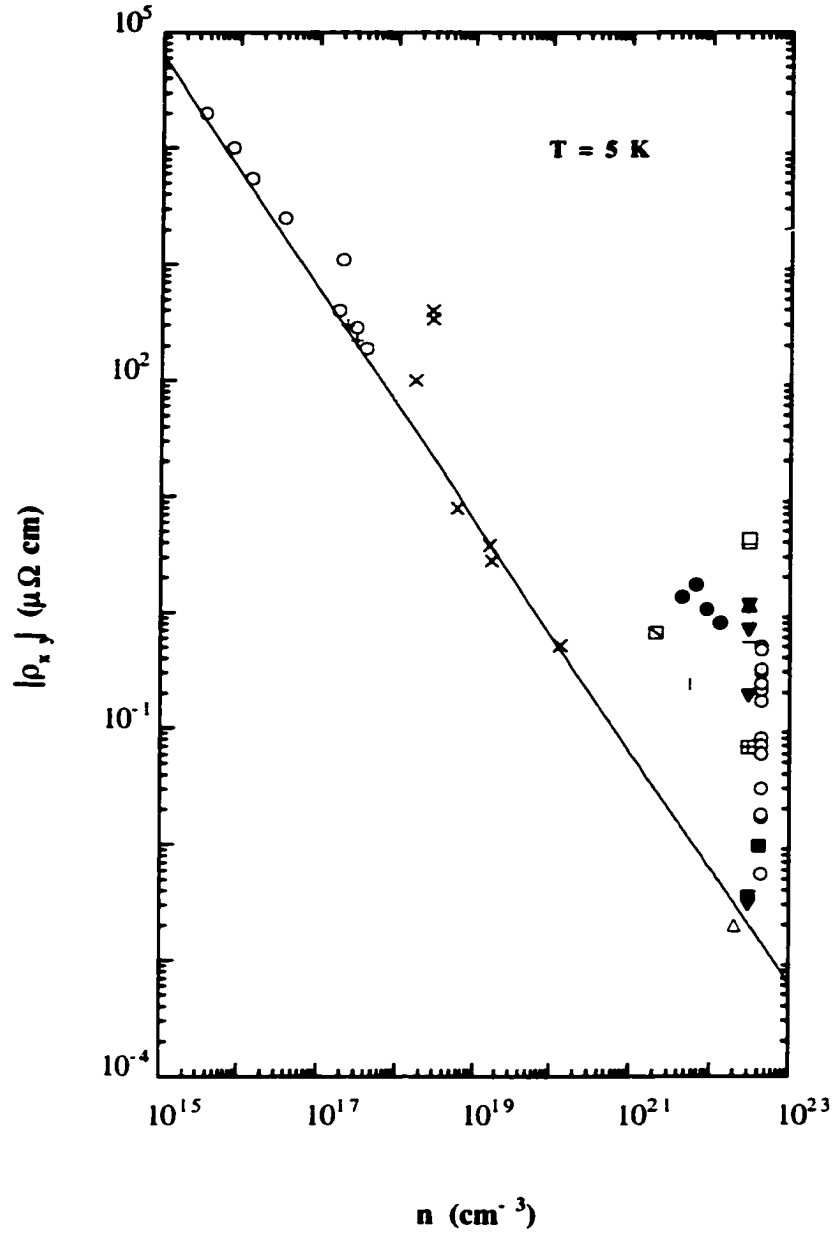

Fig. 3.9. Hall effect of paramagnetic metals, insulators, and ferromagnetic metals at 1 kG at low temperature (~ 5 K) vs carrier concentration (n) (symbols as in Fig. 3.10. Solid line represents $\rho_{xy} = H / nec$ Drude model.

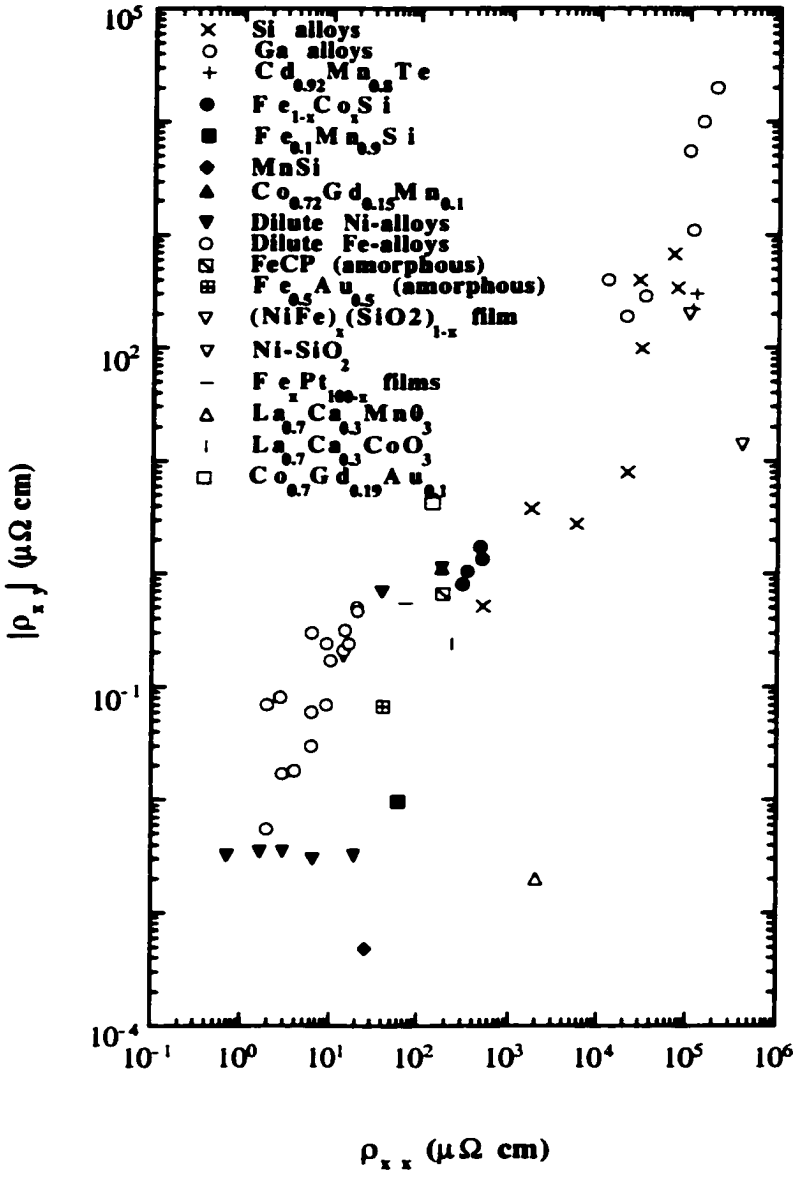

Fig. 3.10. Hall effect of paramagnetic metals , insulators, and ferromagnetic metals at 1 kG and low temperature (~ 5 K) vs resistivity (ρ_{xx}) (symbols as in the figure). References for the following: Si alloys[73], Ge alloys[74, 75], $Cd_{0.92}Mn_{0.08}Te$[76], $Co_{0.72}Gd_{0.15}Mn_{0.1}$[77], Ni alloys[71], Fe alloys[71], FeCP[78], $Fe_{0.5}Au_{0.5}$[79], $(NiFe)_x(SiO)_{1-x}$[80], Fe_xPt_{100-x}[81], $La_{0.7}Ca_{0.3}MnO_3$[82], $La_{0.7}Ca_{0.3}CoO_3$[83], $Co_{0.7}Gd_{0.19}Au_{0.1}$[77].

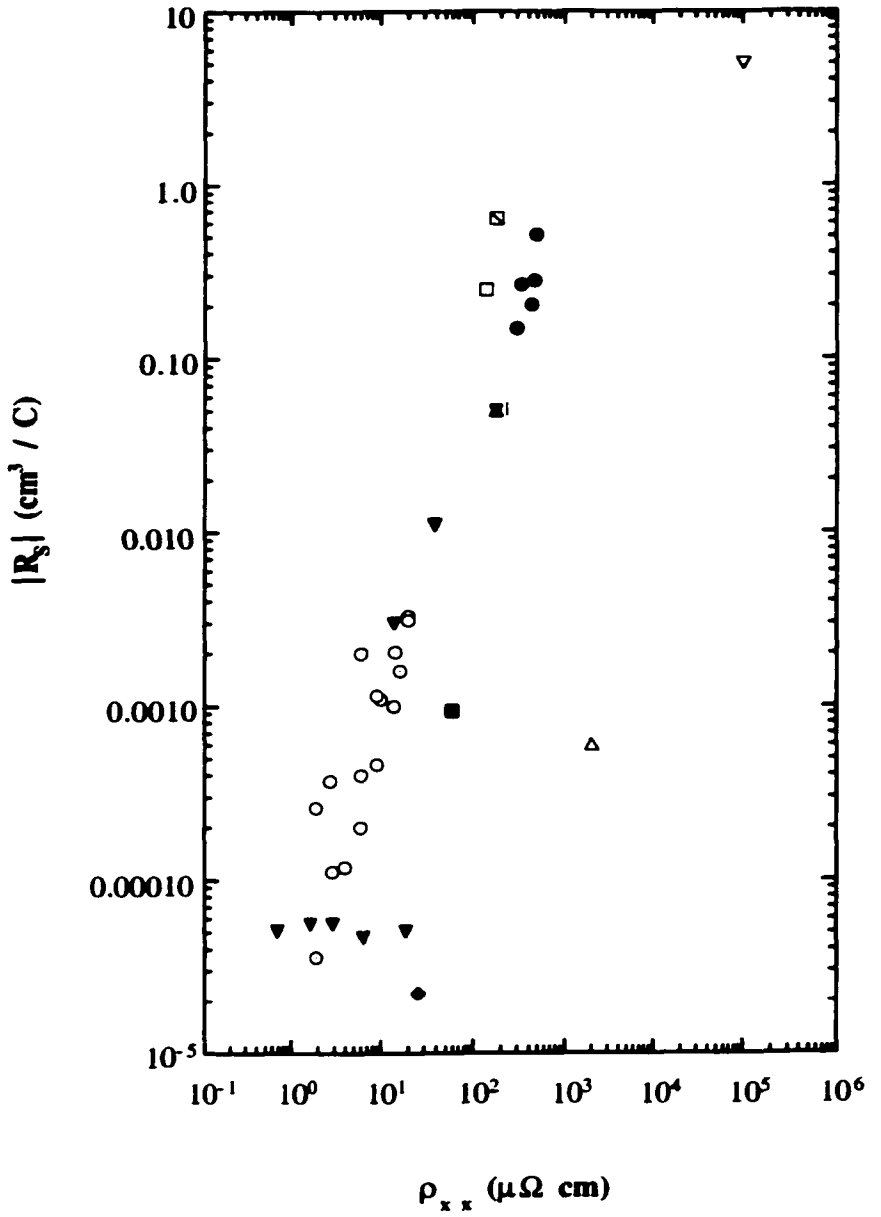

Fig. 3.11. Anomalous Hall constant (R_S) vs. resistivity (ρ_{xx}) at 5 K (symbols as in Fig. 3.10).

CHAPTER 4

$FE_{1-Y}CO_YSI$ AND MNSI: MAGNETIC AND TRANSPORT MEASUREMENTS

In this chapter we will compare the magnetic and transport properties of the helimagnetic metals MnSi and $Fe_{1-y}Co_ySi$ ($0.1 \leq y \leq 0.3$). We have discovered qualitatively different magnetotransport for the low carrier density ferromagnet produced by modest doping of FeSi by Co.

4.1 Introduction

The desire to maximize the sensitivity of read/write heads and thus the information density of magnetic storage devices has produced an intense interest in the magnetoresistance (MR) of magnetic materials. Recent discoveries include "colossal" MR of the manganites[1-3] and the enhanced MR of low carrier density ferromagnets[84]. In the low carrier density systems investigated to date as well as manganites, a key feature is that the electrical conduction is due to a different set of electrons than those responsible for magnetism. To the extent that an external field reduces the disorder among the local spins, the scattering will be reduced, resulting in a negative MR. The MR is especially pronounced when the ordering tendency of an external field is high, such as near a para-ferromagnetic (Curie) transition and can be further boosted by electron-phonon coupling. In this chapter we describe a new mechanism for MR which obtains in low carrier density magnets where magnetism as well as the electrical conduction are due to the same electrons. The MR is very different from that seen when conduction electrons and ordered moments can be treated separately - it is positive and only weakly temperature-dependent below the Curie point.

The oxides of manganese that are famous for high MR are, like the high-temperature superconductors, derived from chemical doping of insulators which are also magnetically ordered. Thus, the local moments which order in the doped materials already

manifest themselves in the insulator, with the result that to first order, metallicity and magnetism are independent properties[84]. To search for a different types of MR, one needs to consider compounds where the insulating parent is non-magnetic, a requirement which is met by many ubiquitous semiconductors such as Si and Ge. In addition though, the parent should have a strong electron-electron interactions so that magnetism appears readily upon doping. Insulators which satisfy this criterion are referred to as strongly correlated, or Kondo insulators of which FeSi is one of the simplest[26].

4.2 Susceptibility and Magnetization Measurements

We plot in Fig. 4.1 magnetic susceptibility at 0.005 T as a function of T / T_C for several $Fe_{1-y}Co_ySi$ samples noted in the figure. These are compared to the classic helimagnetic compounds MnSi and $Fe_{0.1}Mn_{0.9}Si$ samples. For $x < 0.1$ our samples are non-magnetic. These data all show a peak at about T_C associated with the magnetic transition [40]. Above T_C the data obey a standard Curie-Weiss law $(C / T - \Theta_W)$ with $\Theta_W > 0$. We show in Fig. 4.2 the temperature dependence of magnetization at $H = 1$ T for $Fe_{1-y}Co_ySi$, MnSi, and $Fe_{0.1}Mn_{0.9}Si$. The solid lines through the data are the best fits to Moriya's theory of itinerant magnetism (see Eq. 2.26). The agreement shows that this standard theory is well observed below T_C.

The field dependence of magnetization M is shown in Figs. 4.3, 4.4, 4.5, and 4.6 for MnSi, $Fe_{0.1}Mn_{0.9}Si$, $Fe_{0.9}Co_{0.1}Si$ (field up to 32T), and $Fe_{0.85}Co_{0.15}Si$ (showing both negative and positive field and also normalized per Co concentration) respectively. The form of $M(H)$ is standard for helimagnetic (or ferromagnetic) materials. The saturated value of M at low T and high H gives the value of the spontaneous magnetization (P_S) that develops below T_C. It is a standard practice to compare this value to the moment determined from the Curie-Weiss like behavior of the magnetic susceptibility above T_C (P_C) $(C = N_0 \mu_B^2 P_C(P_C + 2) / 3 k_B)$[85]. The ratio of these two quantities (P_C / P_S) for a local moment magnet such as Gd or EuO, is close to 1, while for itinerant magnets this ratio diverges as $P_S \rightarrow 0$ or $T_C \rightarrow 0$[34]. Here we find values of P_C / P_S between 4 and 9

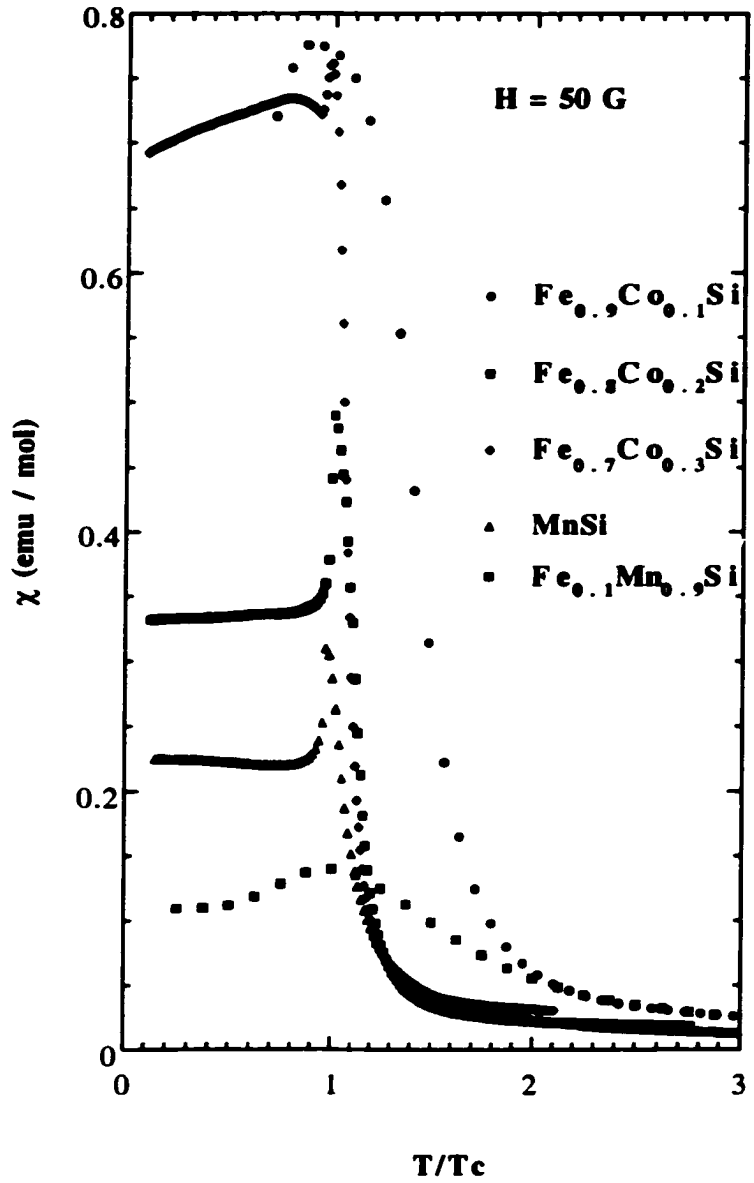

Fig. 4.1 Magnetic susceptibility at H = 0.005 T vs. T / T_C for several samples noted in the figure.

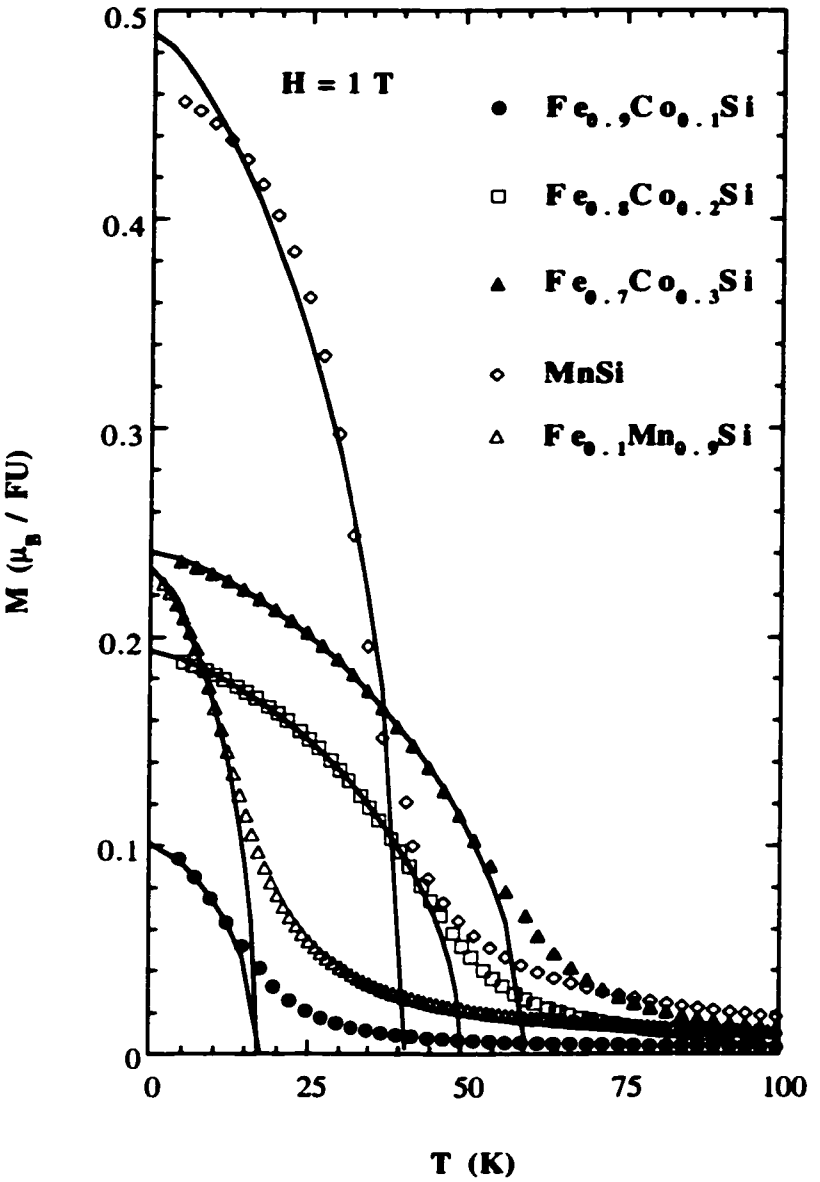

Fig. 4.2 Magnetization vs. temperature for the samples noted in the figure. Solid lines are the best fits to Eq. 2.26.

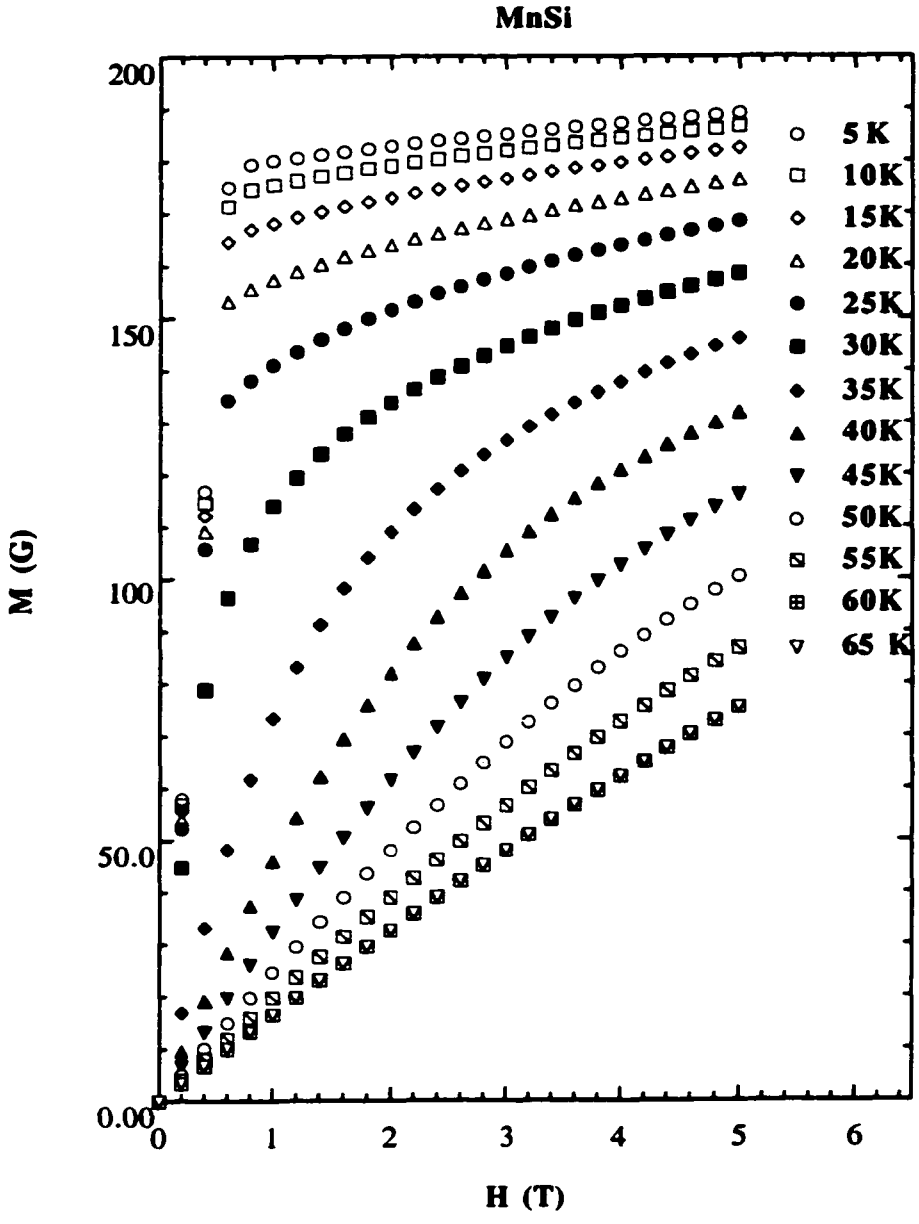

Fig. 4.3 Magnetic field dependence of magnetization for MnSi at the temperatures noted in the figure.

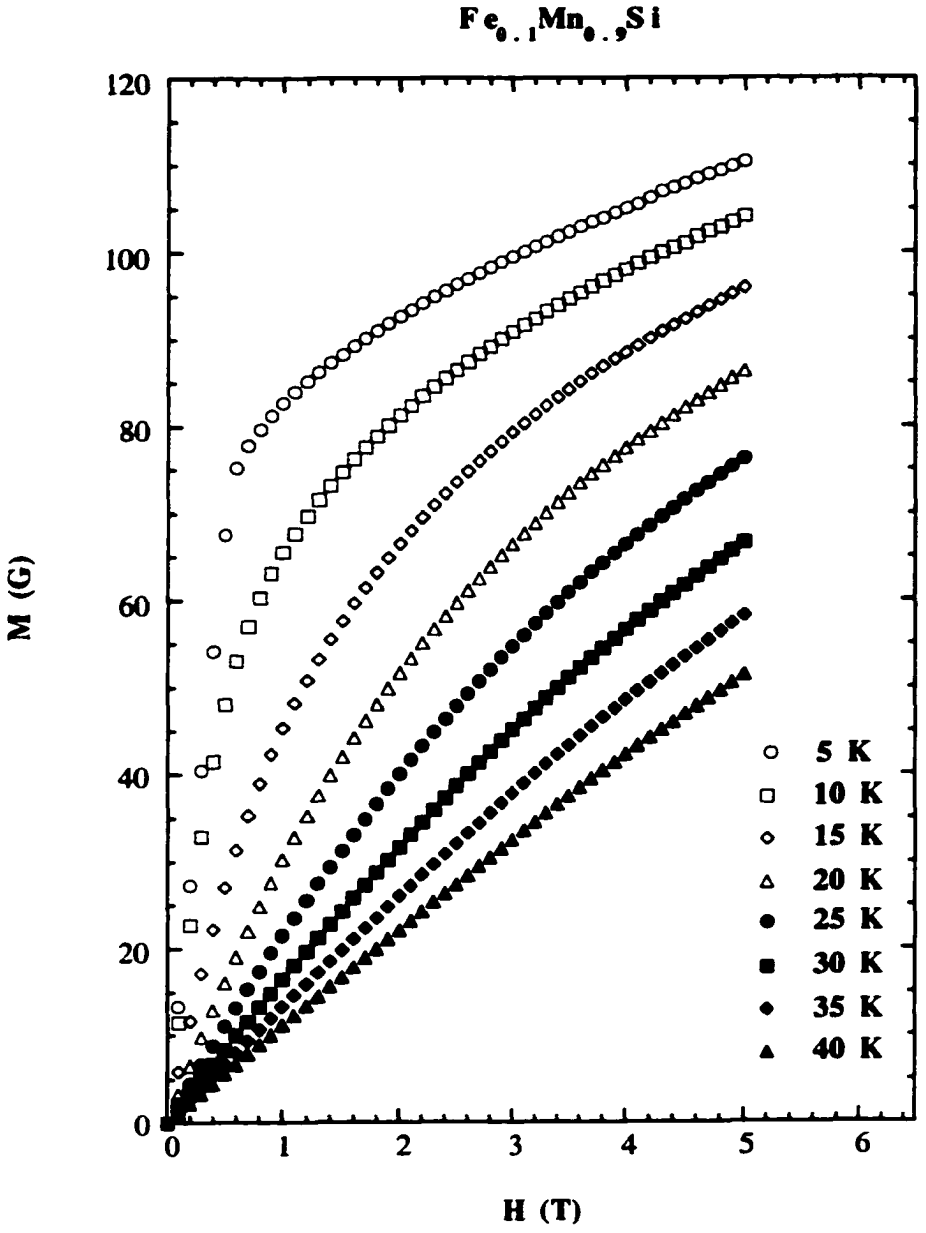

Fig. 4.4 Magnetic field dependence of magnetization for $Fe_{0.1}Mn_{0.9}Si$ at the temperatures noted in the figure.

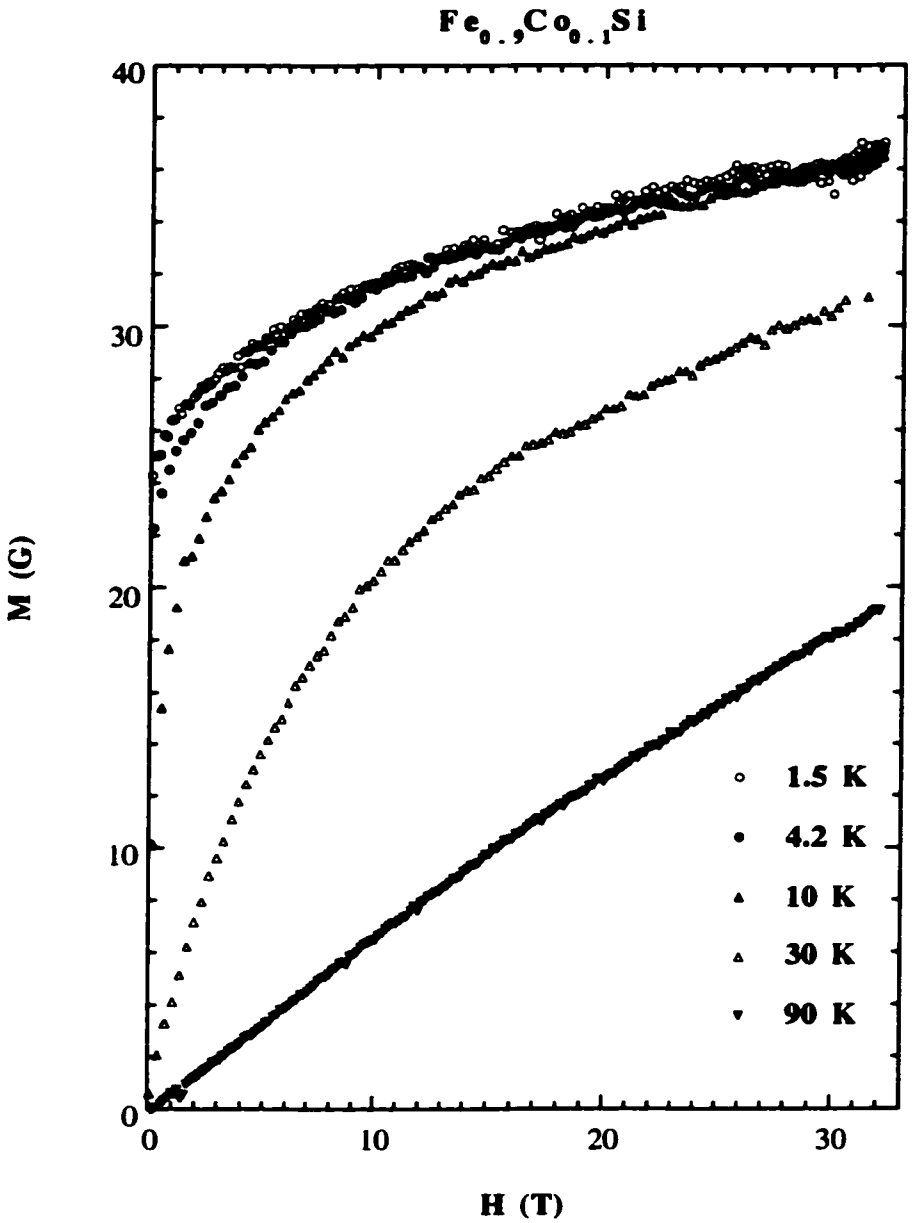

Fig. 4.5 Magnetic field dependence of magnetization for $Fe_{0.9}Co_{0.1}Si$ at the temperatures noted in the figure.

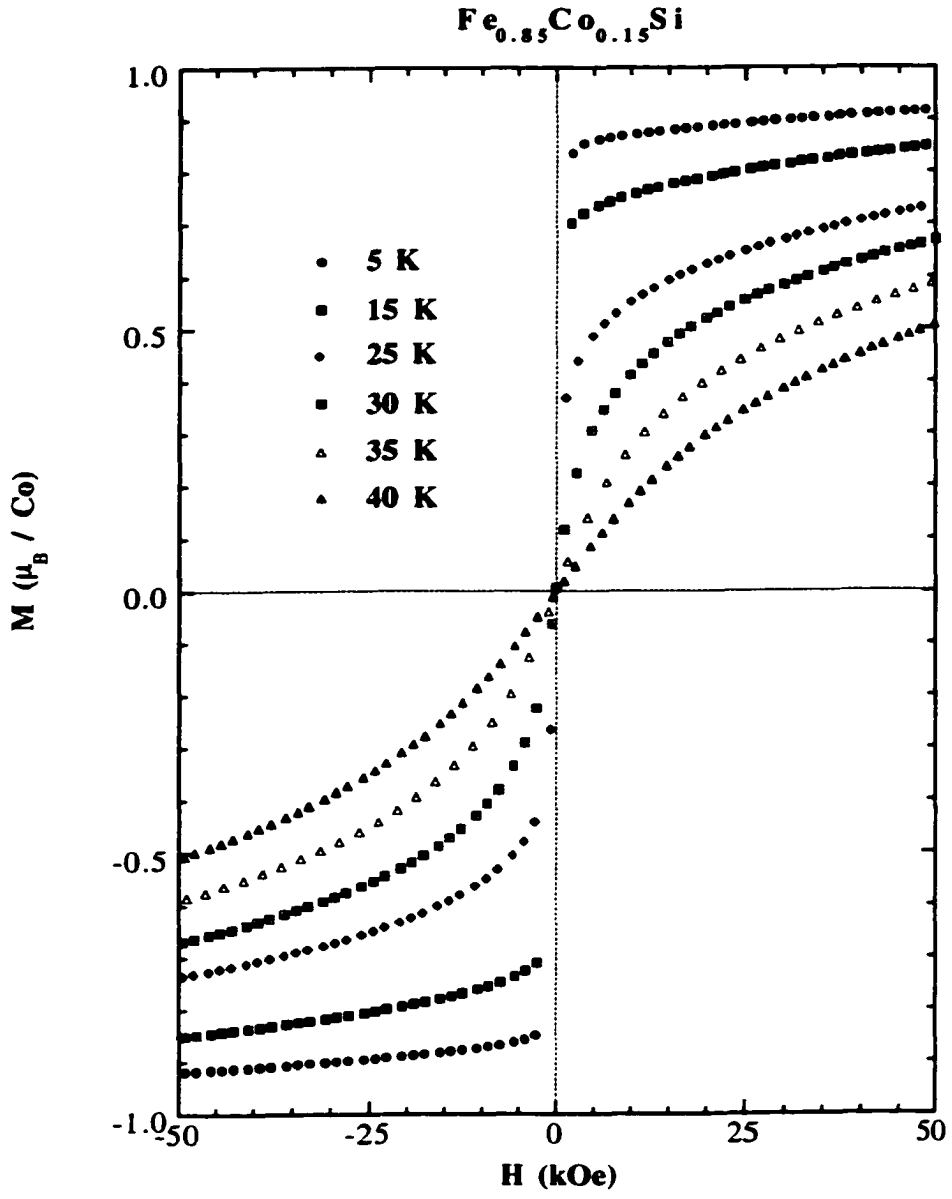

Fig. 4.6 Magnetic field dependence of magnetization for $Fe_{0.85}Co_{0.15}Si$ at the temperatures noted in the figure.

(see Fig. 4.8 (a)) putting these materials well into the itinerant regime[37, 68, 86]. Being itinerant, we can establish the degree of carrier spin polarization simply by comparing P_S to the expected value when all of the carriers are polarized. The value of P_S for our samples shown in Fig. 4.8 (b) and apparent in Fig. 4.6 is consistent with at least 90% of a spin 1/2 per itinerant carrier for the Co samples, while for MnSi and $Fe_{0.1}Mn_{0.9}Si$ it is less than 50%. In Fig. 4.7 we show the low field M revealing a hysteretic form as expected for helimagnetic materials [36]. For fields above 2 kG the spins are aligned in a single domain FM state. The picture that emerges is that while MnSi and $Fe_{0.1}Mn_{0.9}Si$ have magnetization that are common to weak itinerant ferromagnets, $Fe_{1-y}Co_ySi$ is a weak itinerant ferromagnet with a small density of carriers that are completely, or nearly completely spin polarized at low T.

4.3 Resistivity and Magnetoresistance Measurements

The standard T dependence of ρ for weak itinerant ferromagnetic metals is displayed by MnSi (see Fig. 4.9 (a)), and $Fe_{0.1}Mn_{0.9}Si$ (see Fig. 4.10 (a)). This is typified by a peak in zero field $d\rho/dT$ at T_C due to carrier scattering from spin fluctuations (see Figs. 4.9 and 4.11 for MnSi)[38, 87]. The solid line is the best fit to Eqs. 2.14 and 2.15 which reproduce the data quite well with $\eta = \eta' = 0.1$ and $A/A' = 0.17$. In Fig. 4.12 we plot our MnSi data below T_C as a function of T^2 to compare with the standard behavior of itinerant magnets. The solid lines through the data are the best fits to Eq. 2.12 with $B(H)$ ~ 0.022, 0.021, 0.017, and 0.015 $\mu\Omega$ cm K^{-2} for H = 0, 1, 3, and 5 T respectively and ρ_0 ~ 25 $\mu\Omega$ cm. The scattering is suppressed by the application of external magnetic field resulting in the MR shown in Fig. 4.9 (b) for MnSi and Fig. 4.10 (b) for $Fe_{0.1}Mn_{0.9}Si$[88]. Here a strong negative MR (over 20% for MnSi and over 11% for $Fe_{0.1}Mn_{0.9}Si$) is displayed in proximity to T_C. The field dependence of MR for MnSi is shown in Fig. 4.13 where again we see that the largest MR occurs in proximity to T_C.

None of this typical behavior is demonstrated by our $Fe_{1-y}Co_ySi$ samples. The resistivity in zero field is displayed in Figs. 4.14, 4.15 (a), 4.16 (a) for our different

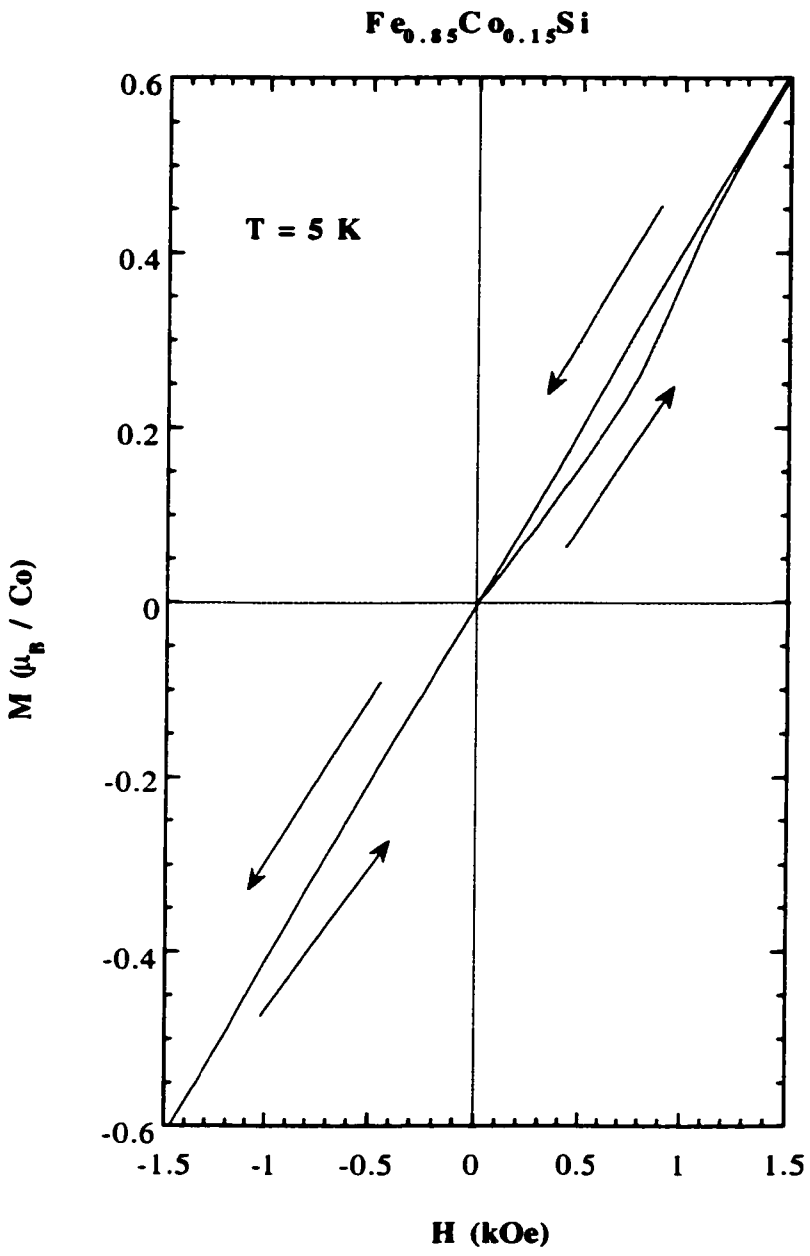

Fig. 4.7 Low field magnetization hysterisis plot for $Fe_{0.85}Co_{0.15}Si$.

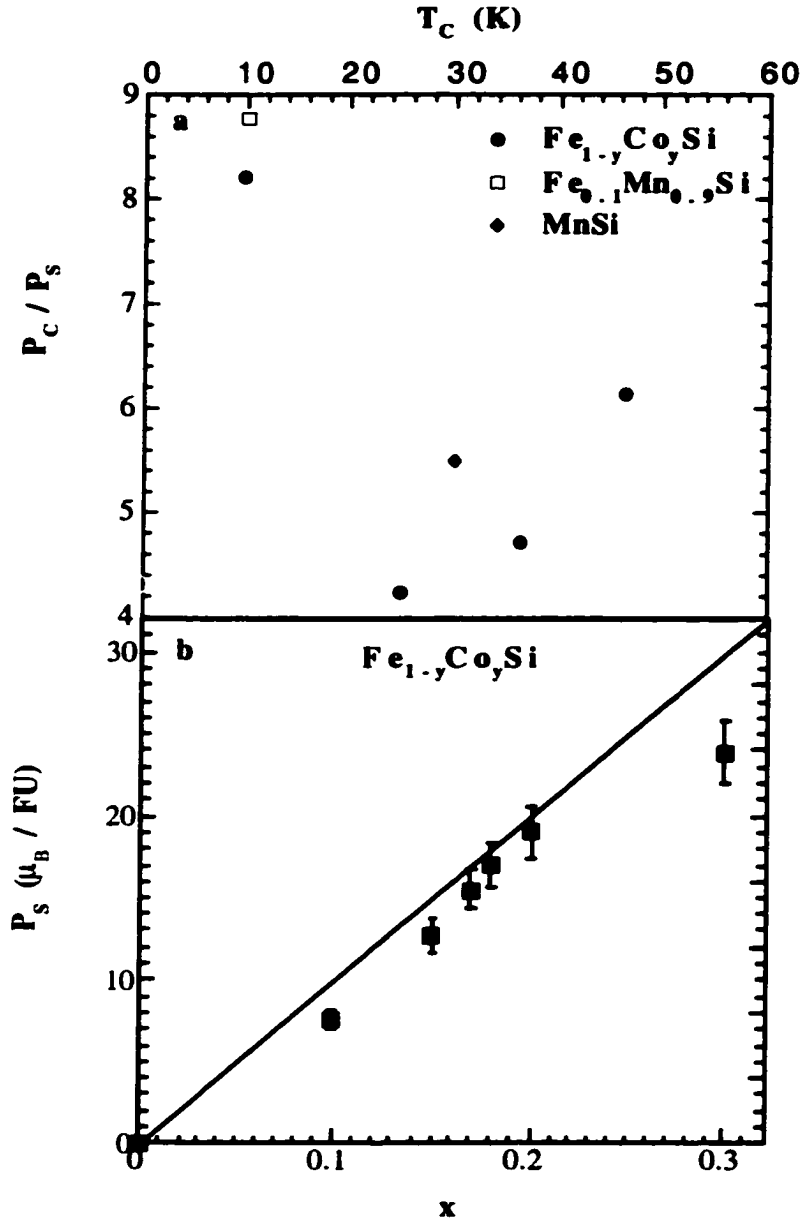

Fig. 4.8 (a) The ratio of spontaneous magnetization *(P_S)* to the magnetic moment *(P_C)* vs. temperature for $Fe_{1-y}Co_ySi$ (y = 0.1, 0.15, 0.2, and 0.3), $Fe_{0.1}Mn_{0.9}Si$, and MnSi. (b) The spontaneous magnetization *(P_S)* vs. nominal Co concentration. The solid line represent complete spin polarization.

samples noted in the figures. ρ of our $Fe_{1-y}Co_ySi$ samples are order of magnitude larger than that of our MnSi sample and shows a strong upturn as T is lowered below T_C[35]. Furthermore, magnetic field does not suppress this effect, but in fact enhances it. The single crystal data ($y = 0.2$) demonstrates that the MR is not the result of grain boundary scattering and that the effect is enhanced as the sample disorder is increased or the carrier density is decreased (see Fig. 4.19 (a)). The MR shown in Figs. 4.15 (b), 4.16 (b) and 4.17 can be as large as 10% near T_C and falls off gradually below this temperature. The effect grows with proximity to the MI transition with our 10% Co sample (see Fig. 4.17 (b)) having the largest MR (10%) at 4 K in 5 T.

The variation of the MR with field is shown in Fig. 4.18 where both the transverse and longitudinal MR are presented for $y = 0$. 15 polycrystalline sample and Fig. 4.19 for the $y = 0.1$, 0.2, and 0.3 samples for the fields up to 32 T. The data displayed in Fig. 4.18 shows that at low fields and low T the longitudinal MR is negative, most likely due to the anomalous MR common to ferromagnets[42]. This MR results from strong spin-orbit coupling in much the same way as the anomalous Hall effect and is dependent on the orientation of M and J (the current density). After the subtraction of the low field anisotropic MR there are only slight differences between the transverse and longitudinal MR. Thus, we conclude that there is a little contamination of our data from an ordinary Lorentz MR which is anisotropic and depend on the orientation of J and B. The symmetry of our MR data about zero field shows that there is little contamination from the Hall effect.

Our $Fe_{1-y}Co_ySi$ samples have a large positive MR that is not associated with an orbital (Lorentz) MR nor with the scattering from spin fluctuations as in MnSi. This leaves coupling to the bulk electron spins as the most likely cause of the anomalous MR. Fig. 4.20 (a) and (b), and Fig. 4.21 give crucial hints about the microscopic origin of our observations. First σ is T and H dependent down to the lowest temperatures measured (200 mK). Furthermore, σ for $H = 0$ is well described by a $\sqrt{T}$ dependence which is a

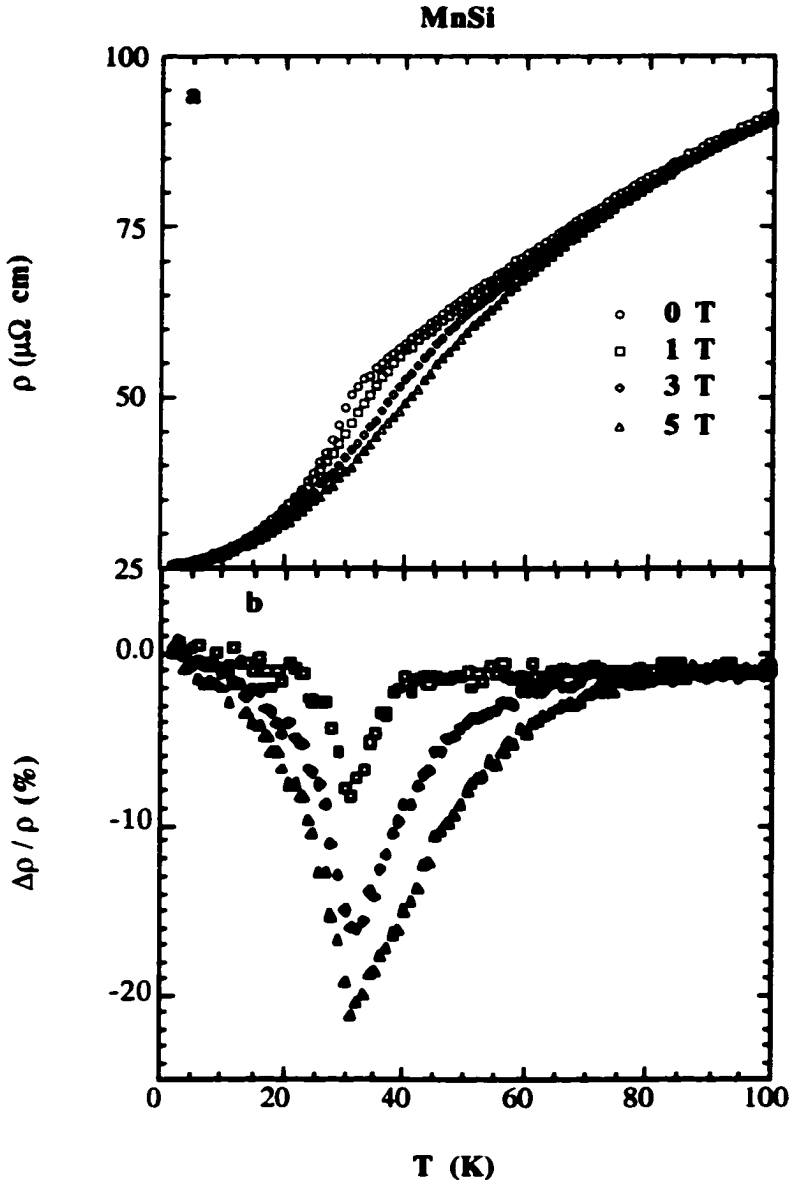

Fig. 4.9 (a) Temperature dependence of resistivity for MnSi at various fields noted in the figure. (b) Temperature dependence of magnetoresistivity $\Delta\rho / \rho$ (%) = ($\rho(T,H)$ - $\rho(T,0)$) / $\rho(T,0)$ for MnSi at the same fields (symbols are the same as in (a)).

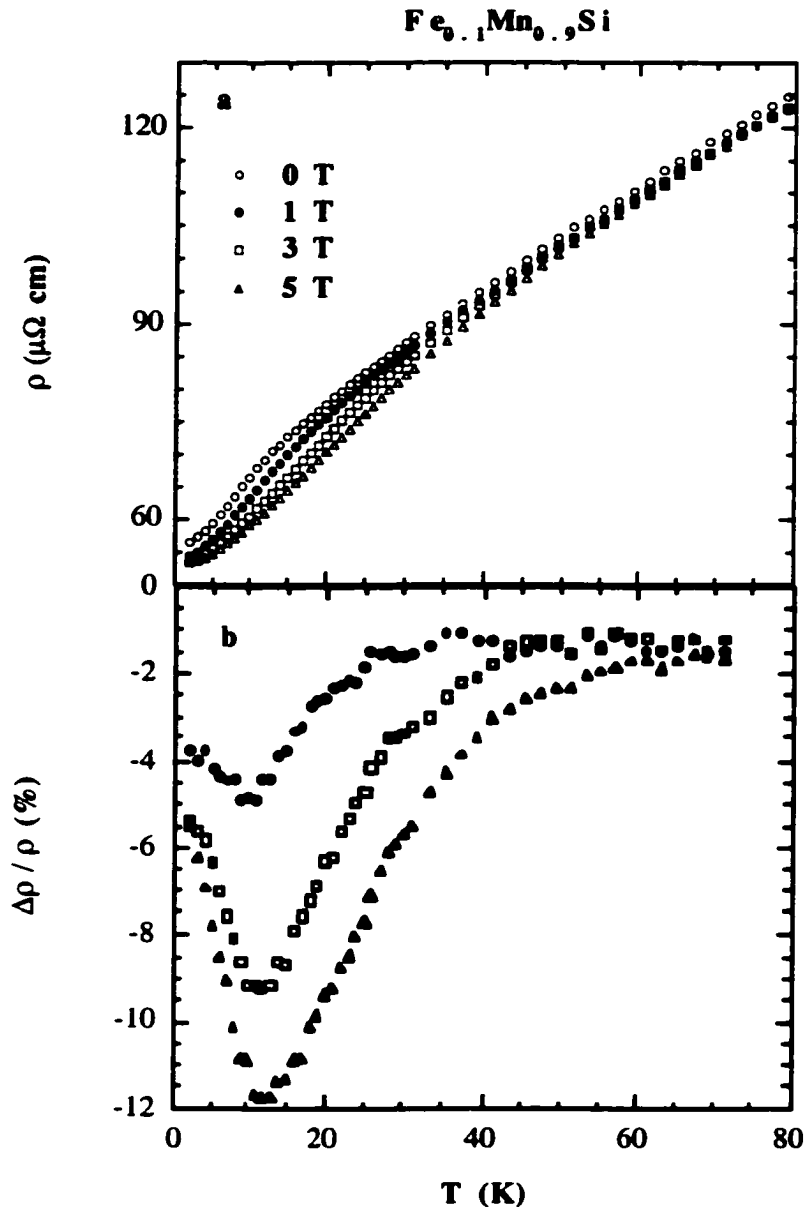

Fig. 4.10 Temperature dependence of resistivity for $Fe_{0.1}Mn_{0.9}Si$ at the fields noted in the figure. (b) Temperature dependence of magnetoresistivity for $Fe_{0.1}Mn_{0.9}Si$ at the same fields (symbols are the same as in (a)).

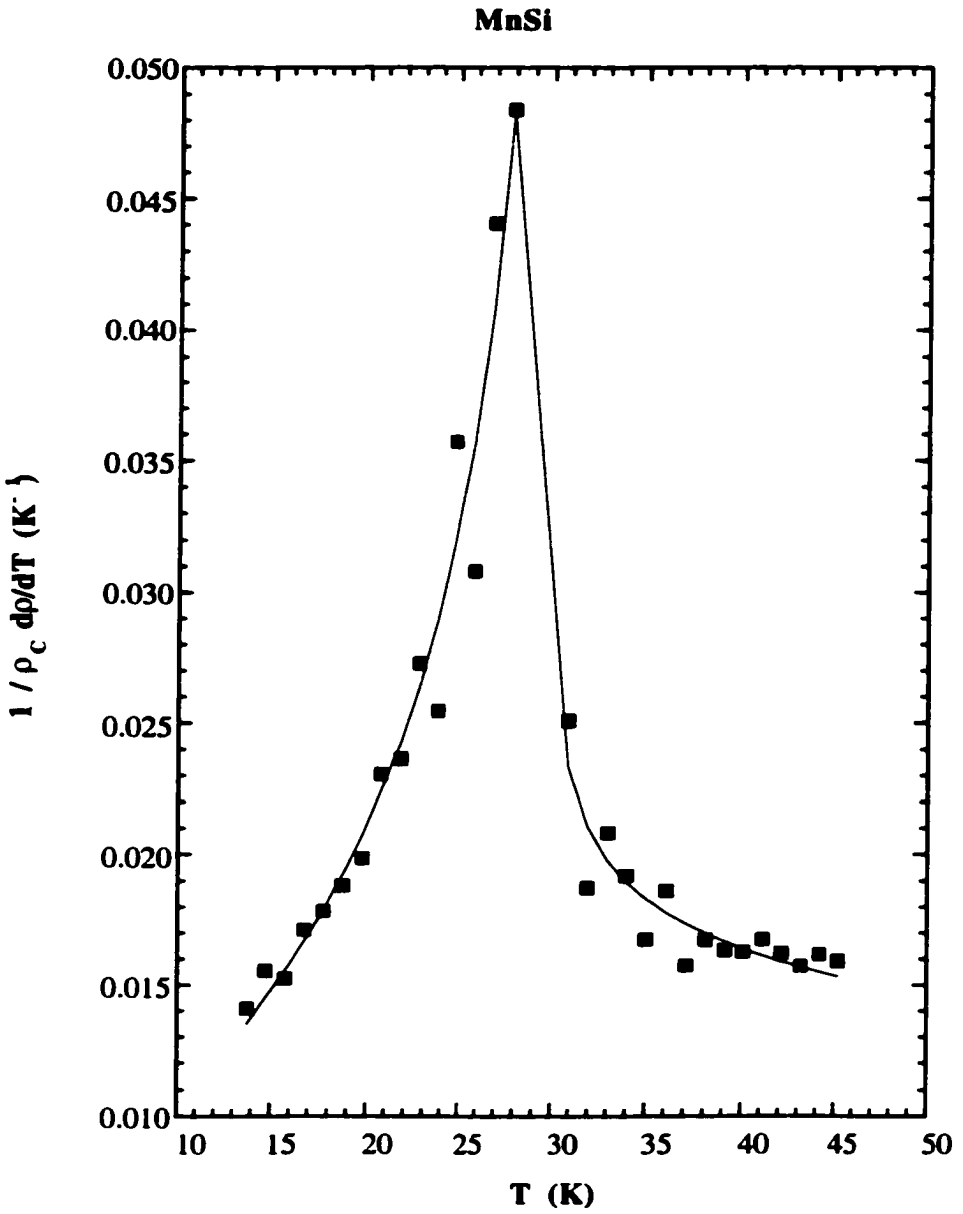

Fig. 4.11 Derivative of resistivity vs. temperature for MnSi. Solid line is the best fit to Eqs. 2.14 and 2.15.

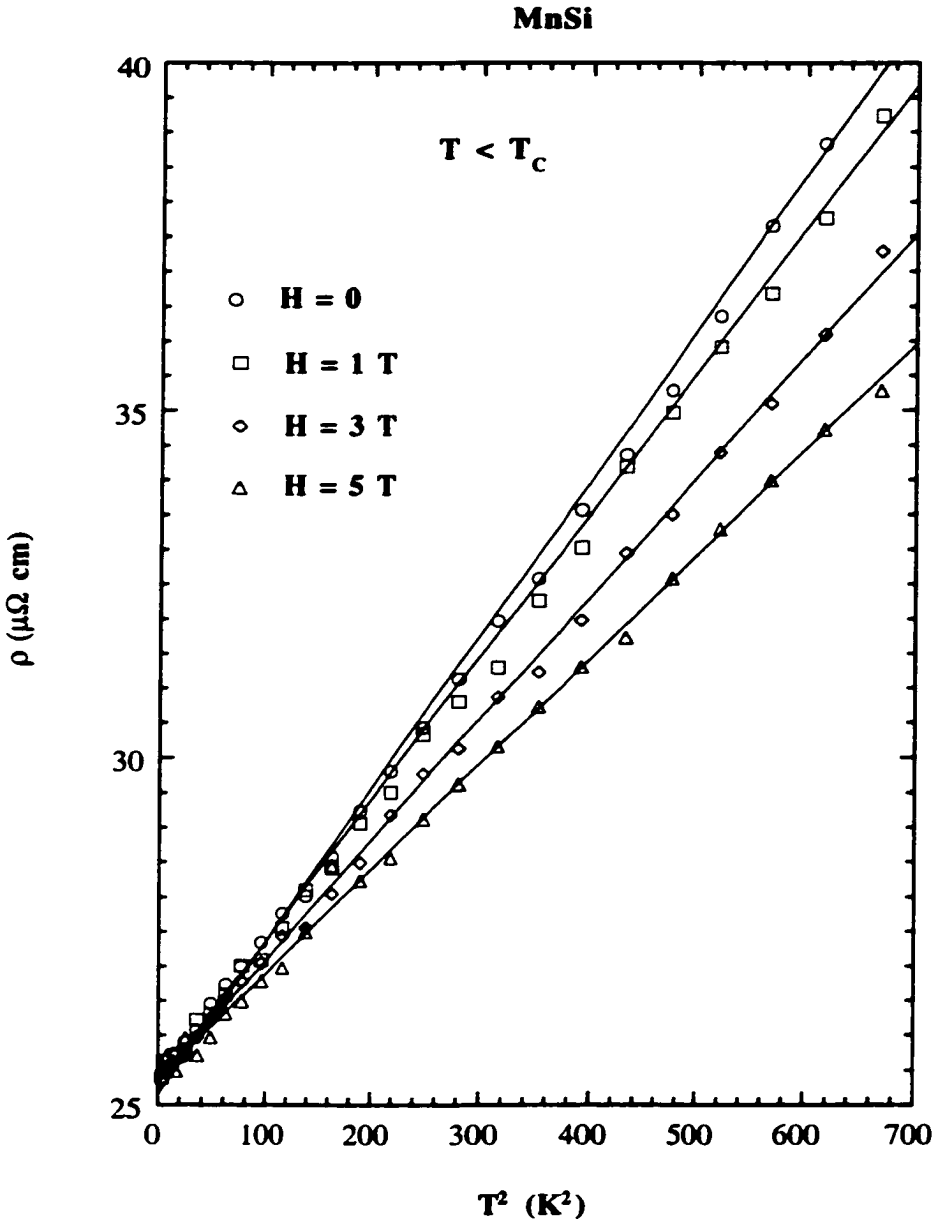

Fig. 4.12 Temperature squared dependence of resistivity for MnSi ($T < T_C$) at fields noted in the figure. The solid lines are the best fits to Eq. 2.12.

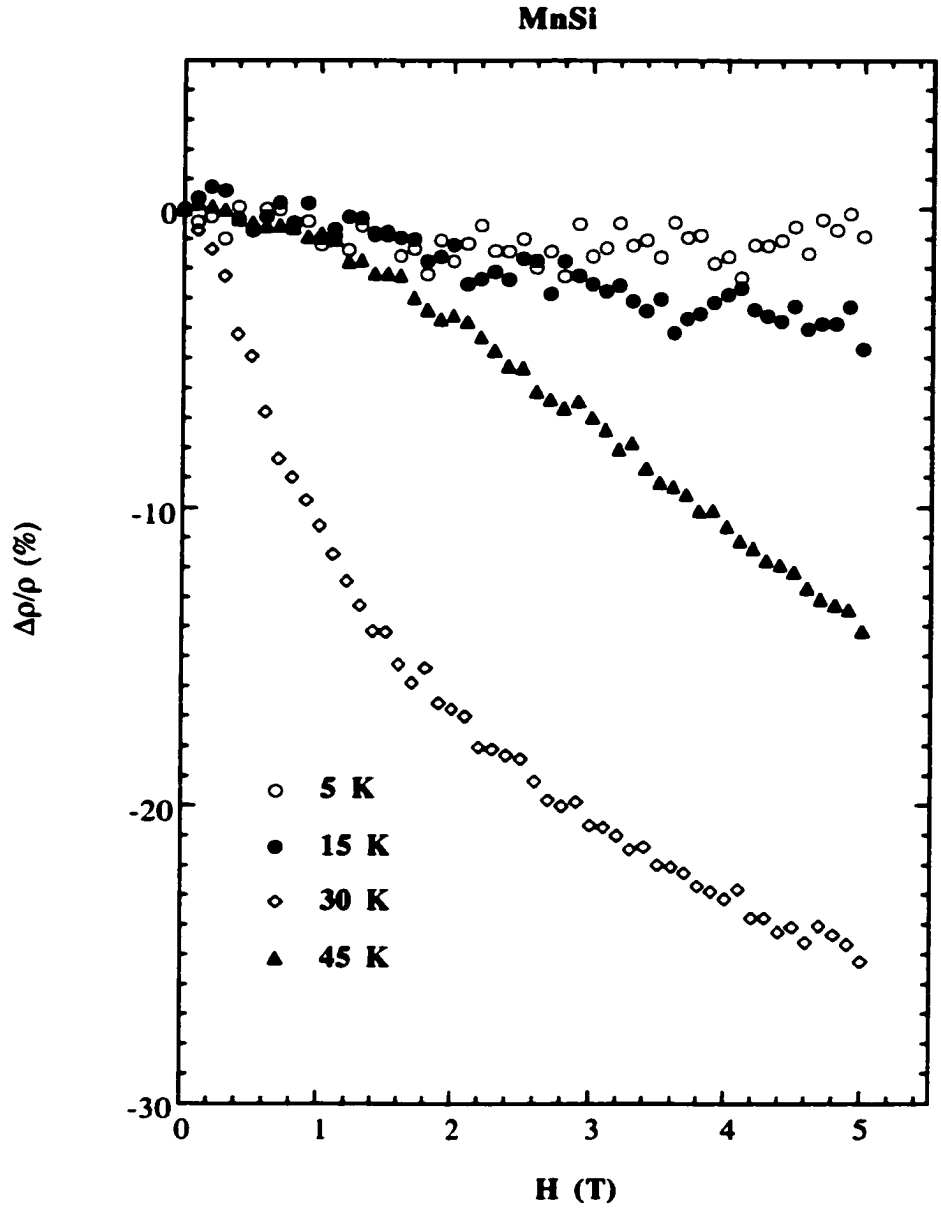

Fig. 4.13 Magnetic field dependence of the magnetoresistivity at temperatures noted in the Figure.

common form for disordered conductors (see Fig. 4.21), while for large H, $\sigma(H,T)$ approaches a $\sqrt{H}$ asymptote (see Fig. 4.20 (b)).

In classic paramagnetic materials , theory has predicted and exhaustive experiments have shown that near the MI transition ($k_F\ell \sim 1$) the Coulomb interactions between carriers are enhanced by the diffusive nature of the transport (e-e interactions)[11, 59, 60, 64, 89]. The enhancement results from the finite probability for two carriers to interact more than once within a phase-breaking scattering time[60]. As such, the scattering amplitudes interfere coherently leading to an increased Coulomb coupling and a square-root singularity in the electronic density of states (DOS) at the Fermi energy. The resulting $\sigma(H,T)$, which measures the energy dependent DOS either thermally or via the Zeeman effect, has square-root T and H dependences (see Eq. 2.19)[59, 60].

Our previous experiments on $FeSi_{1-z}Al_z$ have clearly demonstrated that this e-e interaction dominates the low T transport[32], and that the associated parameters are reasonable. For comparison we have included in Fig. 4.20 (a) and (b) our data for $FeSi_{0.95}Al_{0.05}$ and $Fe_{0.92}Mn_{0.08}Si$ which have similar n and σ, but remain paramagnetic at low T. We can see that the T dependence of these samples is similar in form. Indeed, for H = 9 T, a field chosen to be well above that required to saturate M up to high temperatures in $Fe_{1-y}Co_ySi$, the prefactors of the $\sqrt{T}$ term are actually within 30% of each other for the very different dopants. The field dependences are also similar in form, approaching asymptotes proportional to $\sqrt{H}$, although the amplitudes of the asymptotes are somewhat more diverse, but still remain within factors of three of each other for the different dopants. Given the similarities between the data for paramagnetic Al- and Mn-doped FeSi and ferromagnetic $Fe_{1-y}Co_ySi$, and because parameters found in the detailed comparison between theory and experiment for $FeSi_{1-z}Al_z$ are reasonable, we can attribute the low temperature magnetotransport in $Fe_{1-y}Co_ySi$ to electron-electron interactions in a disordered system. Because $Fe_{1-y}Co_ySi$ is, to our knowledge, the first ordered FM for which $\sqrt{T}$ and $\sqrt{H}$ terms are present, no theory is presently available for ferromagnets.

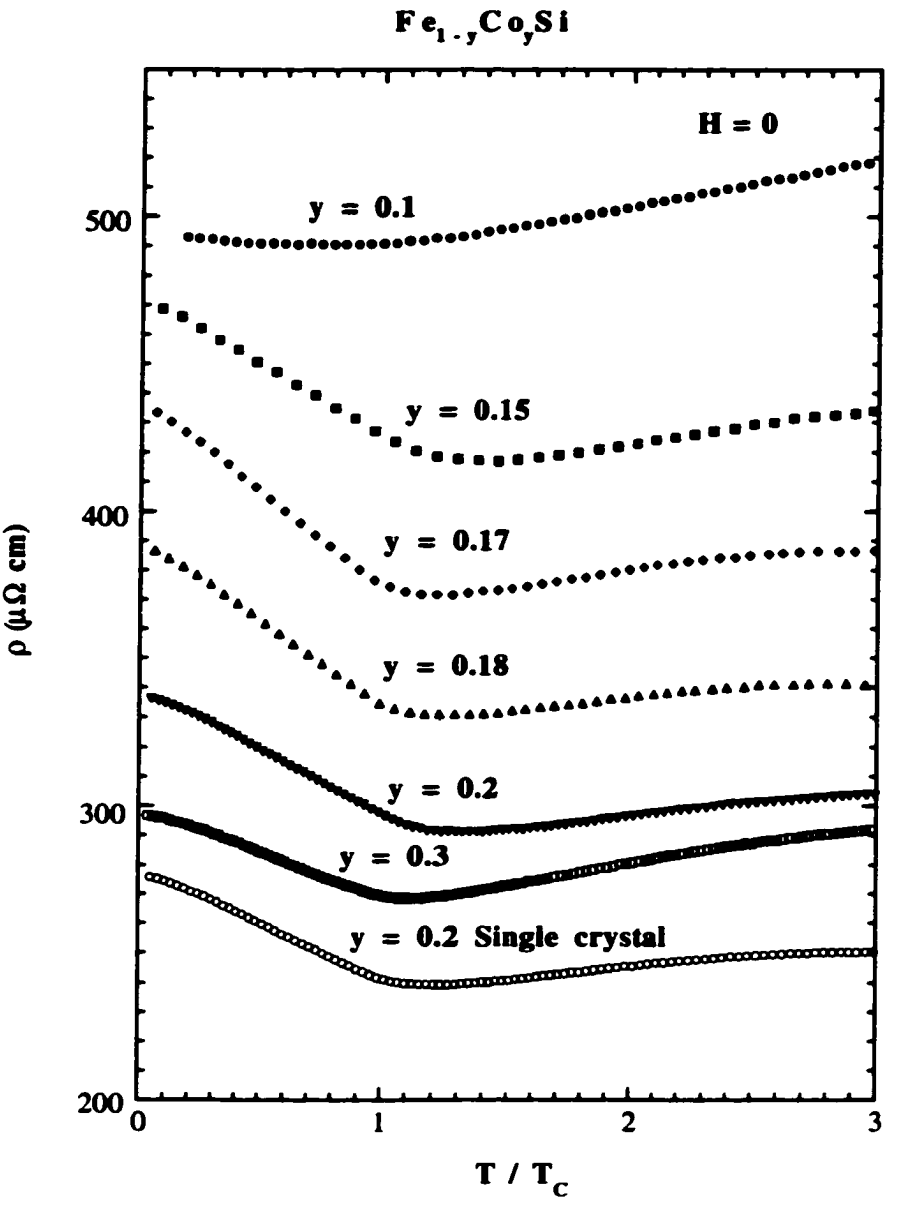

Fig. 4.14 Zero field resistivity vs. T / T_C for the $Fe_{1-y}Co_ySi$ samples noted in the figure.

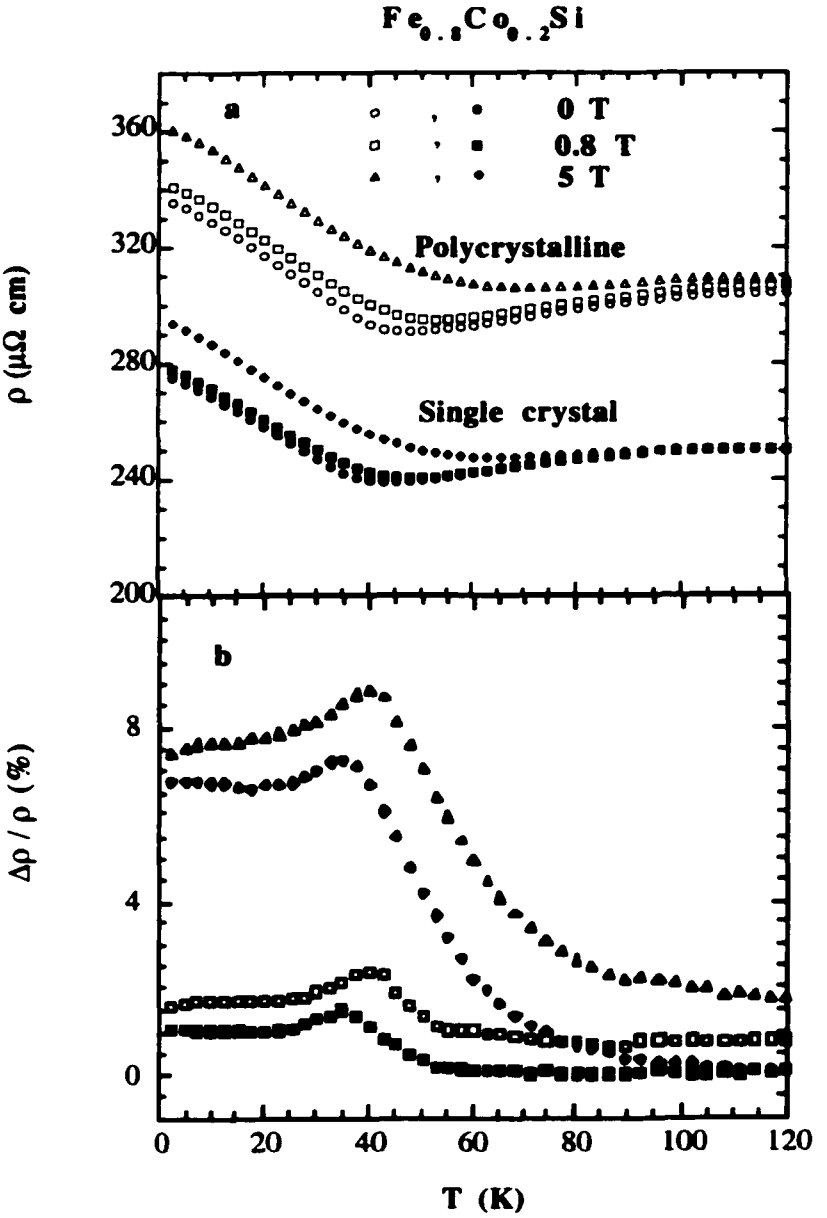

Fig. 4.15 $Fe_{0.8}Co_{0.2}Si$ (a) resistivity, and (b) magnetoresistivity vs. temperature (symbols in (a) are the same as in (b)).

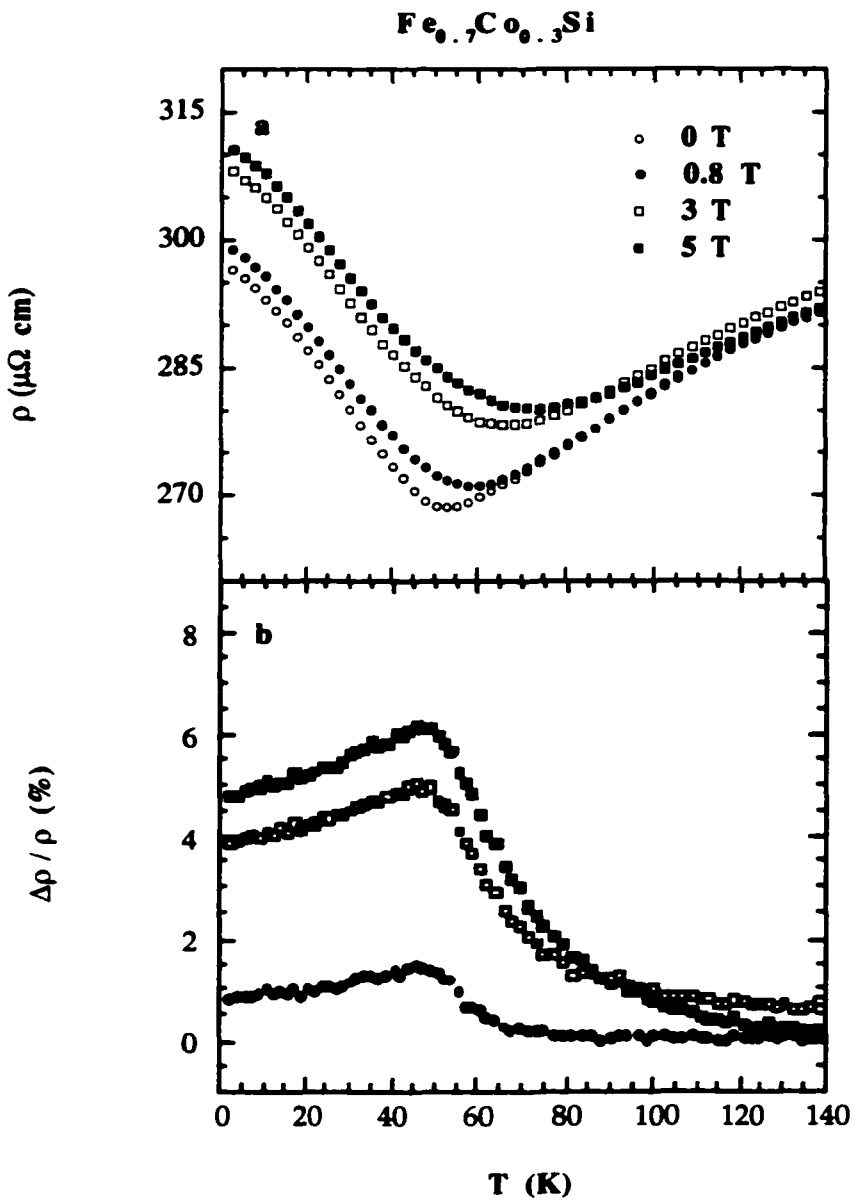

Fig. 4.16 $Fe_{0.7}Co_{0.3}Si$ (a) resistivity, and (b) magnetoresistance vs. temperature (symbols in (a) are the same as in (b)).

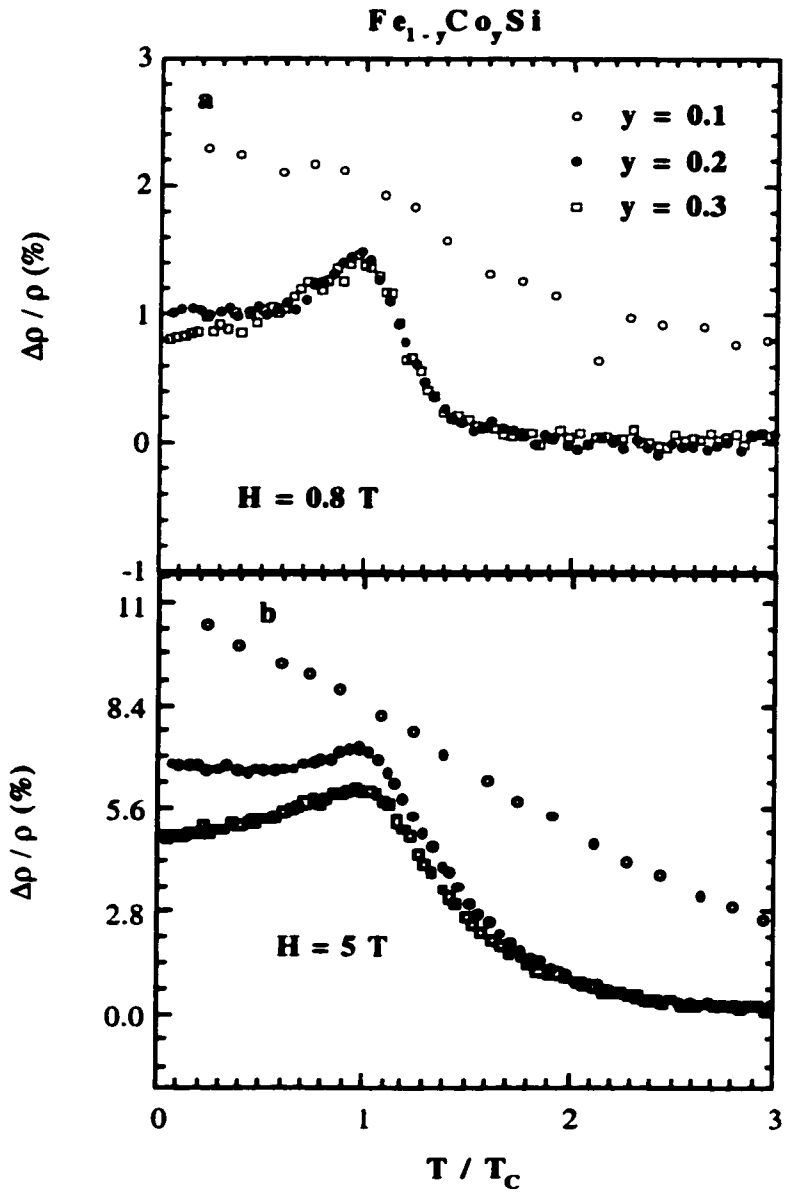

Fig. 4.17 $Fe_{1-y}Co_ySi$ magnetoresistivity at (a) 0.8 T, and (b) 5 T vs. T/T_C.

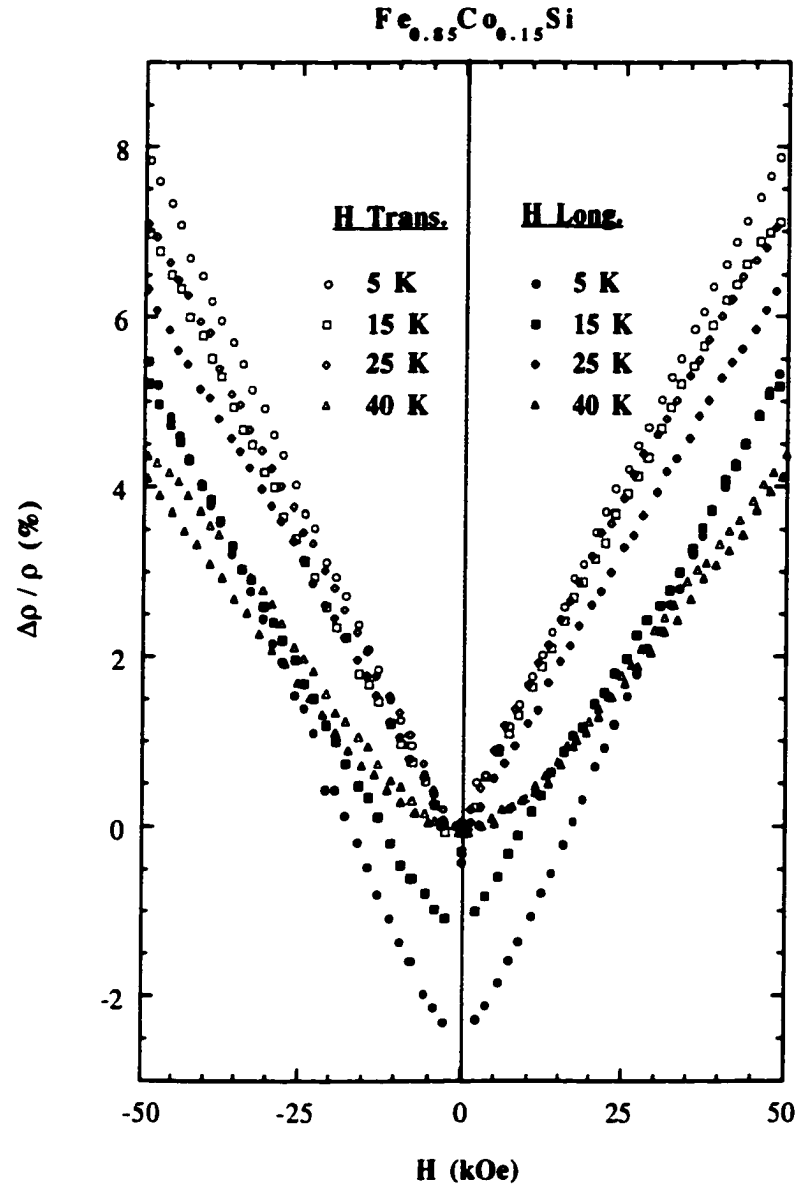

Fig. 4.18 $Fe_{0.85}Co_{0.15}Si$ transverse and longitudinal magnetoresistivity at the temperatures noted in the figure.

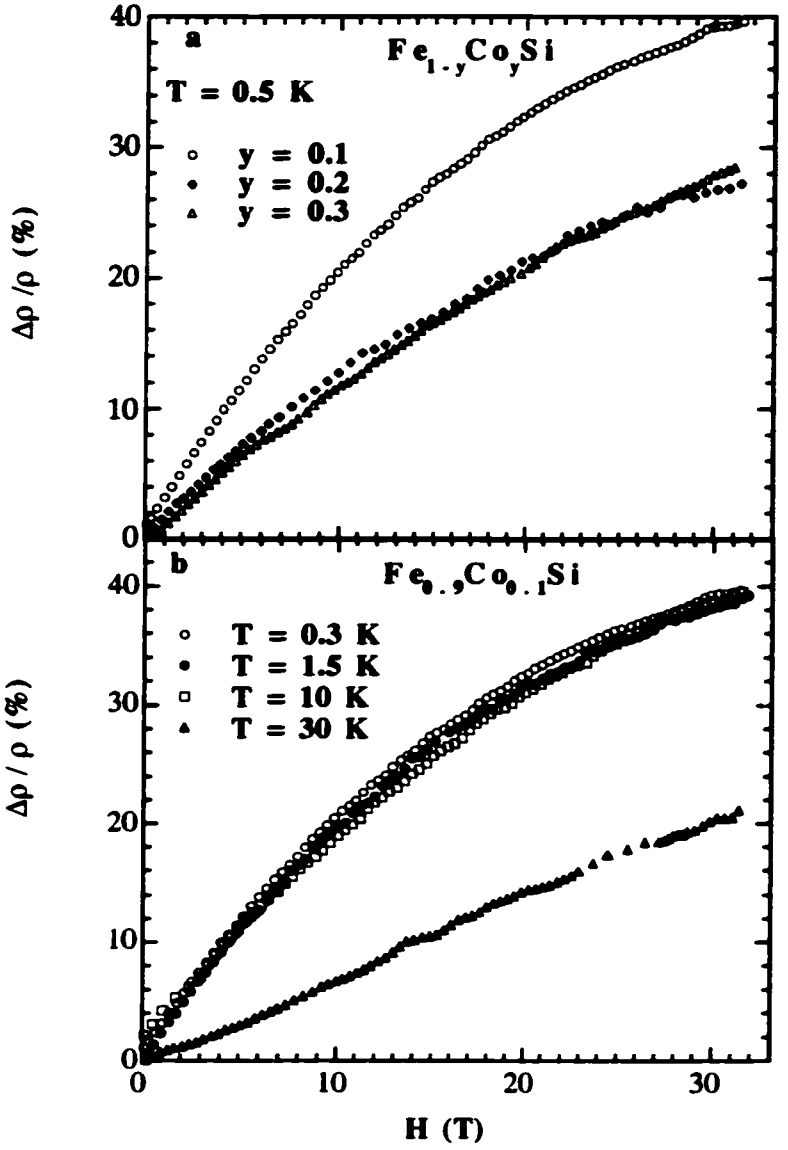

Fig. 4.19 (a) $Fe_{1-y}Co_ySi$ magnetoresistivity vs. field at T = 5K for y = 0.1, 0.2 (single crystal), and 0.3. (b) $Fe_{0.9}Co_{0.1}Si$ magnetoresistivity vs. field at temperatures noted in the figure.

Such theory clearly needs to account for what happens near $H = 0$, especially as T increases through T_C. Even so, it seems reasonable to believe that the key difference between para- and ferromagnets is simply that for a FM, in addition to the external field, there is a large spontaneous field due to the ordered moment. Thus, the effective field is really $H_{eff} = H + \alpha M$ rather than H alone. One can then imagine that for a ferromagnet, one should simply insert H_{eff} where H appears in the expression for $\sigma(H,T)$ derived for disordered paramagnets with electron-electron interactions (see Eq. 2.19). Examining Eq. 2.19 one can write it in the simple form as $(\sigma - \sigma_0)/\sqrt{T} = f(H_{eff}/T)$ and f is the scaling function whose limiting form is $(H_{eff}/T)^2$ for $g\mu_B H_{eff}/k_B T << 1$ and $\sqrt{H_{eff}/T}$ for $g\mu_B H_{eff}/k_B T >> 1$ [59, 60].

We have checked whether the scaling theory posited for the ferromagnets works for ferromagnetic $Fe_{1-y}Co_ySi$. Fig. 4.20 (c) shows the outcome, where we have plotted all of our T and field dependent data below 100 K for the $y = 0.3$ sample in the form $(\sigma - \sigma_0)$ *vs* H_{eff}/T with $\alpha = 1900$ and $\sigma_0 = 4400\ (\Omega\ cm)^{-1}$ chosen to minimize the difference of the data from a piecewise linear form. Note that σ_0 represents the zero H_{eff}, zero T conductivity shown in the inset of Fig. 4.20 (c). It is gratifying that the data scale so well and result in a $(H_{eff}/T)^2$ form for $H_{eff}/T < 0.25$ T / K (dashed line in the figure) and a $(H_{eff}/T)^{1/2}$ form for $H_{eff}/T > 0.25$ T / K (solid line in the figure). The data for the $y = 0.1$, 0.15, and 0.20 samples scale equally well (see Figs. 4.21, 4.22, and 4.23) with the scaling parameters noted in each figure. The zero field and 5 T σ of the $y = 0.3$ sample, along with the fits to these simple forms is shown in the inset to Fig. 4.20 (c). We conclude from the quality of both the scaling and the fits that, outside the small low-field effects of spin-orbit coupling, the field and T-dependent conductivity up to 100 K is entirely determined by a square-root singularity in the DOS most likely associated with enhanced e-e interactions in the disordered low density FM.

To understand the origin of the temperature dependence of σ and the MR of our Co doped samples it is sufficient to make a simple extension of the e-e interaction theory for

paramagnets. The usual picture of a disordered metal with diffusive transport outlined above and detailed in chapter 2 includes a square-root magnetic field dependence of σ. This dependence can be understood as arising from the triplet channel of the interaction. Since a field splits the spin sub-bands the singular contributions from the triplet channel split off from the Fermi energy by $g\mu_B H_{eff}$[63, 64]. If we simply extend this idea into the FM regime these square-root singularities will be separated from the Fermi energy by an amount determined by the magnetization of the ferromagnetic state. As the temperature is lowered below T_C these singularities move out from the Fermi energy in proportion to the spontaneous M of the material. The MC of our $Fe_{1-y}Co_ySi$ samples is thus determined by these singularities along with T and applied magnetic field.

4.4 Conclusions

In summary, we have measured the magnetic field and temperature dependence of σ and M in the alloy series varying from much studied metallic ferromagnet MnSi, through the strongly correlated (Kondo) insulator FeSi, to the diamagnetic metal CoSi. We observe a large negative magnetoresistance peaking sharply near the Curie temperature in MnSi. We discovered quantitatively different magnetotransport for the low carrier density ferromagnet produced by modest doping of FeSi by Co. Here, magnetoresistance is not only positive, but remains essentially temperature independent below Curie temperature. It is thus not due to spin scattering effects responsible for most magnetoresistive phenomena of current interest. Instead, our data suggest that the magnetoconductivity in ferromagnetic $Fe_{1-y}Co_ySi$, and because parameters found in the detailed comparison between theory and experiment for $FeSi_{1-z}Al_z$ are reasonable, we can attribute the low temperature magnetotransport in $Fe_{1-y}Co_ySi$ to electron-electron interactions in a disordered system. Because $Fe_{1-y}Co_ySi$ is, to our knowledge, the first ordered FM for which $\sqrt{T}$ and $\sqrt{H}$ terms are present, no theory is presently available for ferromagnets.*

* Part of this chapter has been published in *Nature*.

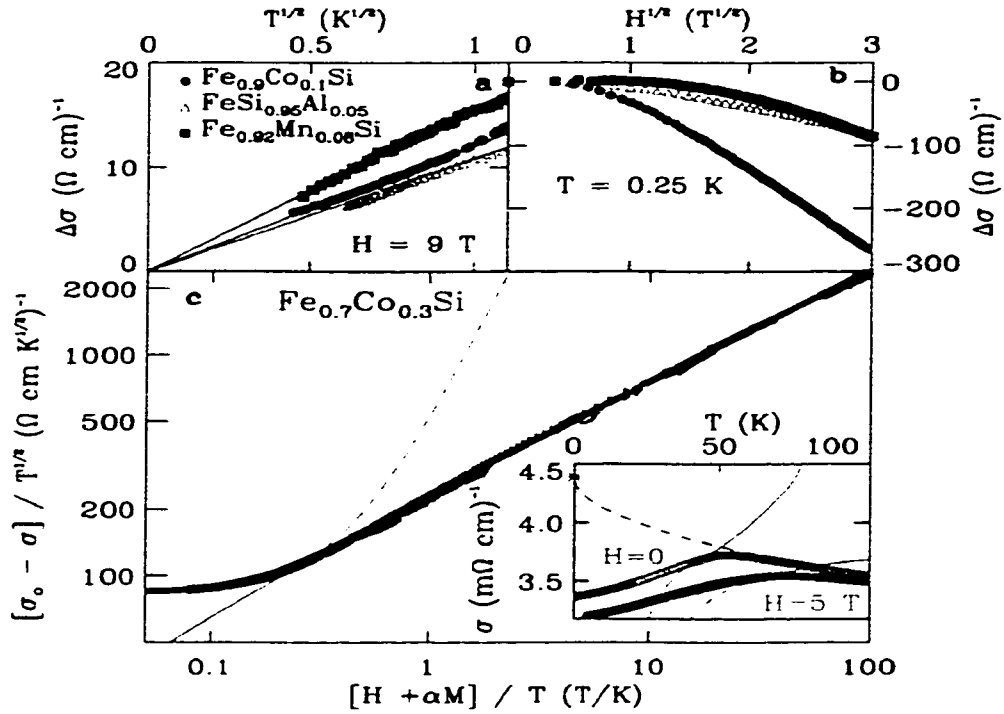

Fig. 4.20 (a) Magnetoconductivity of $Fe_{0.9}Co_{0.1}Si$, $FeSi_{0.95}Al_{0.05}$, and $Fe_{0.92}Mn_{0.08}Si$. Change in conductivity, $\Delta\sigma = \sigma(H,T) - \sigma(H,0)$ with $\sigma(H,0)$ determined from fits of the data to a $T^{1/2}$ dependence, vs. $T^{1/2}$ at 9T. $\sigma(0,0)$ = 1910, 1260, and 1540 $(\Omega cm)^{-1}$ for $Fe_{0.9}Co_{0.1}Si$, $FeSi_{0.95}Al_{0.05}$, and $Fe_{0.92}Mn_{0.08}Si$ respectively. (b) $\Delta\sigma = \sigma(H,T) - \sigma(0,T)$ vs. $H^{1/2}$ at 0.25 K. Symbols represent the same samples as in (a). (c) Scaling plot of the conductivity, $[\sigma - \sigma_0] / T^{1/2}$ vs. H_{eff} / T, for $Fe_{0.7}Co_{0.3}Si$, with H_{eff} taken as $H + \alpha M$ and with σ_0 and α determined by the best scaling of all our T and H dependent data. The data shown include temperature sweeps at constant fields of 0 (0.2 to 100 K, teal o), 0.8 T (2 to 100 K, light-blue •), 3 T (2 to 100 K, dark-blue ▷), and 5 T (2 to 100 K, green +), as well as constant temperature field sweeps at temperatures of 0.3 K (0 to 9T, dark-blue □), 1.2 K (0 to 32 T, black ◁), 1.5 K (0 to 9 T, purple ⊙), 4 K (0 to 32 T, orange ◊), 5 K (0 to 5 T, yellow-green *), 15 K (0 to 5 T, yellow ×), and 30 K (0 to 5 T, violet Δ; and 0 to 32 T, red ▽). Light-blue dashed line represents a fit to the data for $H_{eff} / T < 0.25$ by a $a + b\,(H_{eff}/T)^2$ form. Solid red line represents a fit to the data for $H_{eff} / T > 0.25$ by a $c + d\,(H_{eff}/T)^{1/2}$ form. Inset: Red line and dashed light-blue line represent the same fits as in the main part of the figure. The dashed purple line represents the zero H_{eff} conductivity in our model. Light-blue * represents σ_0, the zero T, zero magnetic field value of the conductivity determined from the scaling of the data.

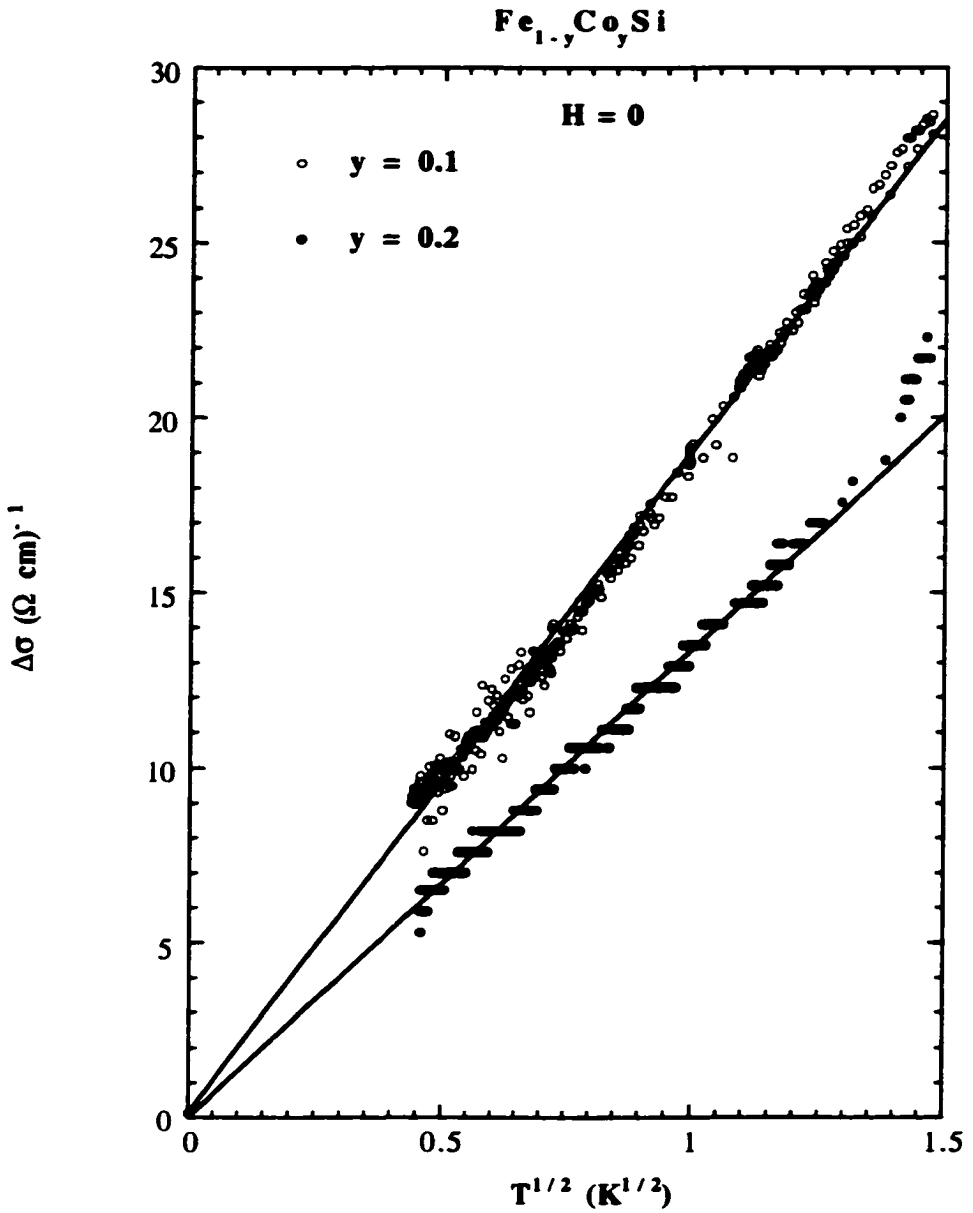

Fig. 4.21 The change in the conductivity ($\sigma - \sigma_0$) for two $Fe_{1-y}Co_ySi$ samples plotted as a function of $T^{1/2}$ with $y = 0.1$ and $y = 0.2$ at zero field.

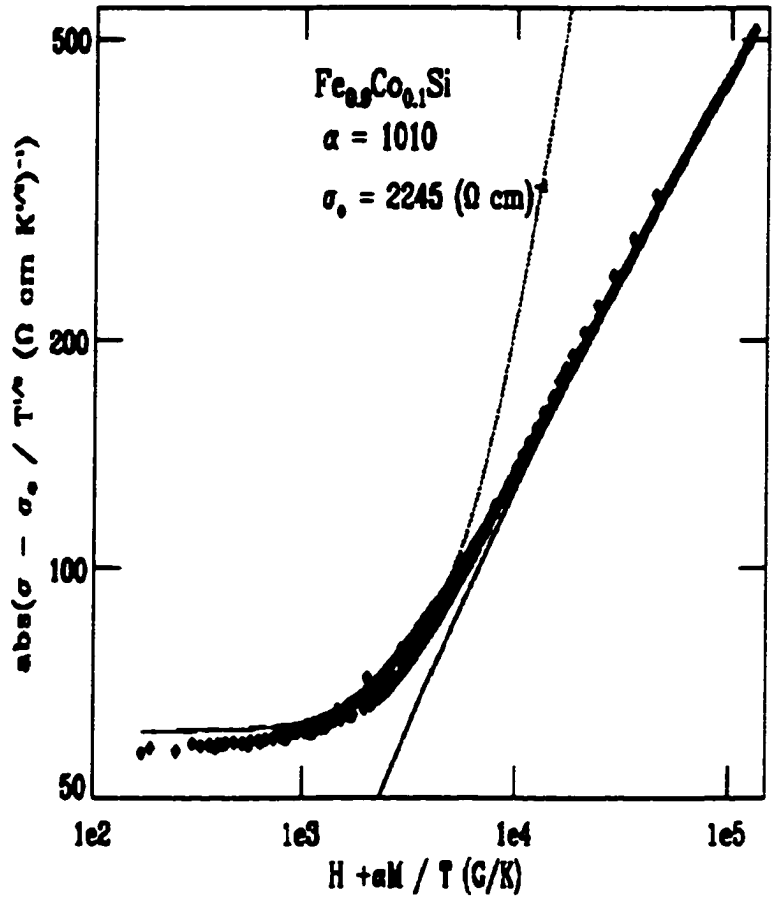

Fig. 4.22 Scaling plot of the conductivity $(\sigma - \sigma_0) / T^{1/2}$ vs. H_{eff} / T, for $Fe_{0.9}Co_{0.1}Si$, with $H_{eff} = H + \alpha M$ and with σ_0 and α determined by the best scaling of all our T and H dependent data. Dashed line represents a fit to the data for $H_{eff} / T < 0.25$ by $a + b\,(H_{eff} / T)^2$ form. Solid line represents a fit to the data for $H_{eff} / T > 0.25$ by $c + d\,(H_{eff} / T)^{1/2}$ form.

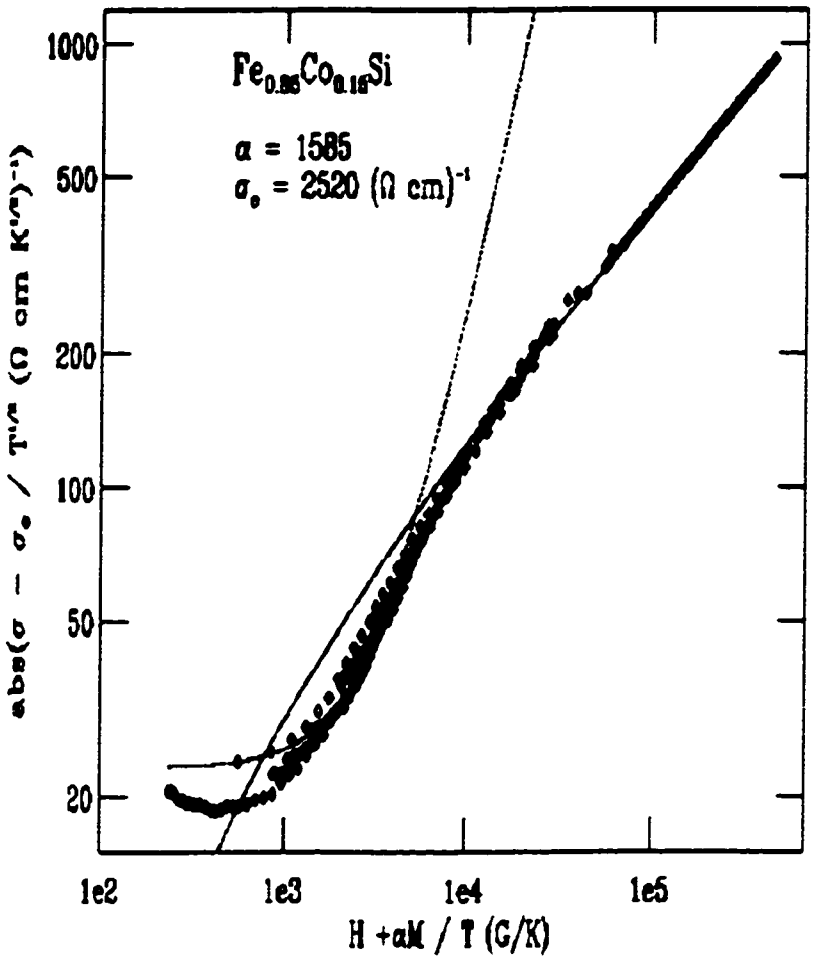

Fig. 4.23 Scaling plot of the conductivity $(\sigma - \sigma_0) / T^{1/2}$ vs. H_{eff} / T, for $Fe_{0.85}Co_{0.15}Si$, with $H_{eff} = H + \alpha M$ and with σ_0 and α determined by the best scaling of all our T and H dependent data. Dashed line represents a fit to the data for $H_{eff} / T < 0.25$ by $a + b\,(H_{eff} / T)^2$ form. Solid line represents a fit to the data for $H_{eff} / T > 0.25$ by $c + d\,(H_{eff} / T)^{1/2}$ form.

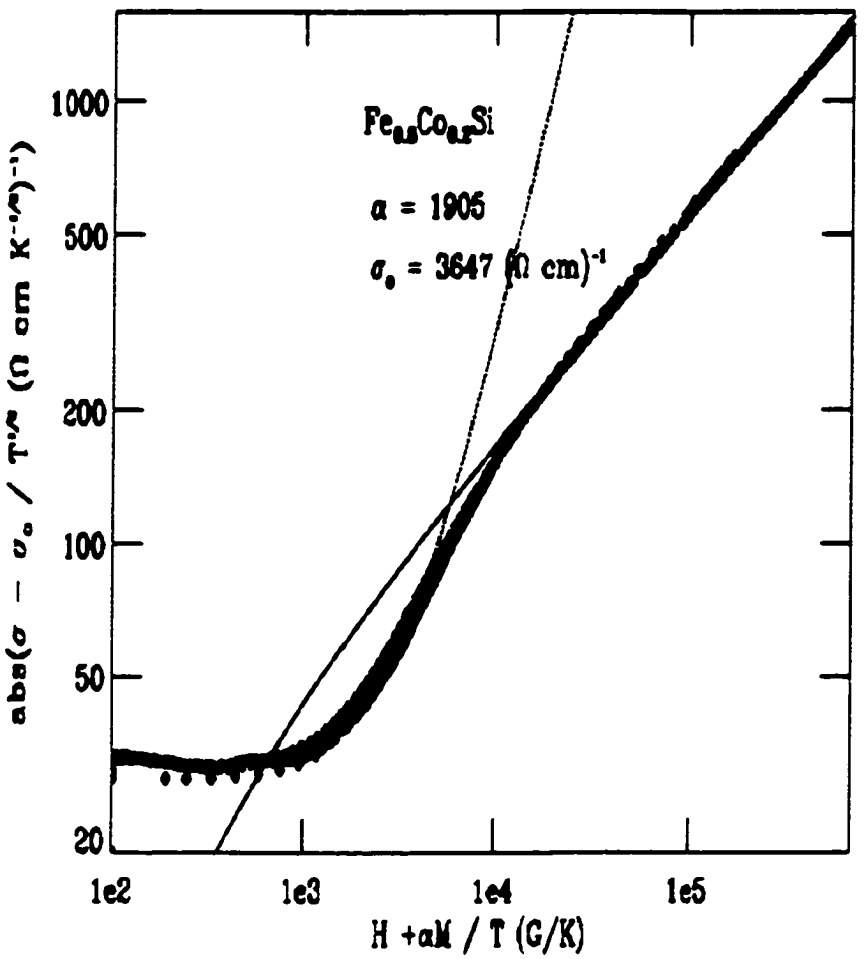

Fig. 4.24 Scaling plot of the conductivity $(\sigma - \sigma_0) / T^{1/2}$ vs. H_{eff} / T, for $Fe_{0.8}Co_{0.2}Si$, with $H_{eff} = H + \alpha M$ and with σ_0 and α determined by the best scaling of all our T and H dependent data. Dashed line represents a fit to the data for $H_{eff} / T < 0.25$ by $a + b (H_{eff} / T)^2$ form. Solid line represents a fit to the data for $H_{eff} / T > 0.25$ by $c + d (H_{eff} / T)^{1/2}$ for

CHAPTER 5

$FE_{1-x}MN_xSI$: MAGNETIC AND TRANSPORT MEASUREMENTS

In this chapter we will be comparing the magnetic and transport properties of $Fe_{1-x}Mn_xSi$ and $FeSi_{1-z}Al_z$ in the concentration range ($0 < x, z \leq 0.08$).

5.1 Introduction

Insulator-to-metal transitions in lightly doped semiconductors have been a central problem in condensed matter physics for many years. A large number of investigations in common semiconductors such as Si, Ge, or GaAs have shown that the disorder and electron-electron (e-e) interactions determine the electronic and magnetic properties of these systems[11, 55, 60, 62, 89]. It is now well established that near the metal-insulator transition the diffusive nature of the carrier transport strengthens the Coulomb interaction among quasi-particles[11, 60]. Recently it has been shown that the correlations can be further enhanced by the addition of elemental dopants containing partially filled d or f shells. The impurity magnetic moments produce a local electron polarization that leads to greatly enhanced exchange interactions[64, 90]. These latter systems, such as n-type $Cd_{0.95}Mn_{0.05}Se$ and p-type $Hg_{0.915}Mn_{0.085}Te$[91, 92] are often referred to as diluted magnetic semiconductors (DMS). In fact, the strong Coulomb interactions are found to stabilize the insulating phase in these materials through the formation of bound magnetic polarons (BMP) or ferromagnetic clouds. The formation of BMP reduces the conductivity below that associated with the singularity in the density of states (DOS) caused by e-e interactions[91]. The magnetic polarons can be unbound by the application of moderate magnetic fields resulting in a more standard MI transition. Thus at zero field the continuous MI transition is delayed by the strongly localizing effect of carrier interaction with localized moments on the impurity atoms.

In this chapter we describe an exploration of the effect of Mn substitution for Fe in the strongly correlated or Kondo insulator FeSi. We find as is true for $FeSi_{1-z}Al_z$, that the

doping yields a paramagnetic metal with roughly a single hole carrier per dopant. In the case of Al substitution for Si in FeSi ($FeSi_{1-z}Al_z$) we found that the metal that results is very similar to Si doped just beyond MI transition except that the quasi-particle mass is greatly enhanced[32]. When we substitute on the transition metal site ($Fe_{1-x}Mn_xSi$) the difference in the number of d electrons in Fe and Mn is responsible for the carrier doping and results in an even larger carrier mass. In addition, we find that the transition from an insulator to a metal is delayed by a localization of the carriers at low temperatures. This weakly insulating state is characterized by a decrease in the conductivity (σ) and thus an increase in the critical concentration for true metallic behavior. The more standard behavior exhibited by $FeSi_{1-y}Al_y$ can be established in $Fe_{1-x}Mn_xSi$ simply by applying a moderate magnetic field. In this sense our data suggest that just as $FeSi_{1-z}Al_z$ represents a renormalized version of Si:P[32], $Fe_{1-x}Mn_xSi$ represents a renormalized version of n-$Cd_{1-x}Mn_xSe$[91], or $Ga_{1-x}Mn_xAs$[93-95] where the strong Coulomb interactions result in the formation of bound magnetic polarons (BMP) near the MI transition. Thus we have identified a Heavy Fermion DMS that results upon carrier doping of a Kondo insulator.

5.2 Susceptibility and Magnetization Measurements

We plot in Fig. 5.1 magnetic susceptibility (χ) at 1 kG for our several $Fe_{1-x}Mn_xSi$ samples noted in the figure. There are systematic changes to χ with doping. This includes the addition of a T independent offset and an increased Curie-Weiss like tail at low T to the χ of pure FeSi. Despite the fact that pure MnSi and $Fe_{1-y}Co_ySi$ are itinerant magnets we find, just as in $FeSi_{1-z}Al_z$, no evidence for a magnetic phase transition for $x \leq 0.8$. In fact, we find no peaks or discontinuities in $\chi(T)$ down to $T = 1.7$ K in fields as small as 50 G. However, at $T < 10$ K there is a small hysterisis below 100 G that grows by ~ 30% as T is lowered (see Fig 5.2 (b)). This demonstrates that there may be frustration of the impurity spins. Fig 5.3 shows the remanent magnetization for a metallic $Fe_{0.97}Mn_{0.03}Si$ samples which could be considered further as the evidence of the possibility of spin glass like behavior[96]. However, the magnetic moment associated with

this glasssy behavior is extremely small ~ 10^{-4} μ_B / FU (see Fig. 5.2). Thus only a small number of impurity spins participate in this glassy behavior. The remanent magnetization depends in a detailed way on the magnetic history of the sample. The isothermal remanent magnetization (IRM) is obtained by first cooling in zero field to the desired temperature to be studied, then a field of a chosen strength is applied for a macroscopic period of time and then switched off again. To obtain the thermo-remanent magnetization (TRM), on the other hand, one applies the field at some initial temperature above freezing temperature T_f and then cools the system slowly in a constant field to the desired temperature. We took our macroscopic time to be 10 minutes, desired field of 1 T and the sample was cooled from 100 K to 2 K.

The comparison to our Al doped samples reveals that there is a much larger change in χ (T) with Mn doping than with Al doping, even at room T. In order to parameterize the changes that occur upon Mn doping we fit a form that includes a high T activated behavior similar to that found in pure FeSi, a T independent Pauli susceptibility ($\delta\chi$), and a Curie-Weiss term, $\chi = x_C\, n\, (g\, \mu_B)^2\, J(J+1) / 3\, k_B\, (T - \Theta_W)$, to the data (see Eq. 2.22). Here, Θ_W is the Weiss temperature, n is the formula unit density, and x_C is the number of spin 5/2 per formula unit. The solid lines through a few of the data sets in Fig. 5.1 is an example of our best fits to Eq. 2.22. Figs. 5.4 (a, b), and 5.5 (a, b) show parameters resulting from these fits for $\delta\chi$, the energy gap (Δ_χ), the ratio x_C / x determined from the low T curie constant, and Θ_W. The parameters found from fitting to this form display the systematic effects with doping: an increase in Pauli susceptibility, an increase in $|\Theta_W|$, and a decrease in x_C / x with x. One can estimate the effective mass m^* from the Pauli term by using Eq. 2.24. We find an m^* of $(56 \pm 5)m_e$ for Mn as compared to m^* of $(14 \pm 2)m_e$ for Al doped FeSi [32] ($\nu' = 8$ for the valance band maximum) . This is an extraordinarily large mass for a d electron compound.

$\Theta_W(x)$ is less than zero revealing an antiferromagnetic interaction that increases with x as the Mn-Mn distance decreases. The ratio x_C / x shows that the percentage of

spins involved in the C-W tail is steadily *decreasing* with x. A simple model assuming that Mn atoms with a nearest (6) or next nearest (6) Mn neighbor form singlet clusters, and do not contribute to the Curie-Weiss tail is shown along with the data in Fig. 5.5 (a) (solid line). This decrease in x_C / x could be a result of an interaction of Mn spins to form singlets resulting in small regions of AFM couplings, a reduction of the number of localized electrons as the carriers become itinerant, or a Kondo like interaction between the induced carriers and the Mn spins. Since $|\Theta_{CW}|$ is increasing with x, we believe that although all three are probably occuring to some degree, the first is most likely the dominant effect. Fig. 5.4 (b) shows that there is at most a 120 K decrease in Δ_χ over this range in x. The small change in Δ_χ can be interpreted as evidence that the addition of itinerant carriers by Mn substitution has not significantly altered the gross features of the band structure of FeSi. We present in Fig. 5.6 (a) *M (H)* data for four Mn concentrations. In Fig. 5.6 (b) the *M* of our 2% Mn sample at various temperatures is displayed. Naively one can interpret these data as consisting of the *linear M (H)* of the free carriers *($\delta\chi H$)* added to the magnetization of noninteracting ions (see Eq. 2.25). The solid lines through data in Fig. 5.6 (a) are the best fits to Eq. 2.25 with the $\delta\chi$ taken from fits to χ *(T)* and Lande g factor taken as 2.

5.3 Resistivity and Magnetoresistance Measurements

Figs. 5.7, and 5.8 present the zero field conductivity (σ) of our Mn doped samples. The low Mn concentrations ($0 < x \leq 0.08$) (Fig. 5.8) data are similar in form to the σ of our $FeSi_{1-z}Al_z$ samples in the same concentration range. In both cases there is a systematic increase in the low T conductivity with doping. This is coupled with small changes in the room temperature σ where the intrinsic activated carriers dominate. However, there are some significant and telling differences from $FeSi_{1-z}Al_z$ that this data set exhibits. Although the carrier concentrations at any particular x *(z)* are similar for the two types of substitution, the low temperature σ of $Fe_{1-x}Mn_xSi$ is factor of two smaller than that of the corresponding $FeSi_{1-z}Al_z$ samples.

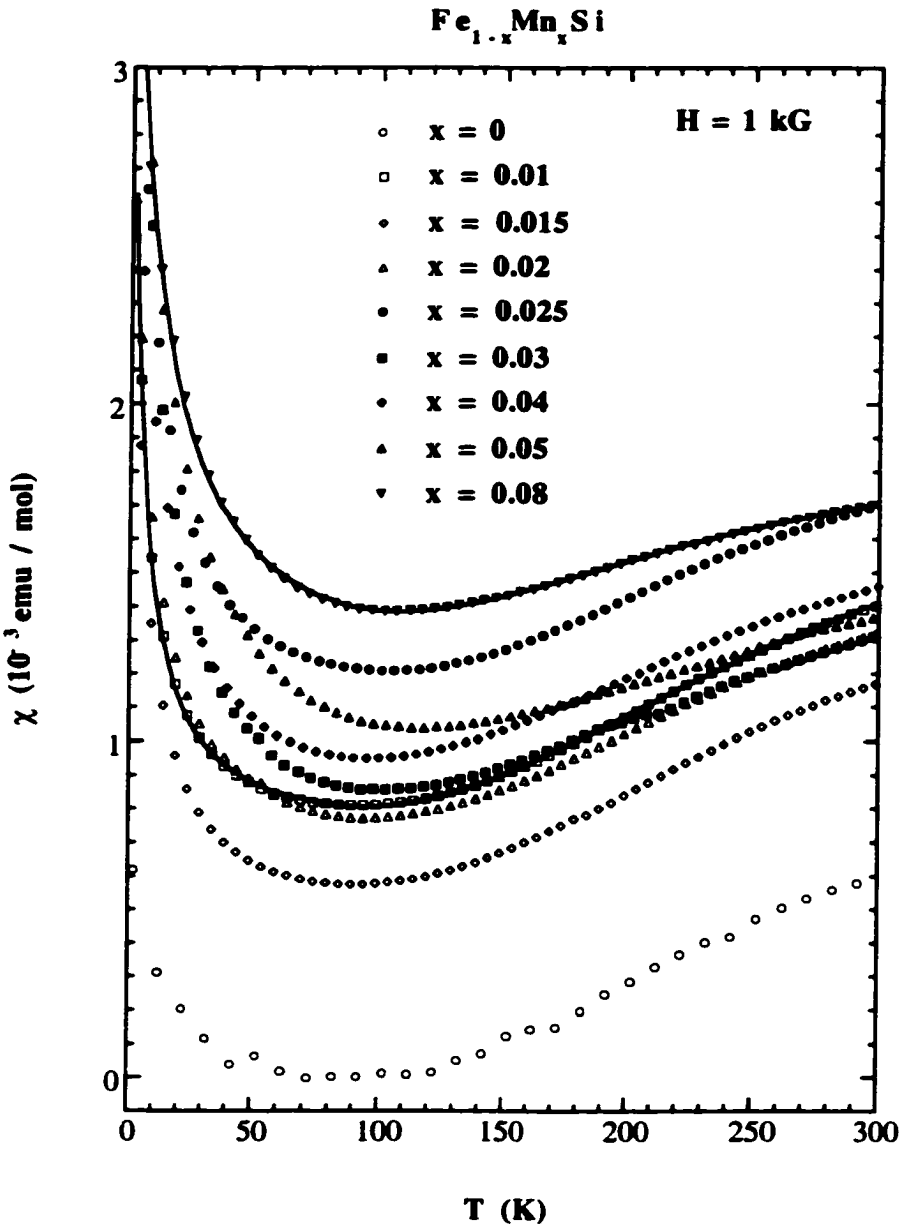

Fig. 5.1 Magnetic susceptibility $\chi(T)$ for $Fe_{1-x}Mn_xSi$ at 0.1 T, with the symbols noted in the figure. The solid lines through a few of the data sets are the best fits to Eq. 2.22.

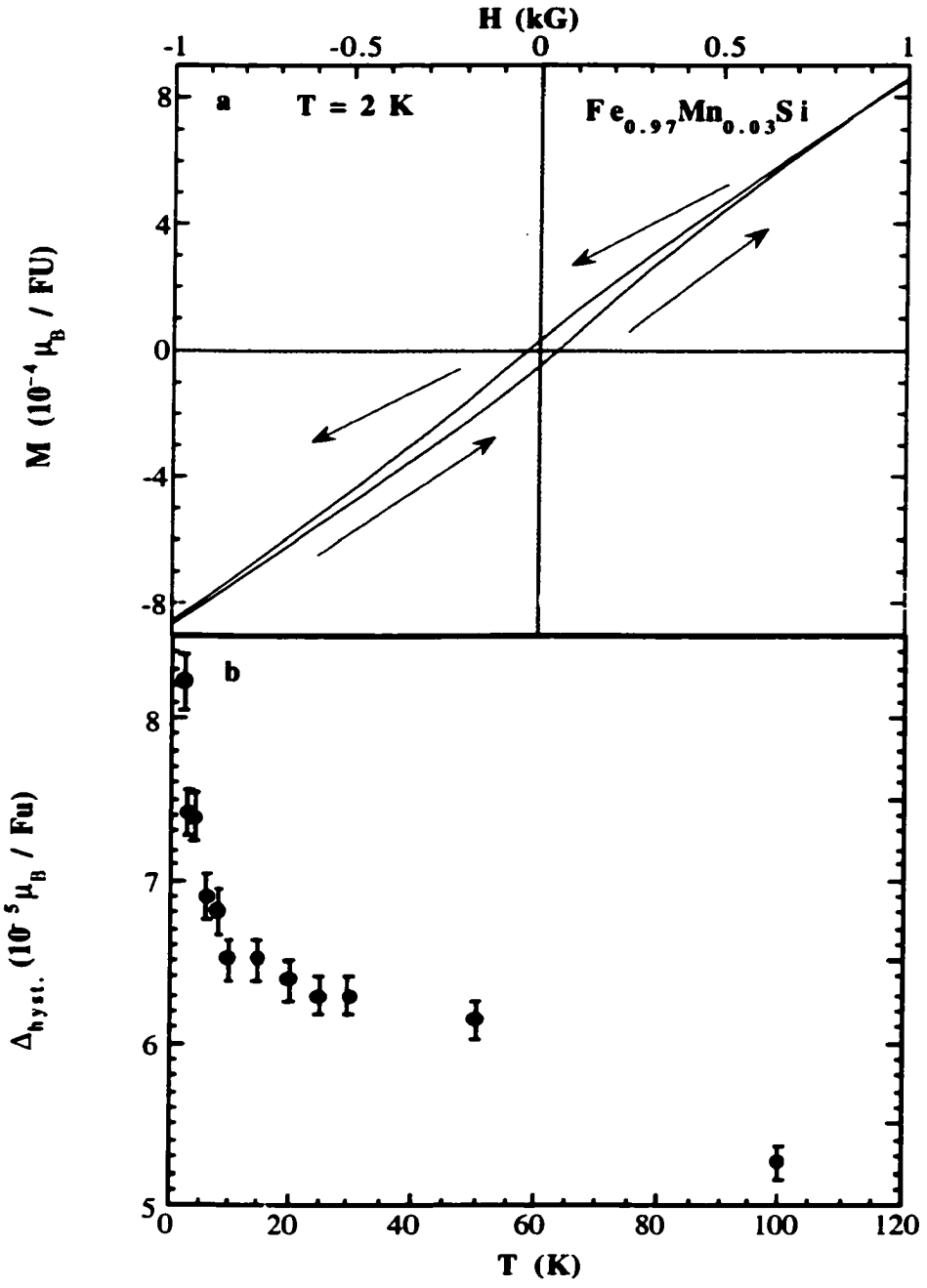

Fig. 5.2 (a) History dependence of the magnetization for $Fe_{0.97}Mn_{0.03}Si$ at T = 2 K showing a small hysterisis upon increasing the field from zero. Sample was initially cooled from 100 K to 2 K in zero field. (b) The size of the hysterisis width as a function of T for $Fe_{0.97}Mn_{0.03}Si$.

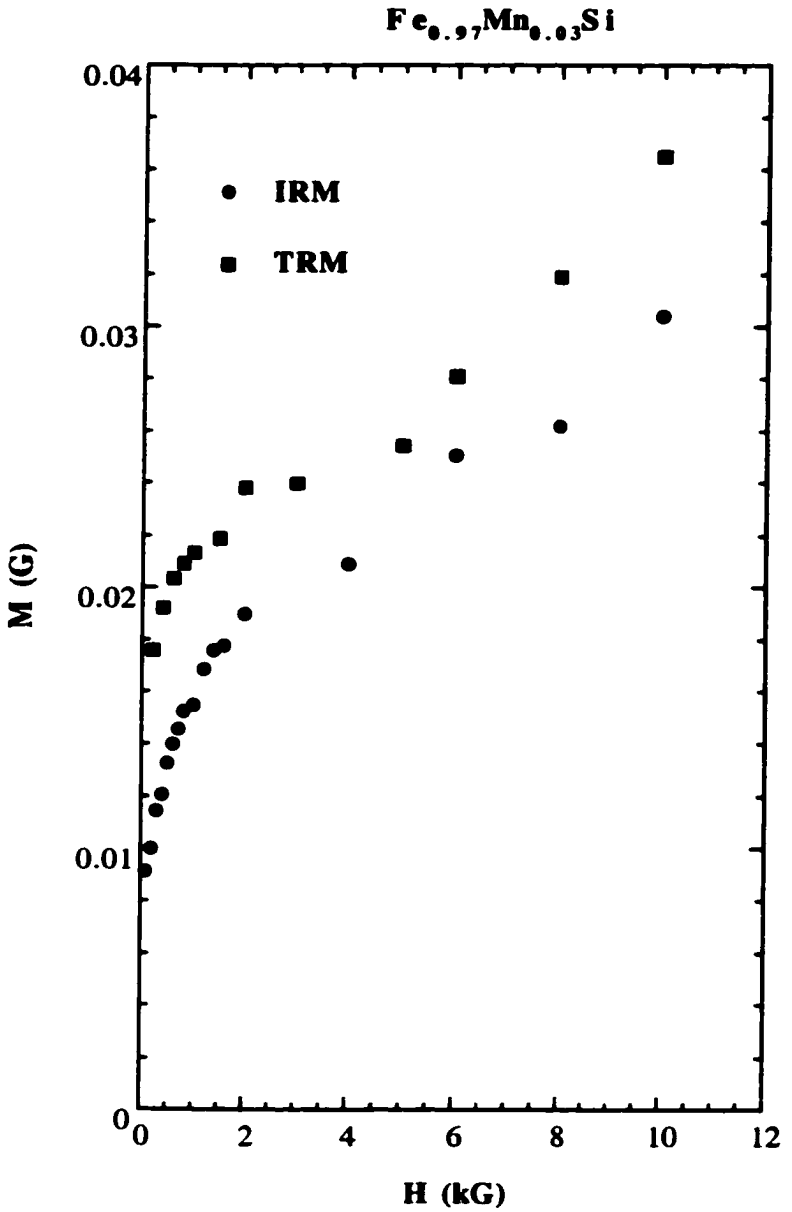

Fig. 5.3 Field dependence of the isothermal remanent magnetization IRM and of the thermo-remanent magnetization TRM obtained after cooling from T = 100 K to T = 2 K in a field H = 1 T.

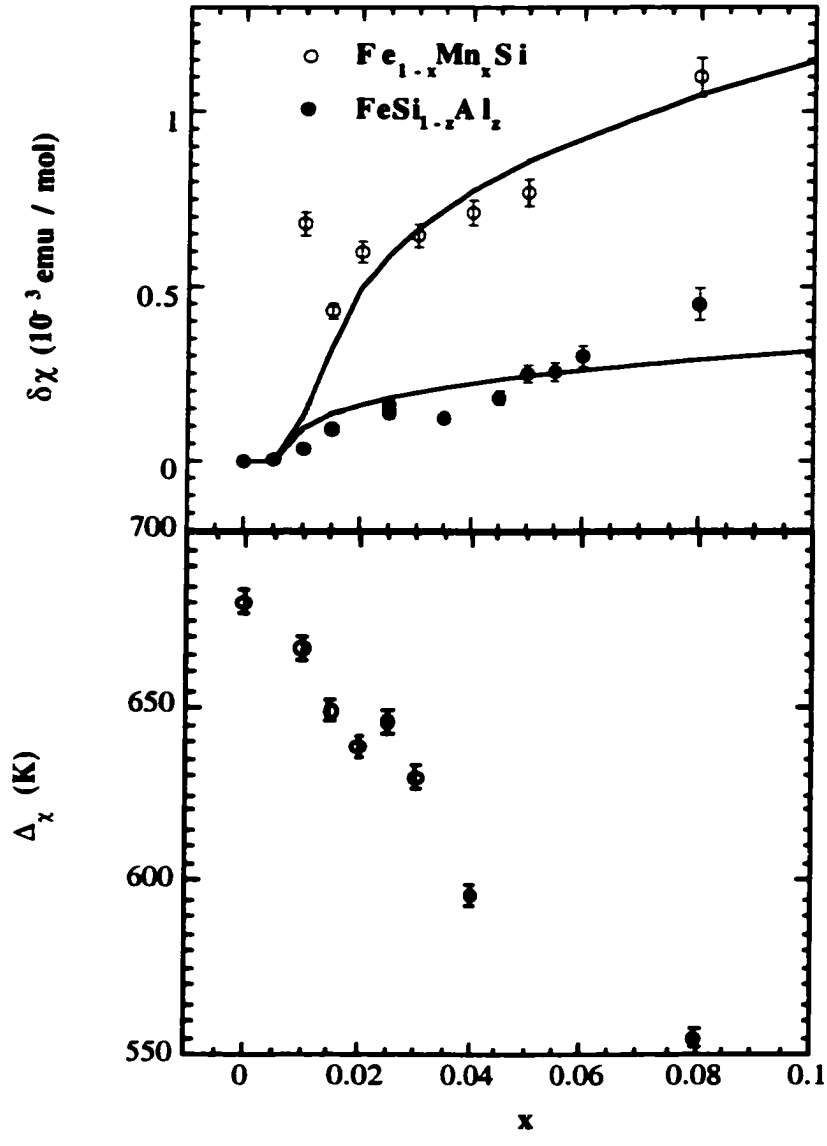

Fig. 5.4 (a) Pauli susceptibility ($\delta\chi$) for $Fe_{1-x}Mn_xSi$ and $FeSi_{1-z}Al_z$ as a function of concentration with the symbols noted in the figure. The solid lines are the best fits to Eq. 2.24. (b) Energy gap as measured from magnetic susceptibility (Δ_χ) for $Fe_{1-x}Mn_xSi$ as a function of concentration with the same symbols as in (a).

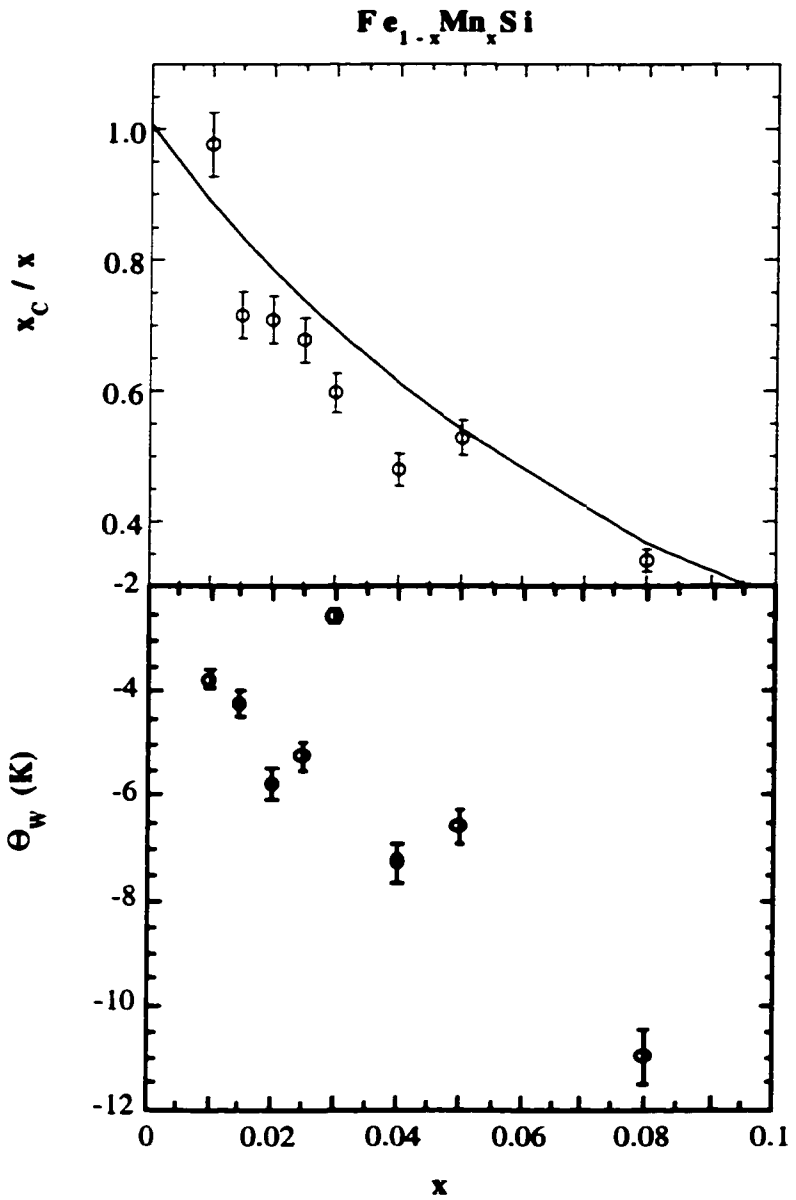

Fig. 5.5 (a) The ratio x_C / x determined from the low T Curie constant. Solid line represents a simple model assuming that Mn atoms with a nearest (6) or next nearest (6) Mn neighbor form singlet clusters, and do not contribute to the Curie-Weiss tail (b) The Weiss temperature from fits of the low$T$ χ (T) (see Eq. 2.22) for $Fe_{1-x}Mn_xSi$.

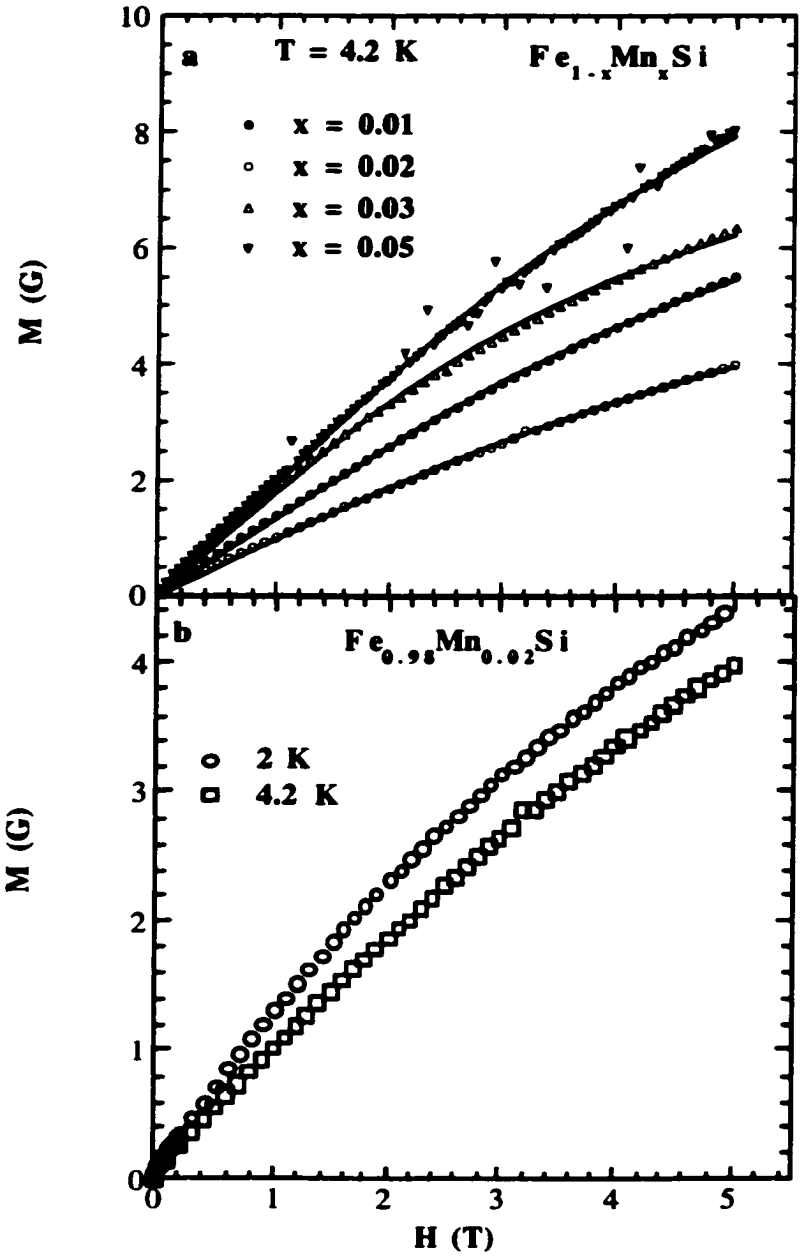

Fig. 5.6 (a) Field dependence of the magnetization for $Fe_{1-x}Mn_xSi$ with symbols noted in the figure. The solid lines are the best fit to Eq. 2.25. (b) Field dependence of magnetization for $Fe_{0.98}Mn_{0.02}Si$ at 2 and 4.2 K.

Furthermore, an examination of σ for $Fe_{1-x}Mn_xSi$ below 20 K shows a maximum in σ which systematically moves to lower *T* with increasing doping (see Figs. 5.8 and 5.9 (a) and (b)). This insulating like behavior was also apparent in $FeSi_{1-z}Al_z$ samples for $z < 0.01$, but persists for $Fe_{1-x}Mn_xSi$ up to $x = 0.10$. The downturn in σ at low *T* makes determining the critical concentration for the MI transition difficult. We have taken a point of view supported by exhaustive experiments in classic semiconductors such as Si:P that the insulating samples will have a conductivity described by either the variable-range-hopping (VRH) model: $\sigma = \sigma_{VR}\, exp(-(T_0 / T)^{1/4})$, or by the electron-electron interaction model: $\sigma = \sigma_0 + m_\sigma T^{1/2}$ with $\sigma_0 = 0$ for insulating samples and $\sigma_0 > 0$ for metallic samples (see chapter 2 for detailed discussion). Using this criterion we determined by comparing the quality of fits to these forms below 1 K that the critical concentration for $Fe_{1-x}Mn_xSi$ is in the range $0.025 < x_c < 0.03$, a much larger critical concentration found in $FeSi_{1-z}Al_z$ ($0.005 \leq z_c < 0.01$)[32].

In order to further the comparison of $Fe_{1-x}Mn_xSi$ and $FeSi_{1-z}Al_z$, as well as to highlight the effects of doping this Kondo insulator on the transition metal site, we have investigated the magnetoconductivity (MC) below 1 K for samples near the MI transition. In our previous investigation of $FeSi_{1-z}Al_z$ we found clear evidence for e-e interaction effects in $\sigma\ (T,H)$ for samples on the metallic side of the transition[32]. Since our $Fe_{1-x}Mn_xSi$ samples also span the MI transition, we expect to find similar metallic behavior, including the $\sqrt{T}$ dependence of σ at low *T* displayed in Fig. 5.10 (a) and (b) for the $x = 0.03$ and $x = 0.04$. However, the changes that occur upon application of moderate magnetic fields to this metallic sample ($x \geq 0.03$) do not correspond to the simple behavior found in $FeSi_{1-z}Al_z$. Although the high field MC assymptotically approaches a $\sqrt{H}$ form, the low field MC is positive as shown in Fig. 5.11 (b) for the $Fe_{0.96}Mn_{0.04}Si$ sample. This figure also shows that transverse and longitudinal MC are very similar showing that the MC is not due to orbital effects. The magnitude of this positive MC is larger than that predicted by weak localization and attempts to fit the data by the sum of

e-e interactions and weak localization effects failed to reproduce the MC for any value of the parameters, these included diffusion constant, g-factor, and the inelastic scattering time. As Fig. 5.10 reveals, there is also an attenuation of the $\sqrt{T}$ contribution to σ at these same fields. Both of these effects, a positive contribution to the MC, and reduction of the value of m_σ, opposite to what was observed in $FeSi_{1-z}Al_z$ (see Fig. 5.15 (a)) cannot be understood within the standard e-e interactions picture that is so well documented for classic semiconductors, even when including the possible effects of weak localization.

Perhaps even more interesting is the effect of field on the samples just on the insulating side of the transition. These samples are identified as insulating since, as Fig. 5.12 (a) points out for $x \leq 0.025$, a variable range hopping form can describe the data at wide T range for $H = 0$ (see Fig. 5.13). T_0 decreases nearly exponentially with x as can be seen in Fig. 5.14 (b). The localization length determined from T_0 and an estimate of the DOS (Eq. 2.17) is displayed in Fig. 5.14 (a). We have introduced the concept of a scaling length near MI transition in section 2.3 (see Eq. 2.16). On the insulating site of MI transition the scaling length or localization length in this case has a concentration dependence $\xi_L \propto (1 - n/n_c)^{-\nu}$. The solid line through the data Fig. 5.14 (a) is the best fit to this form. However, as revealed in Fig. 5.13 (a), for fields greater than ~ 1 T, the VRH form no longer describes the data. In fact, at these fields σ is much better described by a $\sigma = \sigma_0 + m_\sigma T^{1/2}$ form (see Fig. 5.13 (b)).

Thus, we find for $0.015 \leq x \leq 0.025$ (see Fig. 5.12 (b)) an insulator to metal transition with the application of magnetic field. The zero temperature conductivity σ_0 found from the fits to the data at 9 T are displayed along with the $H = 0$ σ_0 in Fig. 5.15 (b) with $FeSi_{1-z}Al_z$ zero field data included for comparison. The zero temperature conductivity σ_0 found from the fits to the data at 9 T are displayed along with the $H = 0$ σ_0 in Fig. 5.15 (b) with $FeSi_{1-z}Al_z$ zero field data included for comparison. The MI transition has been pushed down to $0.01 < x_c < 0.015$ by the magnetic field. At these temperatures the MC is similar in form to those samples on the metallic side of the

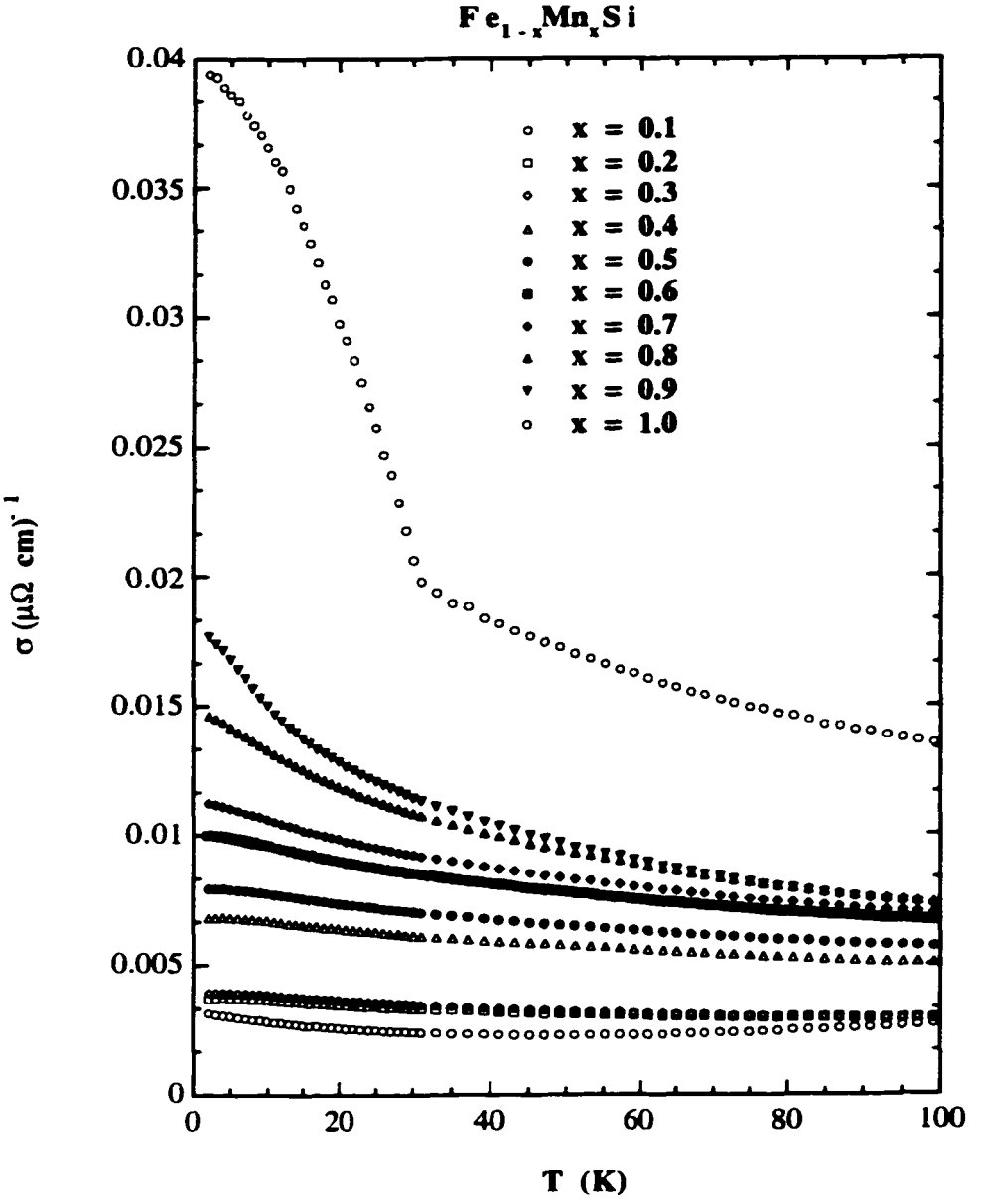

Fig. 5.7 Temperature dependence of conductivity σ *(T)* at zero field for $Fe_{1-x}Mn_xSi$ for $0 < x \leq 1$.

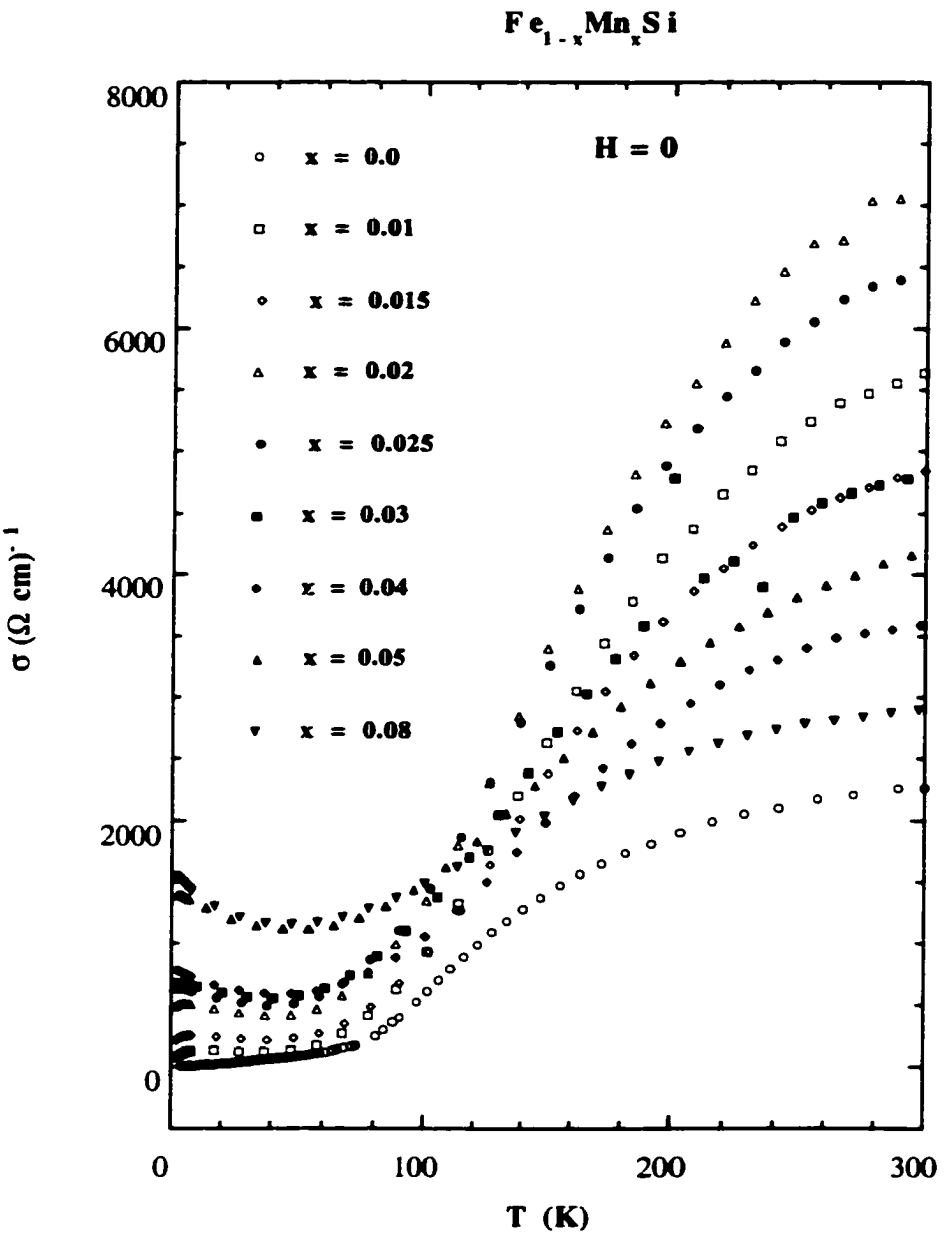

Fig. 5.8 Temperature dependence of conductivity σ *(T)* at zero field for $Fe_{1-x}Mn_xSi$ for $0 < x \leq 0.08$.

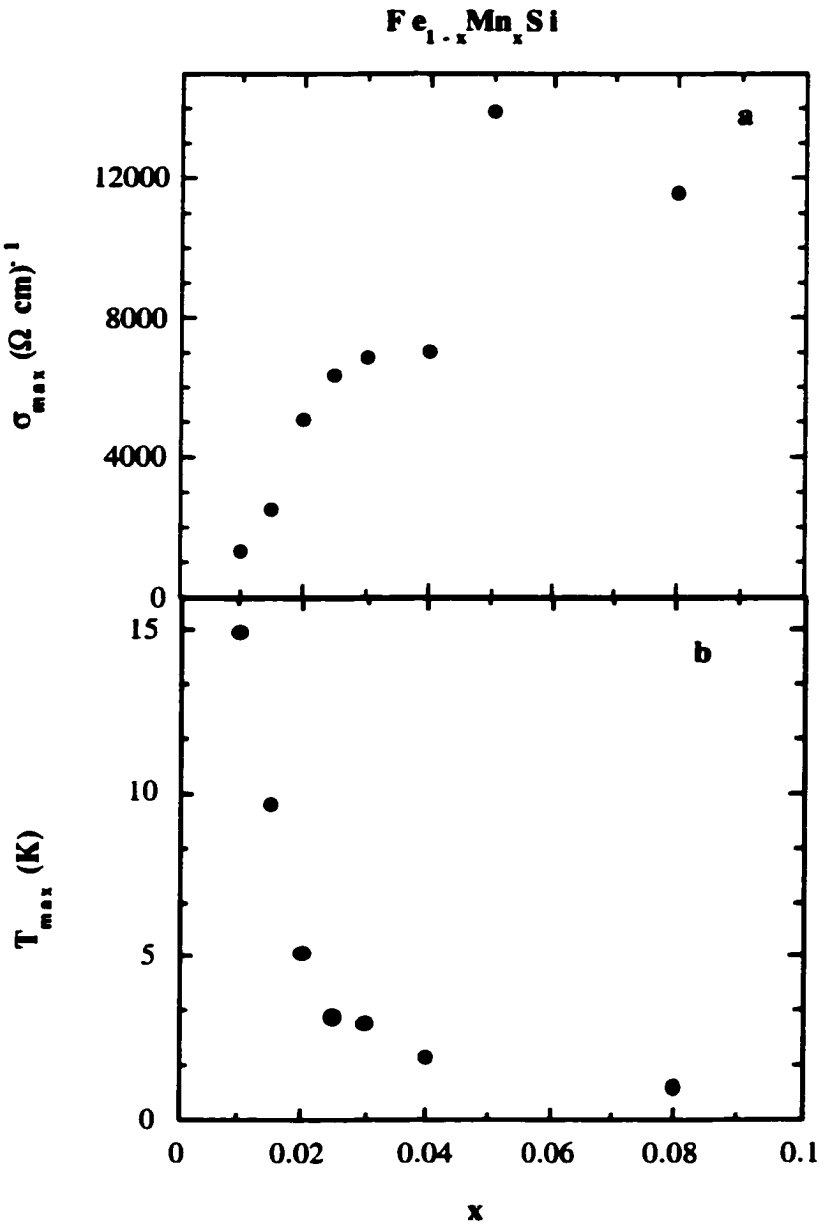

Fig. 5.9 Nominal Mn concentration dependence of (a) zero field conductivity maximum (σ_{max}) and (b) temperature (T_{max}) at which σ_{max} occurs.

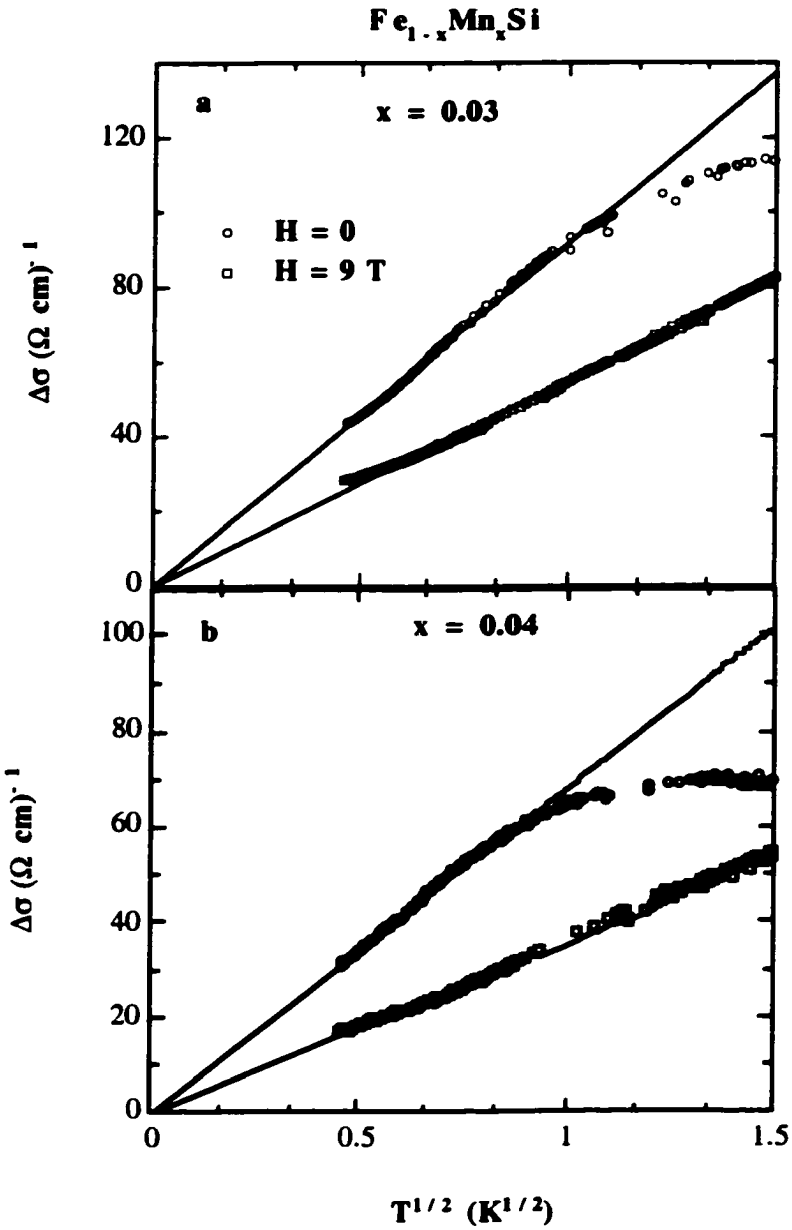

Fig. 5.10 The change in the conductivity (σ - σ_0) below 4 K for two Mn-doped $Fe_{1-x}Mn_xSi$ samples plotted as a function of $T^{1/2}$ with x = 0.03 (a) and x = 0.04 (b) at zero field and at 9 T as labeled in (a). The solid lines represent the best fits to the form $\sigma = \sigma_0 + m_\sigma T^{1/2}$ with σ_0 and m_σ determined from the fits to the data below 1 K.

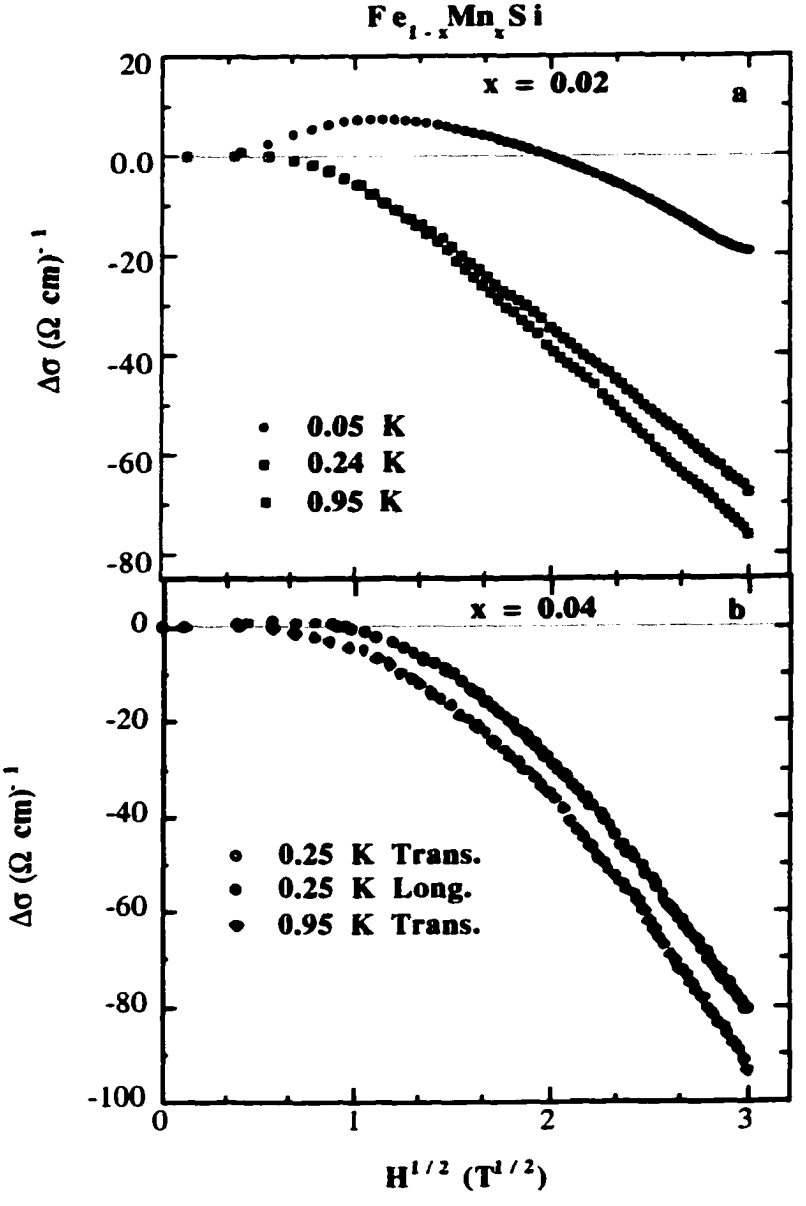

Fig. 5.11 The magnetoconductance $(\sigma(H,T) - \sigma_0(0,T))$ of (a) $Fe_{0.98}Mn_{0.02}Si$ and (b) $Fe_{0.96}Mn_{0.04}Si$ as a function of $H^{1/2}$ for temperatures labeled in the figure. We show in (b) that the MC does not depend on the direction at which the field is applied. Gray line highlights the positive MC ($\Delta\sigma > 0$).

transition. However, at the lowest temperatures the MC is clearly dominated by the positive contribution (see Fig. 5.11 (a) for $Fe_{0.98}Mn_{0.02}Si$ sample). We show in Fig. 5.16 that the magnetoresistivity for $Fe_{1-x}Mn_xSi$ as a function of magnetic field is systematic with Mn concentration. This figure also clearly displays the two separate (positive and negative) contributions to the MC. Fig 5.17 displays the high field MR for 10% Mn sample. We note that the size of the MR decreases with increasing Mn concentration.

An insulator to metal transition with the application of magnetic field has also been reported in In doped $Cd_{0.95}Mn_{0.05}Se$ and $Hg_{0.915}Mn_{0.085}Te$ [91], and in magnetic semiconductor $Gd_{1-x}v_xS_4$ [97]. In these materials similar to our $Fe_{1-x}Mn_xSi$ data, there is a crossover from VRH behavior to a $\sqrt{T}$ dependence at 1 T. Furthermore, as we have seen in $Fe_{1-x}Mn_xSi$ there are two contributions to MC: one positive which dominates at low fields and low T and the other negative which has a $\sqrt{H}$ assymtotic behavior. The behavior of these materials has been associated with the formation of bound magnetic polarons (BMP), a ferromagnetic coupling between local Mn spins with the more itinerant carriers leading to localization of carriers. This localization can be destroyed by the application of a magnetic field which polarizes the Mn spins. Thus, there is a tremendous similarity of $Fe_{1-x}Mn_xSi$ to these dilute magnetic semiconductors, both in transport and magnetization. Recently it has been suggested that the behavior of these materials can be understood as arising from the opening of a psuedogap in the DOS due to a magnetic phase separation [98], [99], [100]. In this description field tends to homogenize the magnetic state of the material removing the psuedogap.

5.4 Conclusions

In summary, we have observed that Mn substitution, like Al substitution, in Fesi results in one hole carrier per impurity being doped into this unconventional insulator. Both of these chemical substitutions lead to the formation of a heavy Fermion metallic ground state as evidenced by the large Pauli susceptibility induced upon doping. However, just as in other Mn doped semiconductors, the presence of Mn has a localizing

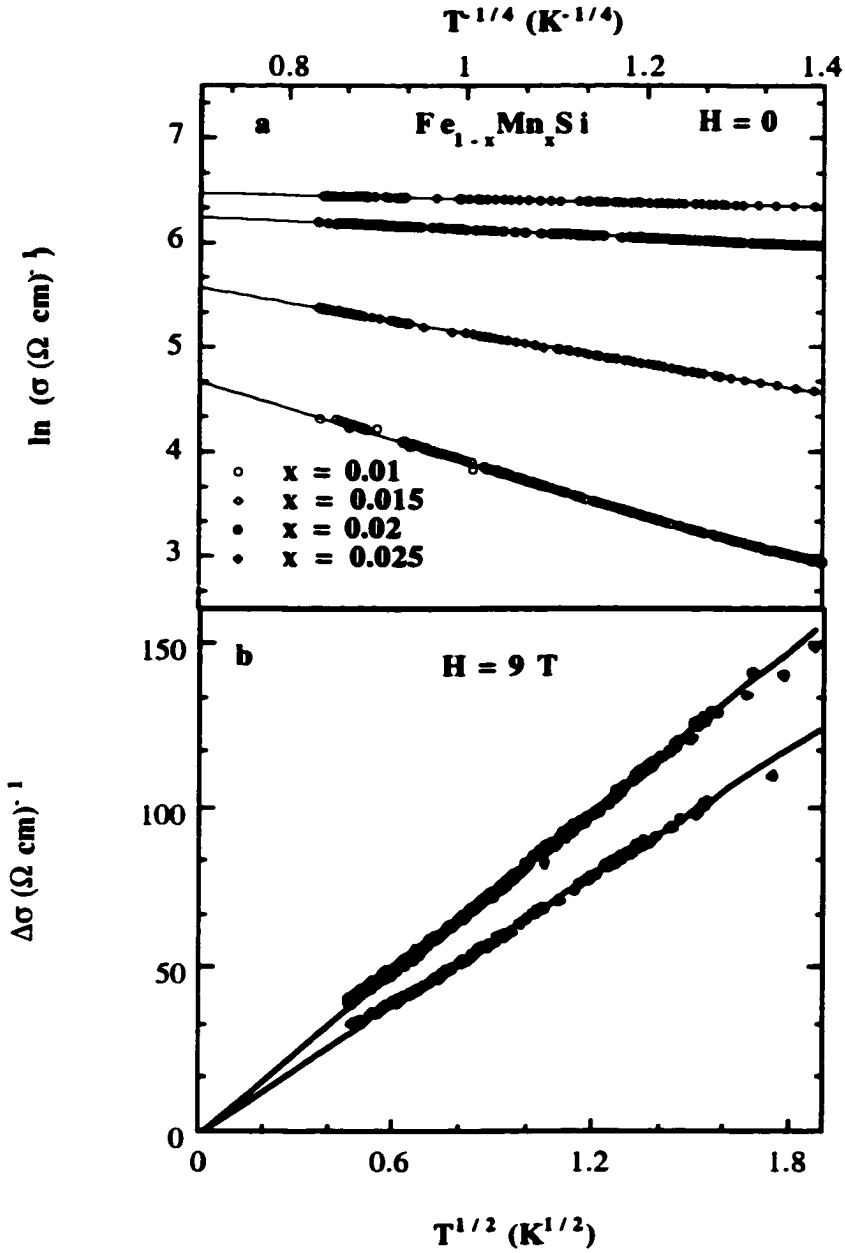

Fig. 5.12 (a) *ln* (σ) vs$T^{-1/4}$ for $Fe_{1-x}Mn_xSi$ at zero field for samples labeled in the figure. Lines represent best fits of $ln(\sigma) \propto T^{-1/4}$ to the low-T data. (b) $\Delta\sigma$ vs $T^{1/2}$ for $Fe_{1-x}Mn_xSi$ at 9 T (symbols as in (a)). Lines represent best fits of a $\sigma(T) \propto T^{1/2}$ form to the low-T data.

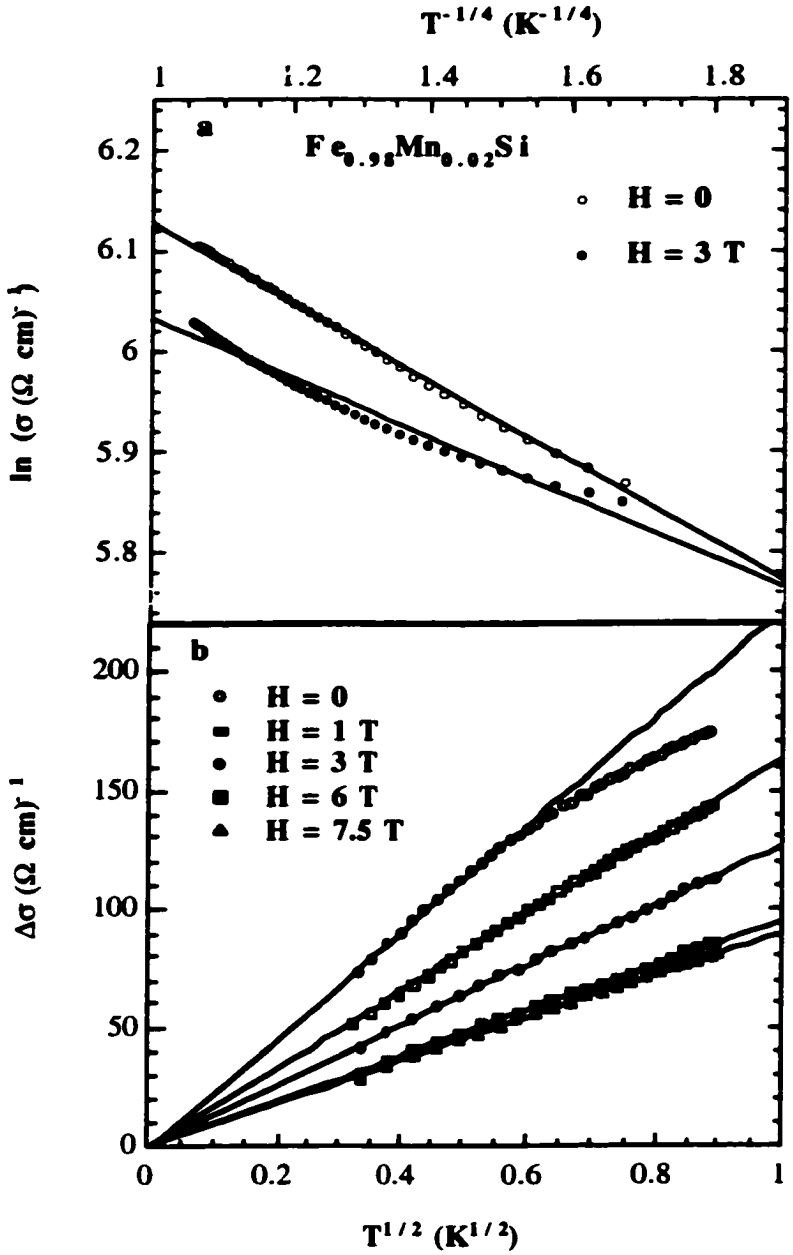

Fig. 5.13 $Fe_{0.98}Mn_{0.02}Si$ (a) $ln\ (\sigma)$ vs $T^{-1/4}$ at zero field and 3 T. The solid lines represent the best fits to $ln\ (\sigma) \propto T^{-1/4}$ form. (b) $\Delta\sigma$ vs $T^{1/2}$ at the fields labeled in the figure. Lines represent best fits to the low-T data to $\Delta\sigma\ (T) \propto T^{1/2}$.

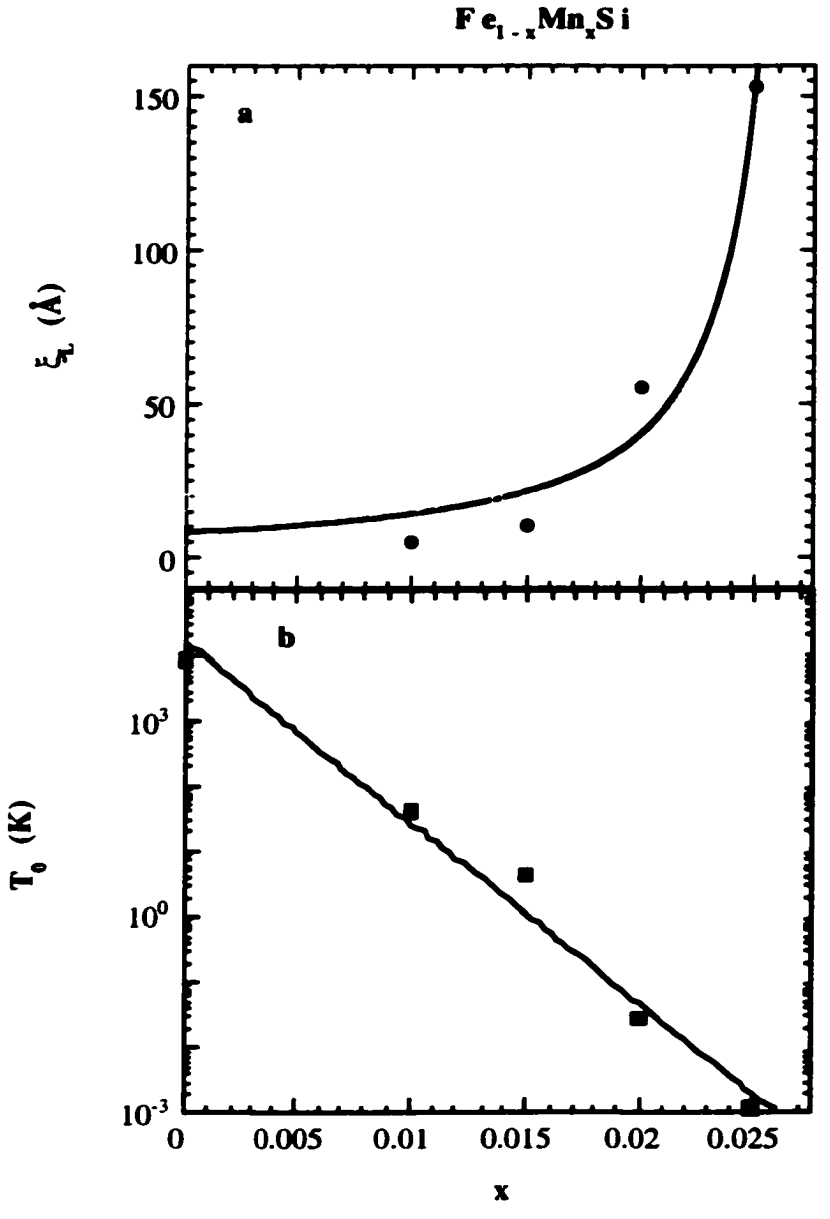

Fig. 5.14 $Fe_{1-x}Mn_xSi$ (a) localization length (ξ_L) vs. nominal Mn concentration. Solid line is the best fit to the form $\xi \propto (1 - n/n_c)^{-\nu}$, with $n_c = (1.2 \pm 1.1) \times 10^{21}$ / cm^3, and $\nu = 1.2 \pm 0.5$. (b) T_0 (K) on log scale plotted as a function of nominal Mn concentration in zero field. Solid line represents a fit of the form $T_0 = exp\,(-a\,x)$ to the data.

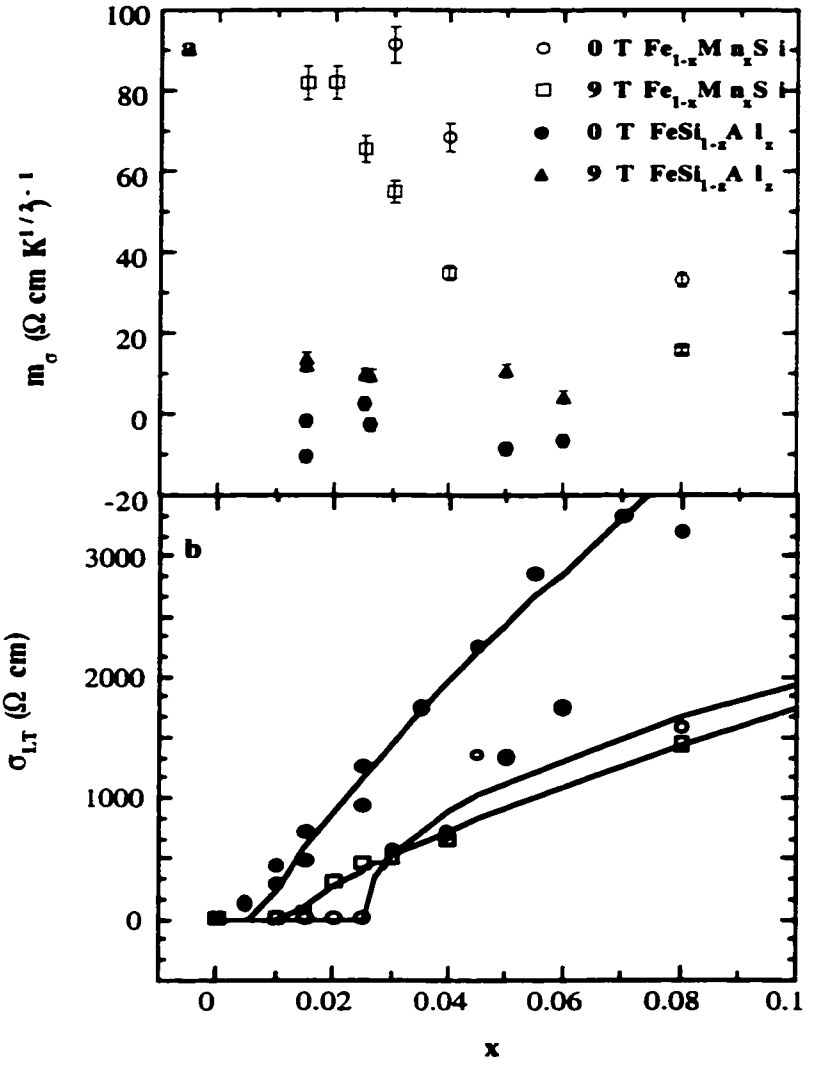

Fig. 5.15 (a) Plot of m_σ from fits of the form $\sigma = \sigma_0 + m_\sigma T^{1/2}$ to the data vs. nominal concentrations of $Fe_{1-x}Mn_xSi$ and $FeSi_{1-z}Al_z$ in fields labeled in the figure. (b) The low-T conductivity vs. nominal concentrations of $Fe_{1-x}Mn_xSi$ and $FeSi_{1-z}Al_z$ (symbols same as in (a)). The solid lines represent a fit to the form $\sigma_{LT} = \sigma_0 (n / n_c - 1)^\nu$. FeSiAl: $\nu = 0.9 \pm 0.1$, $\sigma_0 = 190 \pm 40$ $(\Omega\ cm)^{-1}$, FeMnSi: at $H = 0$, $\nu = 0.41 \pm 0.15$, $\sigma_0 = 1200 \pm 500$ $(\Omega\ cm)^{-1}$, and at $H = 9T$, $\nu = 0.8 \pm 0.1$, $\sigma_0 = 400 \pm 100$ $(\Omega\ cm)^{-1}$.

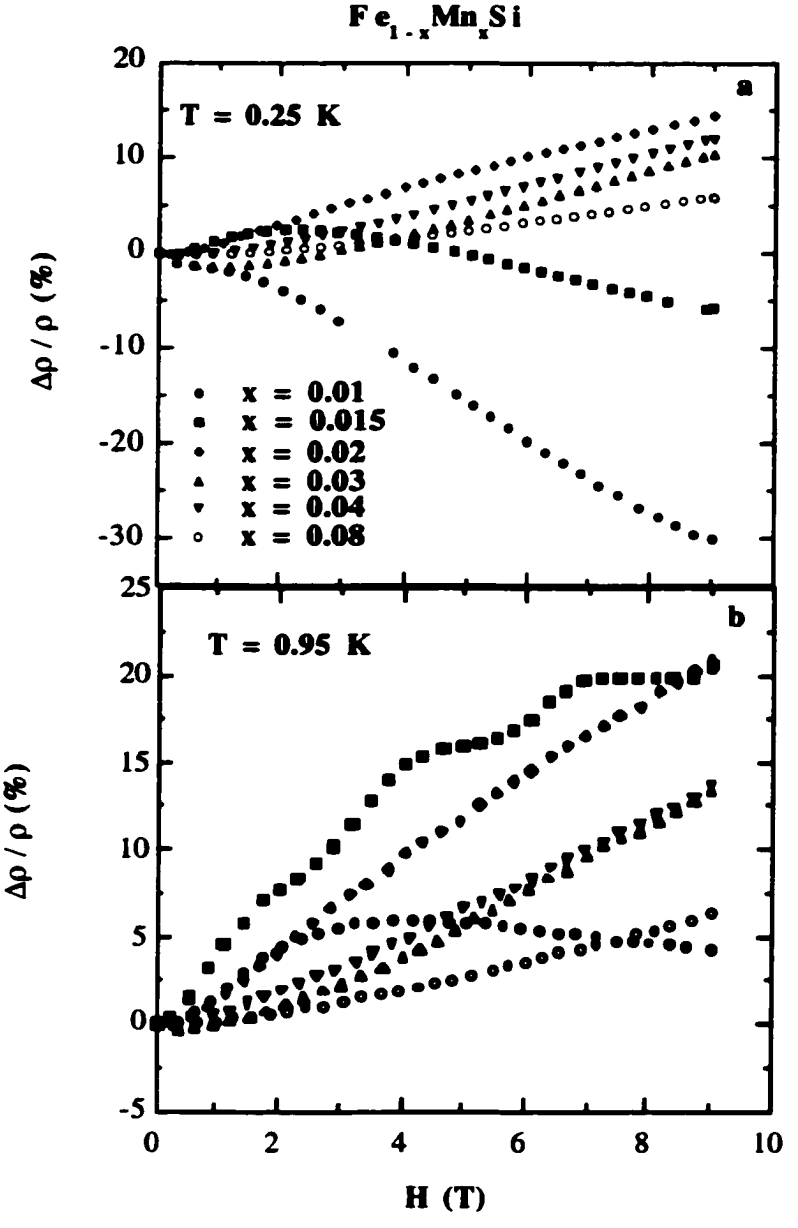

Fig. 5.16 $Fe_{1-x}Mn_xSi$ magnetoresistivity vs. magnetic field for samples labeled in (a) at T = 0.25 K (a) and T = 0.95 K (b).

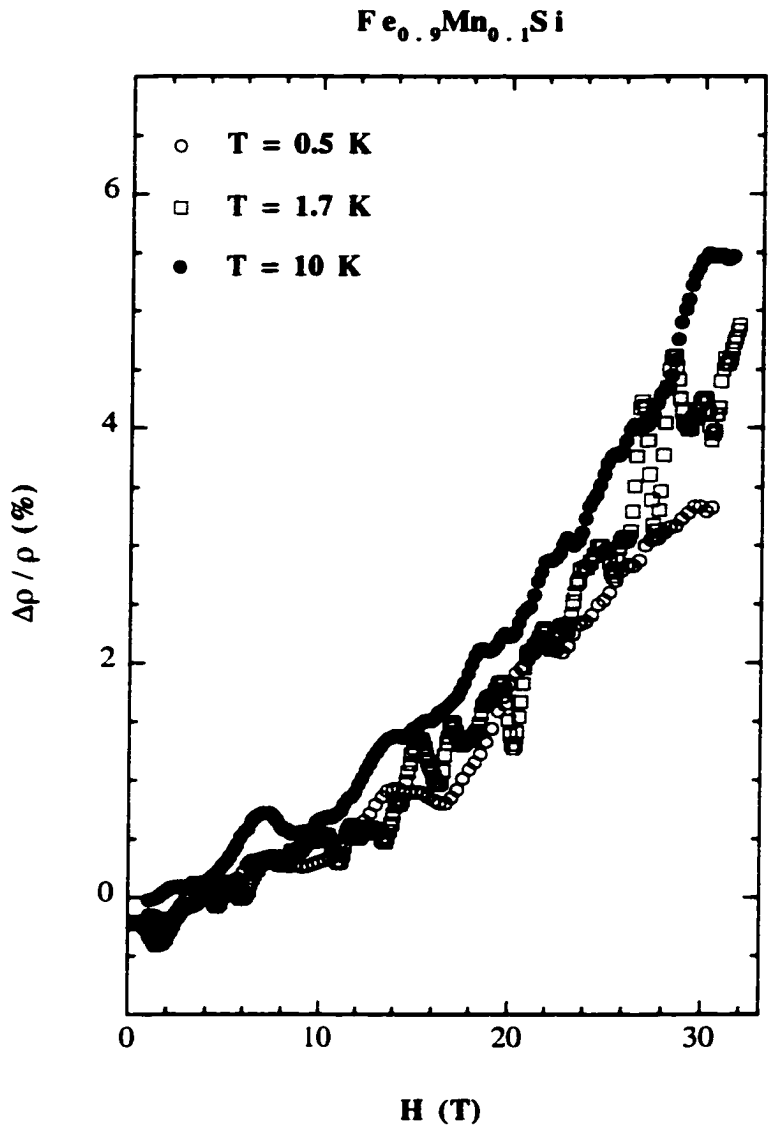

Fig. 5.17 $Fe_{0.9}Mn_{0.1}Si$ magnetoresistivity vs. magnetic field at the temperatures labeled in the figure.

effect on the carriers at low temperature[92]. This localization is removed by fields of order 1 T and can induce metallic behavior in samples just on the insulating side of the MI transition. The similarities in the low temperature transport of $Fe_{1-x}Mn_xSi$ and the more traditional Mn doped semiconductors, such as CdSe, HgTe, and GaAs suggests that $Fe_{1-x}Mn_xSi$ represents the first, to our knowledge, heavy Fermion diluted magnetic semiconductor.

CHAPTER 6

CONCLUSIONS

We have presented the measurements of the magnetic and transport properties of several dilution series of the mono-silicides FeSi, CoSi, and MnSi. The common crystal structure of these materials allowed an investigation of their electronic and magnetic properties as we varied the number of d electrons on the transition metal site. We have investigated the transport and magnetic behavior across this dilution series by carrying out magnetization, Hall effect, resistivity and magnetoresistance measurements. We have discovered an extraordinarily large anomalous Hall effect in $Fe_{1-y}Co_ySi$, a new mechanism for MR in ferromagnets ($Fe_{1-y}Co_ySi$), and a new Heavy Fermion DMS ($Fe_{1-x}Mn_xSi$).

6.1 Hall Effect Measurements

Although our materials are not suitable for technology, our data, as well as recent investigations of $La_{1-x}Ca_xCoO_3$[83] and $La_{1-x}Sr_xMnO_3$[82], suggest that doping of anomalous insulators such as Kondo, Mott-Hubbard, and charge transfer insulators can often lead to magnetic metals with large Hall effects. Our comparison of $Fe_{1-y}Co_ySi$ and $Fe_{1-x}Mn_xSi$ reveals that simple models to predict the size of ρ_{xy} from M and ρ_{xx} are not complete, and thus a true exploration of likely materials is necessary. We hope that our data will motivate such investigations since it suggests that this anomalous Hall effect need not be strongly T dependent, can be large in materials with a few hundred $\mu\Omega$cm resistivity, and has a linear field dependence in helimagnets, or soft magnets.

6.2 $Fe_{1-x}Mn_xSi$

For this dilution series we concentrated on the low Mn concentrations ($0 < x \leq 0.08$) with the intention of comparing it with $FeSi_{1-z}Al_z$. We have observed that Mn substitution, like Al substitution, in Fesi results in one hole carrier per impurity being doped into this unconventional insulator. Both of these chemical substitutions lead to the formation of a heavy Fermion metallic ground state as evidenced by the large Pauli

susceptibility induced upon doping. However, just as in other Mn doped semiconductors, the presence of Mn has a localizing effect on the carriers at low temperature[92]. This localization is removed by fields of order 1 T and can induce metallic behavior in samples just on the insulating side of the MI transition. The similarities in the low temperature transport of $Fe_{1-x}Mn_xSi$ and the more traditional Mn doped semiconductors, such as CdSe, HgTe, and GaAs [91-94]suggests that $Fe_{1-x}Mn_xSi$ represents the first, to our knowledge, heavy Fermion diluted magnetic semiconductor.

6.3 $Fe_{1-y}Co_ySi$

Here we concentrated on the concentration range where this system becomes a helimagnet ($0.05 \leq y \leq 0.8$) with the intention of comparing it with a well known helimagnetic compound MnSi. The picture that emerges from magnetization measurements is that while MnSi has magnetization that is common to weak itinerant ferromagnets, $Fe_{1-y}Co_ySi$ is a weak itinerant ferromagnet with a small density of carriers that are completely, or nearly completely spin polarized at low T. We observe in agreement with previous measurements a large negative magnetoresistance peaking sharply near the Curie temperature in MnSi. We discover qualititatively different magnetotransport for the low carrier density ferromagnet produced by modest doping of FeSi by Co. Here, magnetoresistance is not only positive, but remains essentially temperature independent below the Curie temperature. It is thus not due to spin fluctuation effects responsible for most magnetoresistive phenomena of current interest. Instead, our data suggest that the magnetoconductivity is a spectroscopy of an electronic state density with a $\sqrt{E}$ (E is the energy) singularity of the type generally associated with disorder-induced enhancement of electron-electron repulsion. Until now, such $\sqrt{E}$ terms have been deemed relevant only at ultra-low temperatures (< 1 K). Thus, our discovery not only shows a new mechanism for magnetorestistance in ferromagnets, but also demonstrates the relevance of subtle quantum effects on electrical properties at temperatures beyond 50 K.

REFERENCES

1 C. W. Searle and S. T. Wang, Ca. J. Phys. **47**, 2703 (1969).

2 S. Jin, T. H. Tiefel, M. McCormack, *et al.*, Science **264**, 413 (1994).

3 Y. e. a. Tokura, J. Appl. Phys. **79**, 5288 (1996).

4 H. Y. Hwang and S.-W. Cheong, Nature **389**, 942 (1997).

5 Y. Shimakawa, Y. Kubo, and T. Manako, Nature **379**, 53 (1996).

6 M. N. Baibich, J. M. Broto, A. Fert, *et al.*, Phys. Rev. Lett. **61**, 2472 (1988).

7 R. Fiederling, M. Keim, G. Reuscher, *et al.*, Nature **402**, 687 (1999).

8 Y. Ohno, D. K. Young, B. Beschoten, *et al.*, Nature **402**, 790 (1999).

9 R. Xu, A. Husmann, T. F. Rosenbaum, *et al.*, Nature **390**, 57 (1997).

10 A. E. Berkowitz, J. R. Mitchell, M. J. Carey, *et al.*, Phys. Rev. Lett. **68**, 3745 (1992).

11 T. F. Rosenbaum, R. F. Milligan, M. A. Paalanen, *et al.*, Phys. Rev. B **27**, 7509 (1983).

12 M. A. Paalanen and e. al., Phys. Rev. Lett. **61**, 597 (1988).

13 D. B. McWhan, J. P. Remeika, J. P. Maita, *et al.*, Phys. Rev. B **7**, 326 (1973).

14 S. A. Carter, T. F. Rosenbaum, P. Metcalf, *et al.*, Phys. Rev. B **48**, 16 841 (1993).

15 J. G. Bednorz and K. Muller, Z. Phys. B **64**, 189 (1986).

16 B. Ellman, H. M. Jaeger, D. P. Katz, *et al.*, Phys. Rev. B **39**, 9012 (1989).

17 N. W. Preyer, M. A. Kastner, C. Y. Chen, *et al.*, Phys. Rev. B **44**, 407 (1991).

18 Y. Ando, G. S. Boebinger, A. Passner, *et al.*, Phys. Rev. Lett. **75**, 4662 (1995).

19 Y. Hidaka, Y. Tajima, K. Sugiyama, *et al.*, J. Phys. Soc. Jpn. **60**, 1185 (1991).

20 A. Husmann, D. S. Jin, Y. V. Zastavker, *et al.*, Science **274**, 1874 (1996).

21 L. F. Matheiss and D. R. Hamann, Phys. Rev. B **47**, 13 114 (1993).

22 C. Fu, M. P. C. M. Krijin, and S. Doniach, Phys. Rev. B **49**, 2219 (1994).

23 C. Fu and S. Doniach, Phys. Rev. B **51**, 17 439 (1995).

24 Z. Fisk, J. L. Sarrao, J. D. Thompson, *et al.*, Physica B **206 & 207**, 798 (1995).

25 V. I. Anisimov, S. Yu Ezhov, I. V. Solovyev, *et al.*, Phys. Rev. Lett. **76**, 1735 (1996).

26 G. Aeppli and Z. Fisk, comments Condens. Matter Phys. **16**, 155 (1992).

27 B. Bucher, Z. Schlesinger, P. C. Canfield, *et al.*, Phys. Rev. Lett. **72**, 522 (1994).

28 V. Jaccarino, G. K. Wertheim, J. H. Wernick, *et al.*, Phys. Rev. **160**, 476 (1967).

29 G. Shirane, J. E. Fischer, Y. Endoh, *et al.*, Phys. Rev. Lett. **59**, 351 (1987).

30 Z. Schlesinger, Z. Fisk, H. Zhang, *et al.*, Phys. Rev. Lett. **71**, 1748 (1993).

31 C.-H. Park, Z.-X. Shen, A. G. Loeser, *et al.*, Phys. Rev. B **52**, R16 981 1995).

32 J. F. DiTusa, K. Friemelt, E. Bucher, *et al.*, Phys. Rev. Lett. **78**, 2831 (1997).

33 M. A. Chernikov, L. Degiorgi, E. Felder, *et al.*, Phys. Rev. B **56**, 1366 (1997).

34 T. Moriya, *Spin Fluctuations in Itinerant electron magnetism* (Springer-Verlag, Berlin Hiedleberg New York Tokyo, 1985).

35 J. Beille, J. Voiron, and M. Roth, Solid state Comm. **47**, 399 (1983).

36 J. Beille, J. Voiron, F. Towfiq, *et al.*, J. Phys. F: Metal Phys. **11**, 2153 (1981).

37 K. Ishimoto, M. Ohashi, H. Yamauchi, *et al.*, J. phys. Soc. Jpn **61**, 2503 (1992).

38 J. H. Wernick, G. K. Wertheim, and R. C. Sherwood, Mat. Res. Bull. **7**, 1431 (1972).

39 H. J. Williams, J. H. Wernick, R. C. Sherwood, *et al.*, J. Appl. Phys. **37**, 1256 (1966).

40 N. W. Ashcroft and N. D. Mermin, *Solid State Physics*, New York, 1976).

41 H. Ibach and H. Luth, *Solid State Physics* (Springer-Verlag, Berlin, 1990).

42 I. A. Campbell and A. Fert, *Transport properties of ferromagnets* (North-Holland Pub. Co., Amsterdam, 1982).

43 P. Coleman, P. W. Anderson, and T. V. Ramakrishnan, Phys. Rev. Lett. **55**, 414 (1985).

44 L. Berger and G. Bergmann, *The Hall effect of ferromagnets* (Plenum, New York, 1980).

45 R. C. O'Handley, *Hall Effect Formulae and Units* (Plenum, New York, 1980).

46 C. D. Hurd, *The Hall effect in Metals and Alloys* (Plenum, New York, 1972).

47 P. G. De Gennes and J. Friedel, J. Phys. Chem. Solids **4**, 71 (1958).

48 F. C. Zumsteg and R. D. Parks, Phys. Rev. Lett. **24**, 520 (1970).

49 T. F. Rosenbaum, K. Andres, G. A. Thomas, *et al.*, Phys. Rev. Lett. **45**, 1723 (1980).

50 B. M. Dodson, W. L. McMillan, J. M. Mochel, *et al.*, Phys. Rev. Lett. **46**, 46 (1981).

51 M. A. Paalanen, T. F. Rosenbaum, G. A. Thomas, *et al.*, Phys. Rev. Lett. **48**, 1284 (1982).

52 E. Abrahams, P. W. Anderson, P. C. Licciardello, *et al.*, Phys. Rev. Lett. **42**, 673 (1979).

53 E. Abrahams and T. V. Ramakrishnan, J. Non-Crst. Solids **35**, 15 (1980).

54 B. L. Al'tshuler and A. G. Aronov, Zh. Eksp.Teo. Fiz. (Sov. Phys. JETP) **77 (50)**, 2028 (968) (1979).

55 B. L. Al'tshuler, A. G. Aronov, and P. A. Lee, Phys. Rev. Lett. **45**, 1288 (1980).

56 A. M. Finkel'shtein, sov. Phys. JETP **59**, 212 (1984).

57 C. Castellani, G. Kotliar, and P. A. Lee, Phys. Rev. Lett. **59**, 323 (1987).

58 F. J. Wegner, Z. Phys. **25**, 327 (1976).

59 B. L. Al'tshuler, Sov. Sci. Rev. A phys. **9**, 223 (1987).

60 P. A. Lee and T. V. Ramakrishnan, Rev. modern phys **57**, 287 (1985).

61 G. Bergmann, Phys. Rep. **107**, 1 (1984).

62 P. Dai, Y. Zhang, and M. P. Sarachik, Phys. Rev. B **45**, 3984 (1992).

63 A. J. Millis and P. A. Lee, Phys. Rev. B **30**, 6170 (1984).

64 M. Sawicki, T. Dielt, J. Kossut, *et al.*, Phys. Rev. lett. **56**, 508 (1986).

65 B. T. Matthias and R. M. Bozorth, Phys. Rev. **100**, 604 (1958).

66 B. T. Matthias, A. M. Clogston, H. J. Williams, *et al.*, Phys. Rev. Lett. **7**, 7 (1961).

67 T. Moriya and A. Kawabata, J. Phys. Soc. Jpn. **34**, 639 (1973).

68 S. Kawarazaki, H. Yasuaka, Y. Nakamura, *et al.*, J. Phys. Soc. Jpn **41**, 1171 (1976).

69 P. J. Brown, J. B. Forsyth, and G. H. Lander, J. Appl.Phys. **39**, 1331 (1968).

70 H. Watanabe and H. Nakajima, J. Mag. Mag. Mat. **31-34**, 153 (1983).

71 J. W. Dorleijn, Philips Res. Repts. **31**, 281 (1976).

72 F. E. Maranzana, Phys. Rev. **160**, 421 (1967).

73 P. W. Chapman, O. N. Turfe, J. D. Zook, *et al.*, J. Appl. Phys. **34**, 3291 (1963).

74 O. V. Elmel'yanenko, T. S. Lagunova, D. N. Nalsedov, *et al.*, Fiz. Tver. Tela **7**, 1315 (1965).

75 S. B. Field and T. F. Rosenbaum, Phys. Rev. Lett. **55**, 522 (1985).

76 C. Leighton, I. Terry, and Becla, Phys. Rev. B **58**, 9773 (1998).

77 T. R. McGuire, R. J. Gambino, and R. C. Taylor, J. Appl. Phys. **48**, 2965 (1977).

78 S. C. H. Lin, J. Appl. Phys. **40**, 2175 (1969).

79 G. Bergmann and p. Marquardt, Phys. Rev. B **18**, 326 (1978).

80 A. B. Pakhomov, X. Yan, and Y. Xu, J. Appl. Phys. **79**, 6140 (1996).

81 C. L. Canedy and e. al., J. Appl. Phys. **79**, 6140 (1996).

82 P. Malt and e. al., Phys. Rev. B **57**, 10248 (1998).

83 A. V. Samoilov and e. al., Phys. Rev. B **57**, R14032 (1998).

84 P. Majumdar and P. Littlewood, Phys. Rev. Lett. **81**, 1314 (1998).

85 P. Rhodes and E. P. Wohlfarth, Proc. R. Soc. (London) **273**, 247 (1963).

86 K. Ishimoto, Y. Yamaguchi, Y. Suzuki, *et al.*, Physica B **213 & 214**, 381 (1995).

87 K. Ueda and T. Moriya, J. Phys. Soc. Jpn. **39**, 965 (1975).

88 K. Ueda, Solid state Comm. **19**, 965 (1976).

89 G. A. Thomas, A. Kawabata, Y. Ootuka, *et al.*, Phys. Rev. B **26**, 2113 (1982).

90 N. Manyala, Y. Sidis, J. F. DiTusa, *et al.*, To be published .

91 T. Wojtowicz, T. Dielt, M. Sawicki, *et al.*, Phys. Rev. Lett. **56**, 2419 (1986).

92 J. K. Furdyna, J. Appl. Phys. **53**, 7637 (1982).

93 T. Hayashi, M. Tanaka, T. Nishinaga, *et al.*, J. Crystal Growth **175**, 1063 (1997).

94 H. Ohno, A. Shen, F. Matsukura, *et al.*, Appl. Phys. Lett. **69**, 363 (1996).

95 Ohno, Science **281**, 951 (1998).

96 K. Binder and A. P. Young, Rev. Modern Phys. **58**, 801 (1986).

97 S. von Monar, A. Briggs, J. Flouquet, *et al.*, Phys. Rev. Lett. **51**, 706 (1983).

98 A. Moreo, S. Yunoki, and E. Dagotto, Science **283**, 2034 (1999).

99 A. Moreo, S. Yunoki, and E. Dagotto, Phys. Rev. Lett. **83**, 2773 (1999).

100 M. Fath, S. Freisem, A. A. Menovsky, *et al.*, Science **285**, 1540 (1999).

VITA

Ncholu Ignatius Manyala was born on July 14, 1964, in the Mokhotlong district in Lesotho. He was the tenth of eleven children of Makhathatso and Patliso Manyala.

Ncholu received his primary education at Ha-Matjota primary school in 1979. He found that he liked science courses when attending St. James High School in Mokhotlong. He was introduced to the field of physics when attended pre-college course in Maseru ran by Dutch scholars under the name LESPEC.

In the fall of 1985 he continued his studies at National University of Lesotho where he enjoyed the course work and playing soccer, not really professionally. He graduated in the fall of 1989 and decided to head for graduate school at the University of Witwatersrand, Johannesburg, in the summer of 1990. Ncholu got married to his high school sweetheart Kholu in december 1991, and in May 23, 1992, were blesssed with a beautiful daughter Ithabeleng Manyala.

In winter of 1992 Ncholu joined National University of Lesotho as a lecturer. He thought undergraduate physics for two years and decided to continue his studies. In fall of 1994 he came to Louisiana State University to further his graduate studies. After two years at L.S.U Ncholu found that he enjoyed working in the Low temperature physics group and decided to do his thesis work in the basement of Nicholson Hall with Jonh F. DiTusa. After his graduation here with the degree of Doctor of Philosophy, Ncholu will be going back to Lesotho where he is going to join the physics department in the National University of Lesotho.

DOCTORAL EXAMINATION AND DISSERTATION REPORT

Candidate:

Ncholu Ignatius Manyala

Major Field:

Physics

Title of Dissertation:

Transport and Magnetic Measurements of Mono-Silicides

Approved:

Major Professor and Chairman

Dean of the Graduate School

EXAMINING COMMITTEE:

Date of Examination:

February 18, 2000